ISSN: 1945-3094 (Print), 1945-3108 (Online) Volume 1, Number 5, November 2009

Journal of Water Resource and Protection

Editor-in-Chief : Jian Shen

www.scirp.org/journal/jwarp

Scientific Research

Journal Editorial Board

ISSN: 1945-3094 (Print) ISSN: 1945-3108 (Online)

http://www.scirp.org/journal/jwarp

J. Water Resource and Protection, **2009, 1, 299-380**
Published Online November 2009 in SciRes (http://www.SciRP.org/journal/jwarp/).

TABLE OF CONTENTS

Volume 1 Number 5 **November 2009**

Journal of Water Resource and Protection (JWARP)

Journal Information

SUBSCRIPTIONS

The *Journal of Water Resource and Protection* (Online at Scientific Research Publishing, www.SciRP.org) is published monthly by Scientific Research Publishing, Inc., USA.

E-mail: service@scirp.org

Subscription rates: Volume 1 2009
Print: $50 per copy.
Electronic: free, available on www.SciRP.org.
To subscribe, please contact Journals Subscriptions Department, E-mail: service@scirp.org

Sample copies: If you are interested in subscribing, you may obtain a free sample copy by contacting Scientific Research Publishing, Inc at the above address.

SERVICES

Advertisements
Advertisement Sales Department, E-mail: service@scirp.org

Reprints (minimum quantity 100 copies)
Reprints Co-ordinator, Scientific Research Publishing, Inc., USA.
E-mail: service@scirp.org

COPYRIGHT

PRODUCTION INFORMATION

For manuscripts that have been accepted for publication, please contact:
E-mail: jwarp@scirp.org

J. Water Resource and Protection, **2009, 1, 299-315**
doi:10.4236/jwarp.2009.15037 Published Online November 2009 (http://www.scirp.org/journal/jwarp)

Upstream-Downstream Relationships in Terms of Annual Streamflow Discharges and Drought Events in Nebraska

Hong WU[1], Leen Kiat SOH[2], Ashok SAMAL[2], Tao HONG[2], David MARX[3], Xunhong CHEN[4]
[1]*Texas Institute for Applied Environmental Research, Tarleton State University, Stephenville, USA*
[2]*Department of Computer Science and Engineering, University of Nebraska-Lincoln, Reno, USA*
[3]*Department of Statistics, University of Nebraska-Lincoln, Reno, USA*
[4]*School of Natural Resources, University of Nebraska-Lincoln, Reno, USA*
E-mail: *lksoh@cse.unl.edu*
Received July 21, 2009; *revised August* 19, 2009; *accepted August* 26, 2009

Abstract

Upstream-downstream relationships of annual streamflow discharges and severity and frequency of streamflow drought events are critical in understanding how streamflow droughts propagate over time and space. Such information can be used to resolve water disputes, trigger mitigation strategies, and understand how streamflow changes due to changes in the environment. During drought years, such information is even more critical as water resources are contested. The objective of this research is to study the upstream-downstream relationships of streamflow in Nebraska along four major river systems with diverse hydrologic characteristics and human activities: North Platte, Big Blue, Republican, and Niobrara. The relationships among the upstream and downstream stations along the four rivers are investigated by comparing several statistics derived from the annual flow discharge and on drought events. Trend analysis and coefficient of variation are applied to annual flow discharge values, and a host of drought-related parameters (e.g., annual maximum drought duration, annual accumulated drought duration, number of drought events) are also computed with respect to five different levels of streamflow drought events: water shortage, mild drought, moderate drought, significant drought, and extreme drought. The paired-*t* test and ANOVA with MIXED procedure are subsequently applied to the statistics to observe whether there is a significant difference between upstream and downstream stations along a river. The analysis allows us to characterize the upstream-downstream relationships of the four river systems, laying the groundwork for further investigations to identify the reasons for some of the trends and observations. These findings will be essential in water resources management during or prior to hydrological droughts.

Keywords: Streamflow Drought, Upstream-Downstream Relationship, Paired *T*-Test, Repeated Measures ANOVA with MIXED Procedure, Nebraska

1. Introduction

About 40 percent of the world population lives in 250 major river basins that are shared by multiple countries [1]. Competing uses of these rivers have led to conflicts and disputes between upstream and downstream countries. Downstream water users are directly affected by the water use of the upstream counterparts and are vulnerable to water overuse and misuse upstream. The construction of reservoirs and dams can prevent flooding and drought conditions downstream. On the other hand, if the upstream dams do not release water because of drought or water needs of the reservoirs, serious consequences can occur downstream. If the upstream and downstream water scarcity differs, it could indicate that the causes are not only natural but also management related.

In the High Plains Region of the United States, water resources management is especially critical to rapidly expanding cities, rural communities, the management of public lands (national forests and grasslands, state parks, and wildlife refuges), agricultural communities, and the nation's economy. But the competing demands have created many water conflicts among the users along the same river. Even more, droughts often accelerate the impacts of the water conflicts. During the peak of the

1934 drought, for example, downstream Nebraskans had little water for irrigation because the water users in Wyoming held back as much water as they could, leading to fiercely contested arguments between the two states [2].

Frequent and severe hydrological droughts result in serious environmental, economic, and social consequences in a region. One concern is that extreme hydrological events (e.g., floods and droughts) or observable, statistically significant trends in hydrological measurements will increase in frequency and magnitude. The possible causes for this trend include local and global climate variation and change, water regulations, industrial and urban water withdrawals, excessive irrigation and land use, and loss of vegetation cover [3−12]. If the magnitude and frequency of hydrological droughts change spatially and temporally, the impacts on water management, agriculture, and aquatic ecosystems will be significant. In view of this, water accounting strategies have also been proposed to take into account groundwater and surface water management to use water more productively in parts of the world with water shortages [13]. In addition, Wilhite [14] indicated that drought vulnerability shows an increasing trend. Therefore, the knowledge of the characteristics of hydrological drought event and its spatial and temporal variability is essential for the efficient management of water resources in a specific region.

Thus, the examination of the relationships of streamflow annual discharges and severity and frequency of streamflow droughts among the upstream and downstream stations will be helpful to understand the influence of human activities and its consequences during the low-flow periods. To accomplish this objective, this study investigates these relationships by 1) comparing the basic statistical characteristics (i.e., mean, standard deviation, coefficient of variation, and trend slope) on the annual flow discharges; and 2) comparing the statistics of drought-related parameters (i.e., annual maximum drought duration, annual accumulated drought duration, number of drought events per year, total number of drought events with a duration greater than three weeks, largest drought deficit and its time period, and longest streamflow drought duration and its time period). To facilitate the analysis, we also devise a definition for different levels of drought events based on low flow range. For each river system, we identify two sets of streamflow stations: upstream and downstream. We then compute the above statistics for each set. Subsequently, the paired- *t* test is performed on the trend slopes (as they are scalar values) while the MIXED procedure [15] is used on all other parameters to determine whether the difference between the upstream set and the downstream set along a river is significant. These values help us define upstream-downstream relationships along each of the four river systems in our study area.

2. Study Area

2.1. River Systems

The State of Nebraska in the United States was chosen as the pilot study area because Nebraska, located on the High Plains region, represents a dynamic test bed for the integration of water resources monitoring systems. Nebraska is the transition zone between humid, semiarid, and arid climates, with major streams transecting these climate regions [16]. This study focuses on four major rivers in climatically distinct regions in Nebraska—the North Platte, Niobrara, Big Blue and Republican, as shown in Figure 1.

The North Platte River, originated in Colorado and Wyoming, flows to Nebraska. It is the most important river in western Nebraska. The North Platte River has several small tributaries. A number of canals were constructed in the North Platte River valley for irrigation. Lake McConaughy and Kingsley Dam were constructed more than 60 years ago on the North Platte River for the purposes of irrigation, power development, and recreation. In the River valley, coarse alluvial materials form a principal aquifer unit where wells are constructed for irrigation. The North Platte River on the alluvial sediments can have a good hydrologic connection to the underlying aquifer. The annul precipitation from 1948 to 2001 in Scottsbluff of the North Platte River Valley, about 32 km to the western border of Nebraska, was 39.1 cm.

The Niobrara River originates in far eastern Wyoming and snakes across northern Nebraska. The river in Nebraska is about 491 km in length (Figure 1). The unique nature of this river is its diversity from its wide, verdant valleys to its steep sandstone canyons, waterfalls and cliffs. Thus, recreation such as canoeing, tubing and air boating, is the main activity. A number of small creeks join the river and two major tributaries, the Snake River and Key Paha River, are located down stream. Five dams are constructed in this basin, four on the Niobrara River and one on the Snake River. To the south of the river lies the unique grass-covered Sandhills where a large amount of groundwater is stored. Groundwater feeds numerous lakes and streams in the Sandhills area [17]. Groundwater irrigation exists in the Niobrara River valley but most irrigation wells concentrate in the upstream area. Annual precipitation at Valentine near the middle stream of the Niobrara River was 55.6 cm from 1948 to 2001.

The North Fork Republican River flowing through Colorado and the South Fork Republican River flowing through Kansas conjoin in Nebraska to form the Republican River, which drains southern Nebraska and eventually flows to Kansas. For the river reach in Nebraska, three creeks, Frenchman Creek, Red Willow Creek, and Medicine Creek, join the Republican River on its north side. Beaver Creek joins the Republican River on the

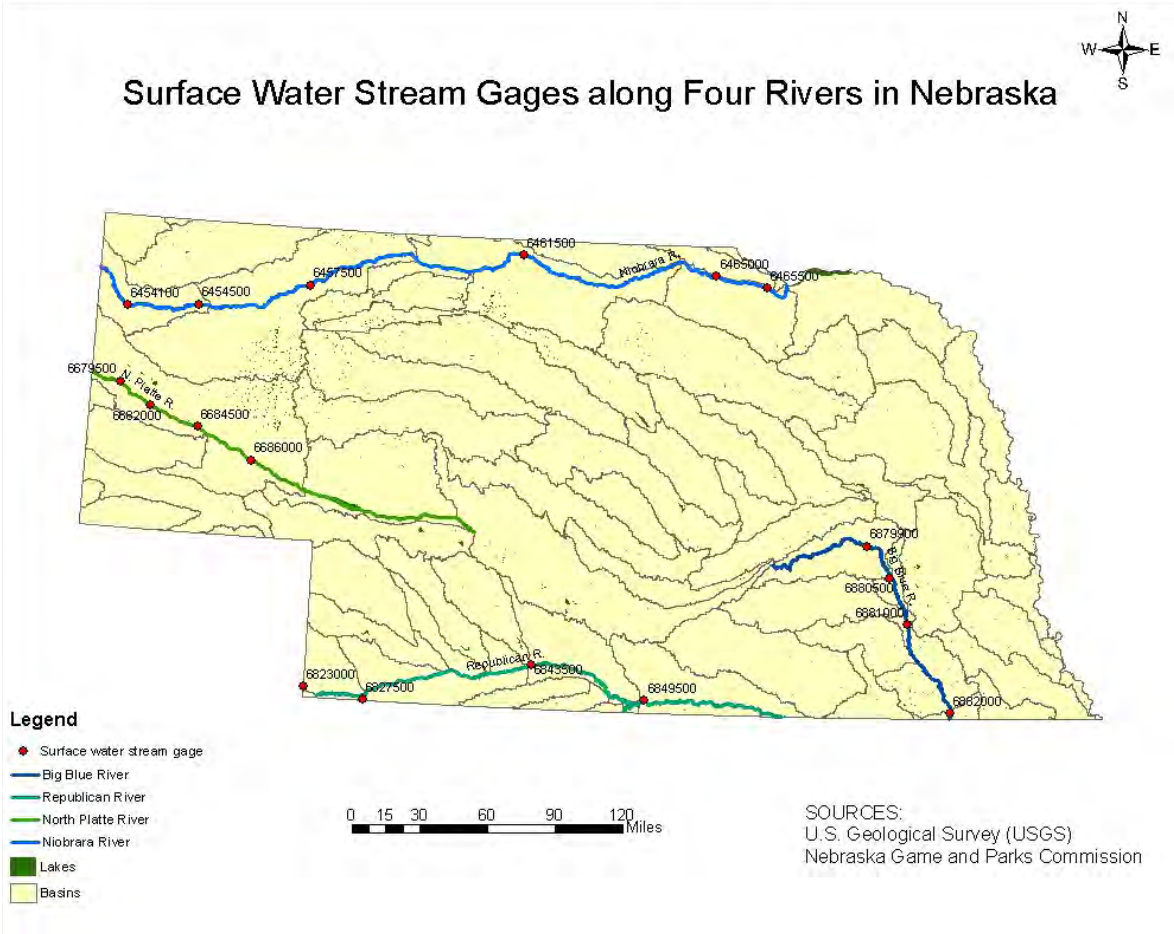

Figure 1. Distribution of the selected surface stream gages along the four rivers in Nebraska.

south side. In the main stem of the river, there are two reservoirs: Swanson Lake in upstream and Harlan County Lake in downstream. One reservoir was constructed on each of the three creeks in the north side of the Republican River: Enders Lake on Frenchman Creek, Hugh Butler Lake on Red Willow Creek, and Harry Strunk Lake on Medicine Creek. Sediments in the river valley of the Republican River consist of alluvial sand and gravel. Groundwater wells were constructed in the Basin for irrigation. There are also several canals which divert streamflow for irrigation. A depletion of streamflow at some specific locations in this river basin has been the starting point of water right disagreements between the users. For instance, rights to the streamflow in the Republican River basin have been in dispute between Nebraska and Kansas, as well as Colorado. The annual precipitation between 1948 and 2001 from a rain gauge of Benkleman (near streamflow gauge 06827500, see Figure 1) in the upstream of the Republican River was 47.4 cm.

The Big Blue River drains southeastern Nebraska. Several tributaries conjoin the river. The river flows to Kansas. The annual precipitation between 1948 and 2001 from a rain gauge of Crete (near the stream gauge 0688100, see Figure 1) was 75.6 cm. The top soil can be glacial or loess deposits. The river banks are usually composed of silt and clay. The groundwater system has a little hydrologic connection to the river [18]. Groundwater irrigation is well developed in the Big Blue Basin. The Big Blue agreement between Nebraska and Kansas has been more amicable than the Republican debates because of the higher annual precipitation levels and reduced threat of water shortage in the Big Blue basin, compared with those conditions in the southwestern and south-central parts of the state, where the Republican River basin lies. Among the four basins, the Big Blue River Basin has little impact of canal diversion or reservoir regulations on streamflow.

2.2. Stream Gauge Station Selection and Streamflow Data Sources

Choice of stream gages for this study posed a significant problem. All stations were chosen from a national database maintained by the U.S. Geological Survey (USGS). However, most stations with the most recent data did not

have long-term historical data and the stations with long-term data were without up-to-date data. We decided to use the long-term data because they will be more meaningful in the statistical analysis. Therefore, the time periods of the selected stations were a somewhat out-of-date. Along the four selected major river systems, thirty eight (38) stream gauge stations were identified based on the relative long-term streamflow data records. Specifically, four stations were chosen along the North Platte River with a period of measurement from 1930 to 1991; six stations along the Niobrara River (1957 – 1991); four stations along the Republican River (1952 – 2001); and four stations along the Big Blue River (1964 – 1994). USGS ended operations on some of these stations in 1990s. As a result, we selected the streamflow series based on the gauge with a shortest record. Nevertheless, the time period is still 30 years or longer for each study area. Figure 1 shows the stations used in this study along with the spatial coverage of the four selected rivers.

3. Methodology

In this study, we compare the streamflow stations on two sets of statistics: 1) the basic statistical characteristics derived from the annual streamflow discharges, and 2) the drought-related parameters derived from the identified streamflow drought events. To identify different levels of streamflow droughts, we devise a definition based on low flow range. Here we discuss these in detail.

3.1. Basic Statistical Characteristics on Annual Streamflow Discharge

Based on the streamflow data over the specific time period for each gauge station, the following basic statistical characteristics on the streamflow discharge were computed:

1) annual mean discharge: the average amount of water through a station per year;

2) standard deviation of the annual mean discharge;

3) coefficient of variation, the ratio of the standard deviation to the annual mean discharge; and

4) trend slope of the annual mean discharge based on linear regression analysis.

The coefficient of variation provides a comparison of the standard deviation of the annual mean discharge in units of the mean. These basic statistical characteristics will be compared among the upstream and downstream stations along each river to study the streamflow drought patterns of the four rivers.

3.2. Definition of a Streamflow Drought

Generally, a hydrological drought event for streams is characterized by three components: *duration*, *severity*, and *magnitude* [19]. Duration is the period during which streamflow stays below the long-term mean. Severity is the cumulative water deficiency. Magnitude is the average water deficiency during the period. Figure 2 illustrates these three drought components and the definition of a drought event schematically. Magnitude is also sometimes known as intensity [20]. Drought severity has also been defined as a combination of duration, deficit and maximum intensity [21].

The relationships among the three components are given by Equation (1):

$$magnitude = \frac{severity}{duration} \tag{1}$$

Prior to computing the three components, one needs to make sure that the distribution of streamflow is *normal*. If it is not, a logarithmic transformation on the flow data is necessary.

To obtain the "above normal" and "below normal" sections of a streamflow time series, the widely used threshold-based approach was employed [22]. A threshold level (or truncation level) divides a time series into two quantized sections. It is considered desirable to use a *mean* truncation level, since the mean is more sensitive to the extreme values of the distribution. Particularly in the study of drought events, these extreme droughts are generally of primary interest. In order to keep a consistent analysis of drought events, the average annual low- and high-flow seasons for each station were identified based on the multi-year average monthly discharge [23, 1]. Consequently, the stream drought events were defined in the low- and high-flow seasons separately.

3.3. Drought-Related Parameters

To describe the severity and frequency of streamflow droughts over the study period for each station from different aspects, several parameters were derived based on the three components of an event: duration, severity, and magnitude. The derived parameters were:

1) the annual maximum drought duration (AMD);

2) the annual accumulated drought duration (ACD);

3) the number of drought events per year (ND) [1];

4) the total number of drought events with a duration greater than three weeks over the study period;

5) the largest drought deficit and its time period over the study period; and

6) the longest streamflow drought duration and its time period over the study period [24].

Using annual results allows us to analyze the long-term trends and sensitivity of the streamflow. Similar parameters have also been used in analyzing other climate data such as evapotranspiration [25]. Comparisons of these parameters among the stations along a river

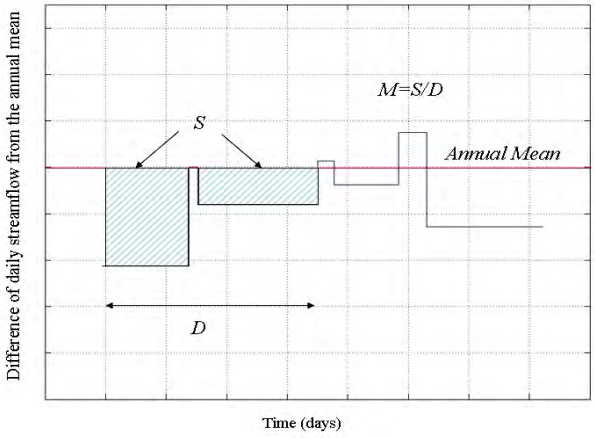

Figure 2. The three components of a drought event. *M* denotes the *magnitude* of a drought event; *S* the *severity*; and *D* the *duration*.

will reveal the upstream-downstream relationships in term of the severity and frequency of streamflow drought. Streamflow drought condition is essential information in the evaluation of water storage in rivers.

Two statistical tests were used to determine the differences of those statistical parameters between the upstream and downstream stations: the paired t-test and ANOVA using MIXED procedure. The paired t-test is commonly used for evaluating matched pairs of data with the assumption that the paired differences are normally distributed [7]. Since the parameters were driven from the daily streamflow data, repeated measurement data were involved. Therefore, the MIXED procedure was used to run an analysis of variance (ANOVA) because the MIXED procedure is able to accommodate data that have both fixed and random factors [5]. The two analyses were performed using SAS [20]. The level of significance was set at 0.05.

3.4. Classification of the Streamflow Drought Levels

In order to obtain greater resolution in the understanding of drought we propose a multi-level approach. We define six levels of droughts of increasing intensity from *no drought* to *extreme drought*. Based on the range of values of daily stream flow, we define the low flow range for a stream for a given day as follows:

$$lfr\ (d) = mean(d) - min(d), \tag{2}$$

where *lfr (d)* is the low flow range, *mean(d)* and *min(d)* are the average value and the minimum value of the stream flow for the day (*d*), respectively. The six levels of droughts are defined using the computed *lfr(d)* and daily flow (*water(d)*) as follows:

$$drought\ level(d) = \begin{cases} no\ drought & water(d) \geq mean(d) \\ water\ shortage & \min(d) + 0.5\,lfr(d) < water(d) \leq \min(d) + 1.0\,lfr(d) \\ mild\ drought & \min(d) + 0.25\,lfr(d) < water(d) \leq \min(d) + 0.50\,lfr(d) \\ moderate\ drought & \min(d) + 0.10\,lfr(d) < water(d) \leq \min(d) + 0.25\,lfr(d) \\ significant\ drought & \min(d) + 0.05\,lfr(d) < water(d) \leq \min(d) + 0.10\,lfr(d) \\ extreme\ drought & 0 \leq water(d) \leq \min(d) + 0.05\,lfr(d) \end{cases} \tag{3}$$

The time scale of streamflow used in the drought analysis is important. Using daily streamflow to define the drought events will introduce two particular problems: *mutually dependent droughts* and *minor droughts* [26]. Mutually dependent droughts are produced when the flow, which exceeds the threshold level in a short time period, divides a long-term drought event into a number of droughts of shorter duration. Minor droughts are results of flow fluctuations around the threshold level. In such cases, pooling successive events to define an independent sequence of droughts is necessary. The moving average procedure (MA) is a method for pooling dependent droughts into a single event. Based on a sensitivity analysis, Tallaksen *et al.* [27] and Hisdal *et al.* [1] concluded that an averaging interval 10 or 11 days is the "optimal" value in MA, respectively. As a result, the 11-day moving average procedure was applied to the daily streamflow data before performing drought identification on the data in this study. Thus, the streamflow data were smoothed by removing small, insignificant peaks and valleys above the threshold level and pooling some minor and dependent droughts together.

4. Results and Discussions

Here we discuss the results from two statistical comparative studies on the upstream-downstream relationships of the four major river systems in Nebraska. In each study, we will first present the statistics derived from the streamflow stations before comparing the upstream and downstream stations.

Note that the orientation of the Big Blue River is basically north-south while others are west-east. Since climatic condition varies largely across west-east, it probably has a larger effect on the streamflow for the Republican, Niobrara, and the North Platte rivers, especially on the Niobrara due to its significantly large distance between the most upstream and most downstream stations used in our studies. Further, the Big Blue watershed has a relatively small drainage area and that might cause the

Table 1. Basic streamflow statistics of the stations along the four rivers and high- and low-flow seasons. Stations are listed in order of flow directions, i.e. the upstream stations are listed before the downstream stations. Note: the Distance value is the distance between the most upstream and most downstream stations.

River (Drainage area in square km)	Streamflow Station	Up-stream/Down stream	Mean Dis-charge (m^3/yr)	Std. Dev. (m^3/yr)	Coeff. of Var.	Slope of annual mean discharge (m^3/yr)	High- Flow Season	Low- Flow Season
Big Blue (11,805) Distance: ~122 km	06879900 (BB1)	Up	295.60	199.86	0.68	3.20	Mar. – Jul.	Aug. – Feb.
	06880500 (BB2)	Up	1537.19	887.68	0.58	31.01	Mar. – Jul.	Aug. – Feb.
	06881000 (BB3)	Down	4521.40	2522.51	0.56	98.29	Mar. – Jul.	Aug. – Feb.
	06882000 (BB4)	Down	9954.64	6882.53	0.69	224.44	Mar. – Jul.	Aug. – Feb.
Niobrara (32,633) Distance: ~490 km	06454100 (N1)	Up	139.86	16.88	0.12	-1.02	Feb. – Jun.	Jul. - Jan.
	06454500 (N2)	Up	279.77	36.02	0.13	-1.50	Feb. – Jun.	Jul. - Jan.
	06457500 (N3)	Up	1158.19	132.18	0.11	-7.02	Feb. – Jun.	Jul. - Jan.
	06461500 (N4)	Down	7643.98	778.72	0.10	-25.51	Feb. – Jun.	Jul. - Jan.
	06465000 (N5)	Down	15179.50	2322.53	0.15	39.47	Feb. – Jun.	Jul. - Jan.
	06465500 (N6)	Down	16781.25	2758.47	0.16	-6.74	Feb. – Jun.	Jul. - Jan.
North Platte (80,025) Dis-tance: ~115 km	06679500 (NP1)	Up	7546.42	5664.76	0.75	100.47	Sep. -. Jun.	Jul.- Aug.
	06682000 (NP2)	Up	9879.66	5868.87	0.59	106.76	Sep. -. Jun.	Jul.- Aug.
	06684500 (NP3)	Down	12748.94	6061.23	0.48	97.67	Sep. -. Jun.	Jul.- Aug.
	06686000 (NP4)	Down	13728.68	5919.73	0.43	97.81	Sep. -. Jun.	Jul.- Aug.
Republican (58,015) Dis-tance: ~273 km	06823000 (R1)	Up	436.51	85.09	0.19	-4.50	Oct. – Apr.	May. – Sep.
	06827500 (R2)	Up	318.91	225.06	0.71	-9.71	Mar. – Jun.	Jul. – Feb.
	06843500 (R3)	Down	2269.15	1051.10	0.46	-47.54	Jun. – Aug.	Sep. – May.
	06849500(R4)	Down	2275.02	1733.68	0.76	-50.06	Jun. –Aug.	Sep. – May.

streamflow characteristics to be more volatile over time. The downstream flow is much larger than that in the upstream for this small Big Blue watershed because a larger precipitation in eastern Nebraska leads to large surface runoff on less permeable top soils. Soils in other three basins are more permeable; this can likely accelerate precipitation infiltration and reduce surface runoff during rain events.

4.1. Study 1: Upstream-Downstream Relationships of Streamflow

4.1.1. Statistical Characteristics of Streamflow

Table 1 summarizes the basic statistics of streamflow including the 1) annual mean discharge, 2) its standard deviation, 3) its coefficient of variation, 4) its slope of trend, and the distribution of the annual 5) high- and 6) low- flow seasons for each station along the 4 river systems. (The measurements are shown in British units since the original streamflow measurements are reported as such.) As expected, the annual mean discharges of downstream stations generally are greater than those of upstream stations. This is because the discharges increase downstream in a river as tributaries enter and most rivers tend to increase downstream hydraulic parameters (i.e. width, depth, and mean velocity) [28].

The coefficients of variation shown in Table 1 indicate that the variability of the annual discharges is between 60-70% among the 4 stations on the Big Blue River, while the variability is about 10% among the 6 stations on the Niobrara River. The common thing between the two rivers is that the coefficients of variation are consistent among the stations along each river. On the other hand, the coefficients of variation for the stations on the other two rivers of North Platte and Republican are discrepant. For the North Platte River, the station NP1, located at the very beginning of the river, has the highest coefficient (0.75) among the 4 stations. The coefficient of variation decreases downstream. In contrast, the station R4, located on the lower Republican River, has the highest coefficient of variation (0.76) compared with other upstream stations, especially R1. This could be explained by the fact that the Harlan County Reservoir is located between the two stations R3 and R4. In addition, a canal system originates just below this reservoir. The canals divert streamflow during each irrigation season, leading to a high variation of the downstream station. A high coefficient of variation (0.71) is also observed for R2. This is very likely due to Haigler Canal constructed above R2 which diverts water from the North Fork Republican River.

All stations along the Big Blue and North Platte indicate a positive trend in the annual discharge over the study period, while the stations along the Republican indicate a negative trend. All stations along the Niobrara show a negative trend except for one downstream station. The detected negative trend along the Republican is consistent with what has been reported in Wen and Chen [29] as results of groundwater irrigation. Streamflow diversion to canals and consumption of water by riparian vegetation can also reduce streamflow. According to Chen and Shu [30], the rate of groundwater use by riparian vegetation can be up to 5 mm/day in the Republican River Valley. The negative trend is also consistent with the primary reasons for the dispute between the two states of Nebraska and Kansas.

The long-term monthly average discharge distribution over the given time period for each station shows that the high-flow season is a bimodal distribution, and the high- and low-flow seasons for the stations along the Big Blue are consistent (Figure 3). For convenience, this study combined the two high-flow seasons into a single one, i.e., the high-flow season is from March through July, and the low-flow season is from August through February. This pattern is also exhibited by the stations along the Niobrara and North Platte Rivers. However, the distribution patterns of the monthly average streamflow of the stations along the Republican are *inconsistent*. One station's high-flow season is another station's low-flow season, for example. This *inconsistency* is probably due to the lower stream of the river being diverted via irrigation canals during the crop growing season. Note that the Republican River Basin has five major dams on the main stem and its tributaries. These reservoirs regulate water for irrigation and flood control. They can also contribute to the inconsistency.

4.1.2. Upstream-Downstream Relationships of Streamflow

Based on the results described in Table 1, we use the paired *t*-test to determine whether the trend slopes for the stations upstream are different from the trends for downstream stations. To test the differences on other parameters, we utilize the MIXED procedure in SAS to account for year.

```
PROC MIXED DATA=R1
    COVTEST;
    CLASS YEAR S T;
    MODEL Y = T/DDFM=KR;
    RANDOM YEAR YEAR*T S(T);
    LSMEANS T;
```

In the above model, * denotes factor interaction and the parentheses denote factor nesting. That is, S(T) denotes the station id of type T, where the type can be either upstream or downstream. YEAR is the year of measurement.

Table 2 summarizes the results obtained from the two tests. There is no significant difference between upstream and downstream stations along the Big Blue and the Republican rivers, in terms of mean annual streamflow, variability and trend slope. For the North Platte River, there is no significant difference in terms of all the statistics but standard deviation between upstream and downstream streamflow. For the Niobrara River the characteristics between the upstream and downstream stations are significantly different in the annual mean streamflow, variability and the trend slope, with an exception of coefficient of variation. The variability between upstream and downstream stations is probably caused by its long stretch for the analysis, lower annual precipitation in the upstream area, potential effect of intensive groundwater irrigation in parts of the watershed, and surface water regulation (e.g., reservoirs and dams).

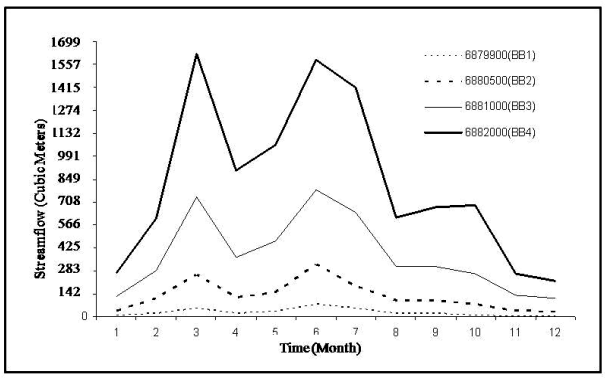

Figure 3. Long-term monthly mean discharge of the four stations along the Big Blue.

4.2. Study 2: Upstream-Downstream Relationships of Drought Events and Durations

The parameters associated with the severity and frequency of the streamflow drought—such as the annual maximum drought duration (*AMD*), the annual accumulated drought duration (*ACD*) and the number of drought events per year (*ND*) were compared among the upstream and downstream stations along the same river to

Table 2. The results of statistical tests to compare the streamflow statistical characteristics between upstream and downstream stations.

	Streamflow Characteristics			
	Annual	**Standard**	**Coefficient**	**Trend**
Big Blue	×	×	×	×
Niobrara	√	√	×	√
North Republican	×	√	×	×
	×	×	×	×

√: Difference between upstream and downstream is statistically significant (p=0.05)
×: The difference is not statistically significant

study the association of the severity and frequency of streamflow drought occurring along the same river.

In the following, due to space consideration, we present figures and tables to show only results of two representative stations of each river, one from the set of upstream stations and one from the downstream stations.

4.2.1. Number of Drought Days

Figures 4-7 show the distribution of drought days of different levels for the stations of the four rivers.

4.2.2. Annual Maximum Drought Duration (AMD)

Figures 8-11 show the distribution of AMD of different levels for the stations of the four rivers.

4.2.3.Annual Accumulated Drought Duration (ACD)

Figures 12-15 show the distribution of ACD of different levels for the stations of the four rivers.

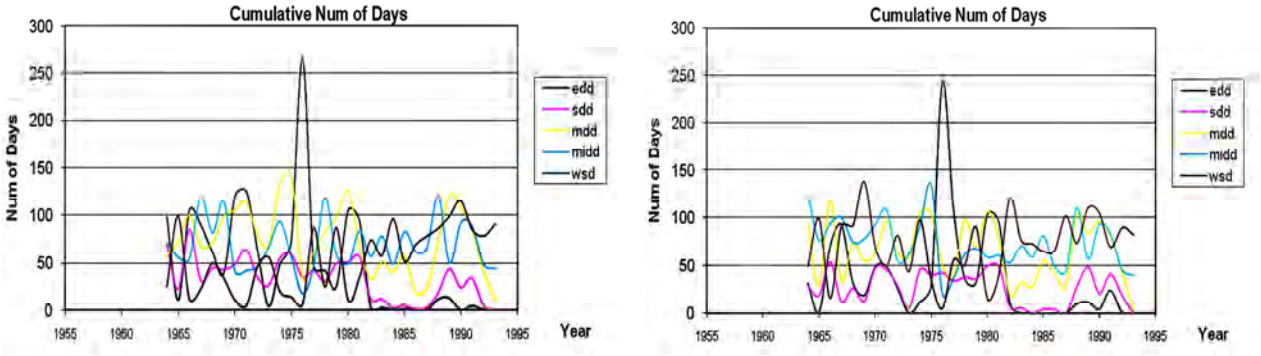

(a) Upstream Station (b) Downstream Station

Figure 4. Number of drought days of different levels for the Big Blue River. "edd" denotes extreme drought days; "sdd" significant drought days, "mdd" moderate drought days, "midd" mild drought days; and "wsd" water shortage days.

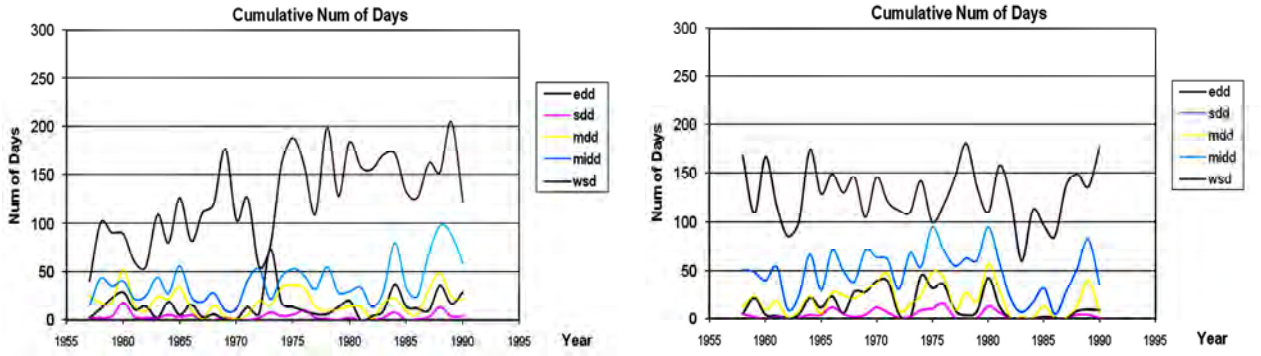

(a) Upstream Station (b) Downstream Station

Figure 5. Number of drought days of different levels for the Niobrara River.

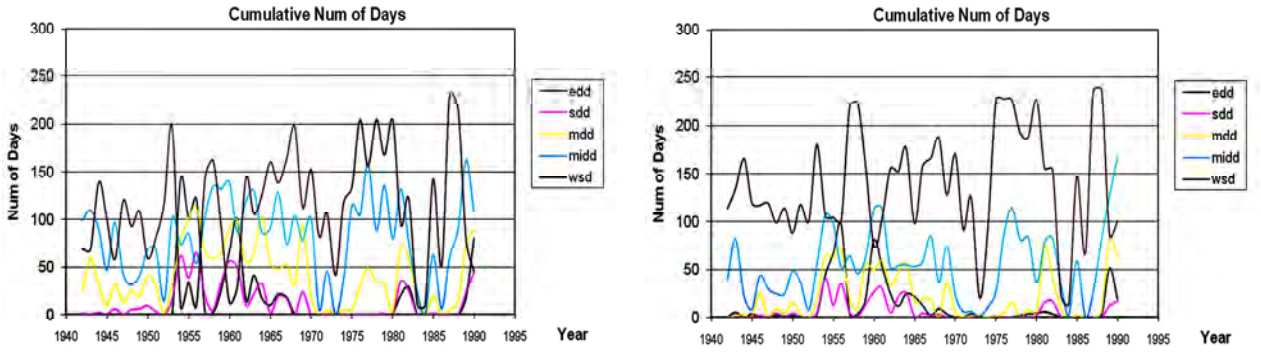

(a) Upstream Station (b) Downstream Station

Figure 6. Number of drought days of different levels for the North Platte River.

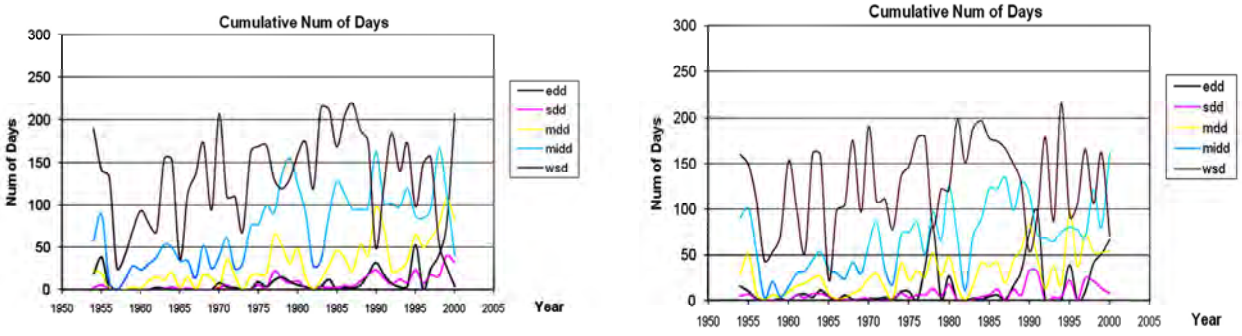

(a) Upstream Station (b) Downstream Station

Figure 7. Number of drought days of different levels for the Republican River.

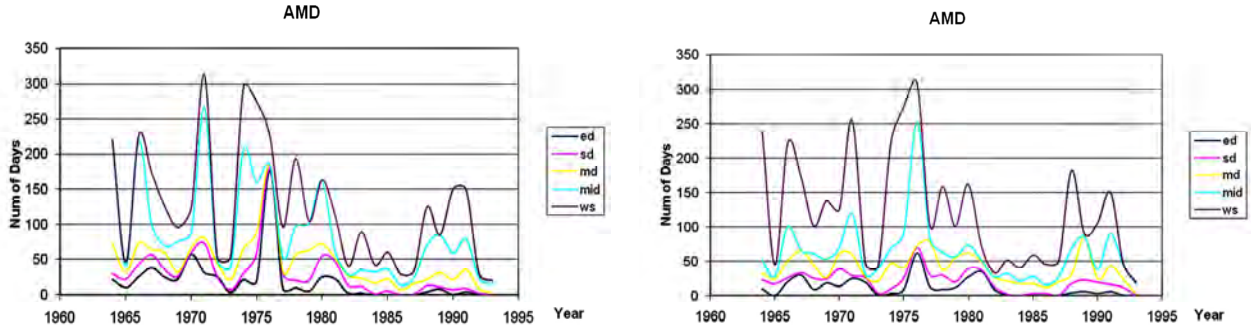

(a) Upstream Station (b) Downstream Station

Figure 8. AMD of different levels for the Big Blue River.

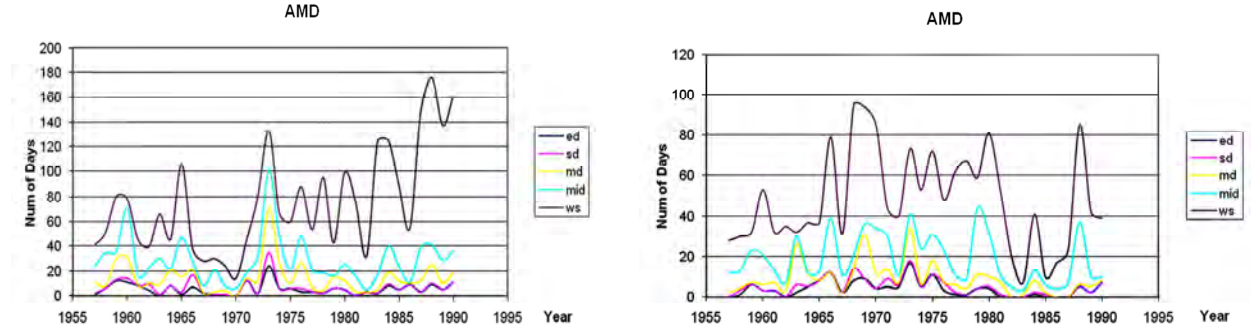

(a) Upstream Station (b) Downstream Station

Figure 9. AMD of different levels for the Niobrara River.

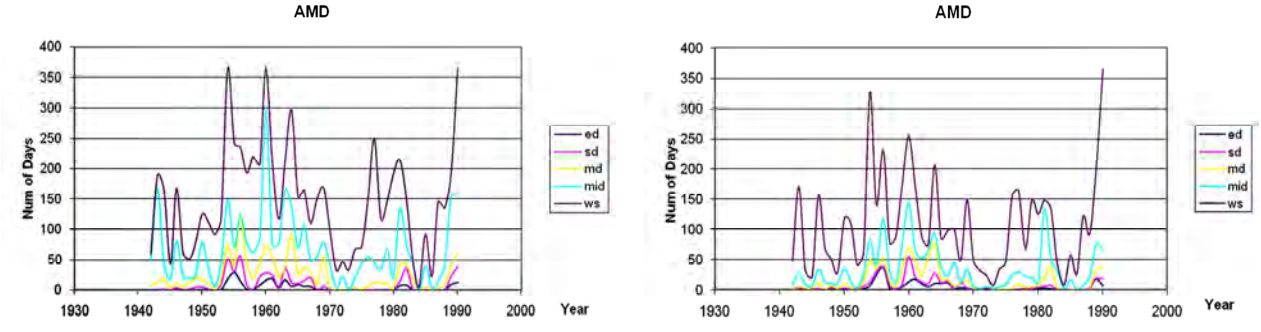

(a) Upstream Station (b) Downstream Station

Figure 10. AMD of different levels for the North Platte River.

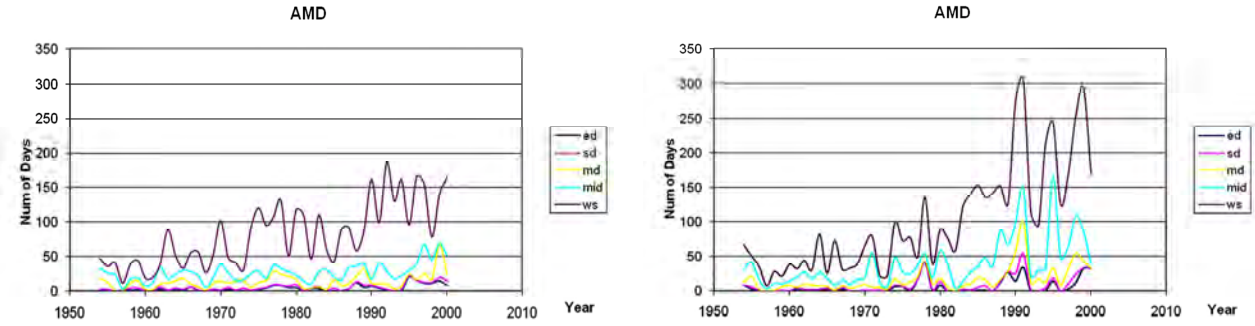

(a) Upstream Station (b) Downstream Station

Figure 11. AMD of different levels for the Republican River.

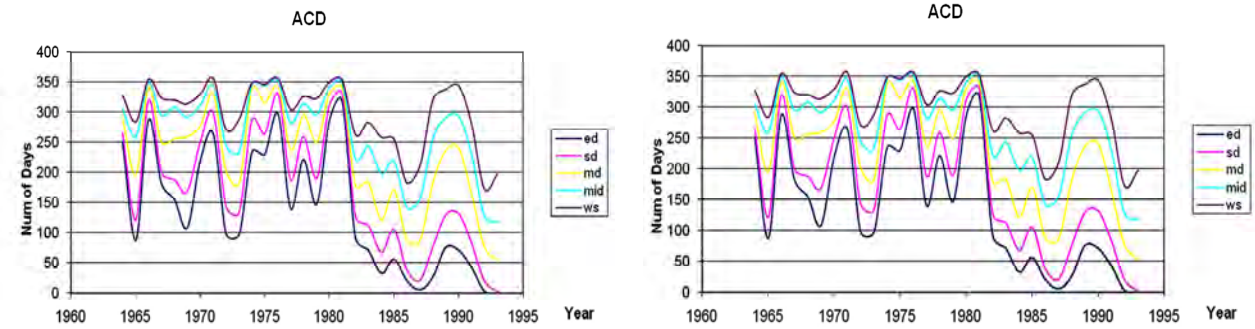

(a) Upstream Station (b) Downstream Station

Figure 12. ACD of different levels for the Big Blue River.

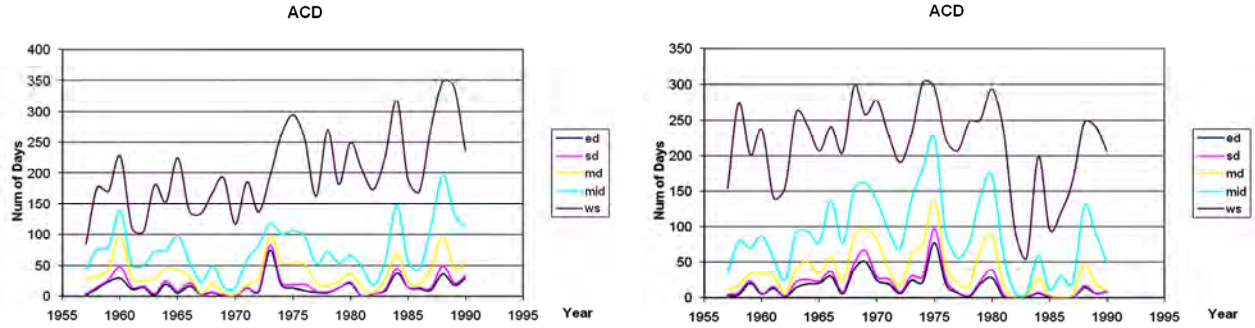

(a) Upstream Station (b) Downstream Station

Figure 13. ACD of different levels for the Niobrara River.

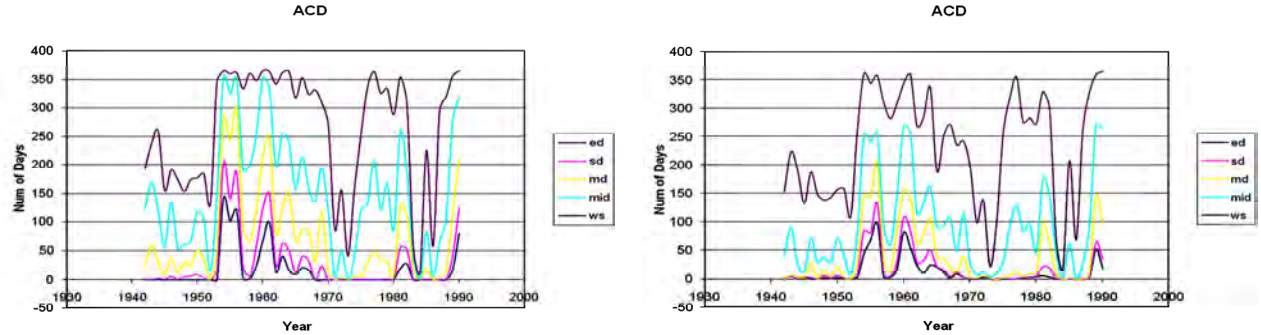

(a) Upstream Station (b) Downstream Station

Figure 14. ACD of different levels for the North Platte River.

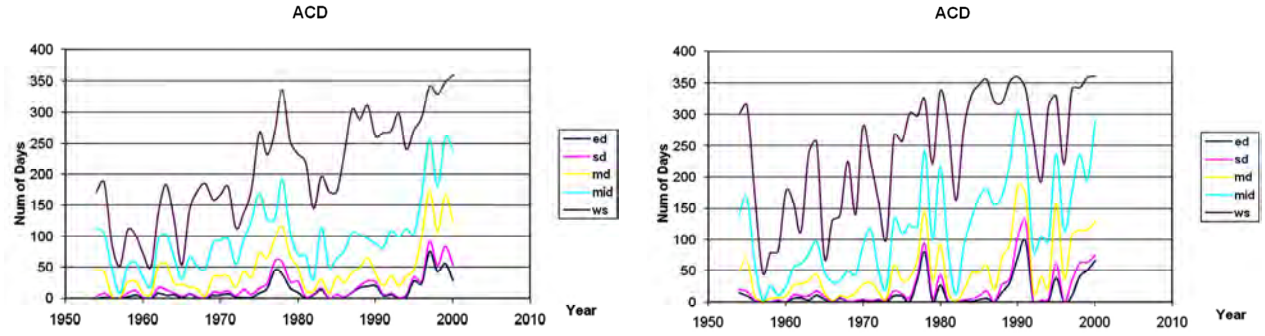

(a) Upstream Station (b) Downstream Station

Figure 15. ACD of different levels for the Republican River.

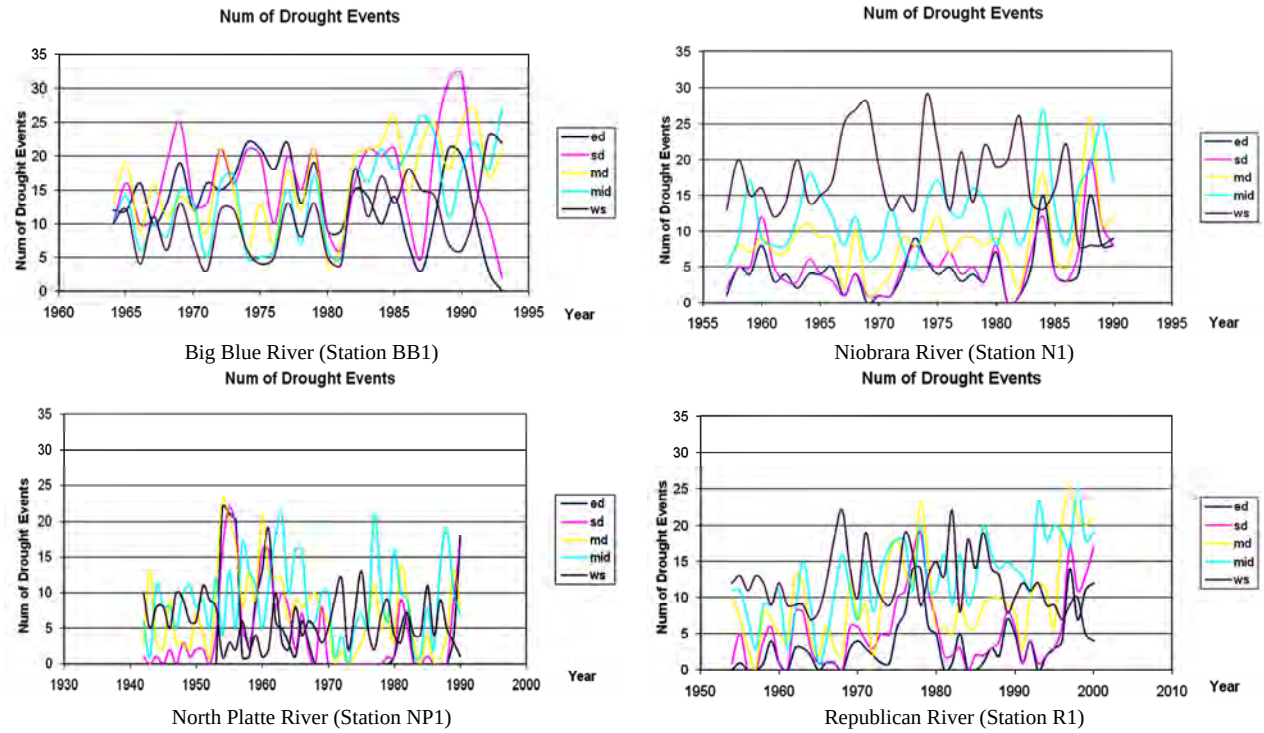

Big Blue River (Station BB1) Niobrara River (Station N1)

North Platte River (Station NP1) Republican River (Station R1)

Figure 16. Number of drought events of different levels for the four rivers.

4.2.4. Number of Drought Events per Year (ND).

Drought events could be defined according to one of the five drought levels as defined earlier in Equation (3). For each level, the drought event is further classified based on the duration to show how long the water deficit will last. We tried durations of 2 weeks, 3 weeks, 4 weeks, 6 weeks, and 8 weeks for each drought type. Therefore there are 25 different combinations. To compare those different combinations, we constructed a 5×5 matrix for each station. Each entry in the matrix is one of the 25 different combinations of different drought duration thresholds and drought types. The upper left corner corresponds to the combination of water shortage drought and a threshold of 2 weeks. The lower right corner corresponds to the combination of extreme drought type and a threshold of 8 weeks. Tables 3-6 summarize the distributions of drought events of different levels and durations for some stations along the four rivers.

Figure 16 shows a graph of number of drought events versus year for different levels of drought for some stations along the four rivers.

4.2.5. Discussion on Upstream-Downstream Relationships of Severity and Frequency of Drought Events

For the Big Blue River, the *AMD*, *ACD* and *ND* are consistent among the 4 stations over the period 1965-1985 (Figures 4, 8, 12, and 16), indicating that the severity and frequency of streamflow droughts among the upstream and downstream stations are statistically similar during this period. For the time around 1985, the trends of the three parameters slightly decrease, and then bounce back

Table 3. Distribution of number of droughts for the Big Blue River (Station BB1).

	2 weeks	3 weeks	4 weeks	6 weeks	8 weeks
Water Shortage	144	142	120	79	62
Mild	105	103	73	54	40
Moderate	88	78	54	34	28
Significant	57	43	32	24	22
Extreme	42	31	25	21	16

Table 4. Distribution of number of droughts for the Niobrara River (Station N1).

	2 weeks	3 weeks	4 weeks	6 weeks	8 weeks
Water Shortage	115	51	18	5	2
Mild	79	29	9	1	1
Moderate	61	18	6	1	0
Significant	42	7	1	0	0
Extreme	32	3	1	0	0

Table 5. Distribution of number of droughts for the North Platte River (Station NP1).

	2 weeks	3 weeks	4 weeks	6 weeks	8 weeks
Water Shortage	109	130	68	30	13
Mild	94	101	45	18	2
Moderate	88	79	35	9	2
Significant	77	55	19	3	0
Extreme	59	34	9	1	0

Table 6. Distribution of number of droughts for the Republican River (Station R1).

	2 weeks	3 weeks	4 weeks	6 weeks	8 weeks
Water Shortage	165	109	36	7	5
Mild	130	52	11	1	1
Moderate	112	33	5	0	0
Significant	75	8	1	0	0
Extreme	44	3	1	0	0

for the four stations. In addition, in late 1980's and early 1990's, the droughts at downstream stations have become more intense, more frequent and last longer than the upstream droughts. In 1976, the annual precipitation measured from the rain gauge of Crete was 46.6 cm, compared to annual average precipitation of 75.6 cm of 53 years. This below-normal precipitation led to a large number of drought days for up- and downstream stations (Figure 4), as well as a large value of AMD for these stations (Figure 8).

For the Niobrara River, the *AMD* of the upstream stations is more severe for most of the study period compared to that of the downstream stations. The *ACD* of the upstream stations has an increasing trend and exceeds that of the downstream stations after 1980. Clearly, the number of droughts (ND) each year at the downstream stations is greater than the upstream stations (Figures 5, 9, 13 and 16). Thus, for this river, the upstream stations encounter more severe droughts, especially in recent years, while the downstream stations encounter droughts more frequently. Severe drought in upstream may come from the combination of two factors: lower annual precipitation rate in the western Nebraska and groundwater irrigation. In western Nebraska, the Niobrara River flows through the north border of Box Butt County where intensive groundwater pumping has caused a large decline of the water table in the aquifer for several decades. The decline has been up to 9 m at some locations, compared to the water table in 1950's and 1960's. If the river is hydrologically connected with the underlying aquifer, the depleted aquifer will have induced infiltration of streamflow to the surrounding aquifers. The trend analysis of streamflow by Wen and Chen [29] indicated that annual discharge in upstream of the Niobrara River had a decreasing trend in 1946-2003 at station 06454500 (N2) and in 1945-1991 at station 6457500 (N3).

The relationships of the parameters on the North Platte River among the 4 stations are shown in Figures 6, 10, 14, and 16. With regard to the *AMD* and *ACD* development over the years, the upstream stations are similar with the downstream stations. However, the upstream stations show a higher value of *ND* for most drought categories than the downstream stations for the entire period.

Figures 7, 11, 15, and 16 show a unique pattern along the Republican River. The parameters of the downstream stations more intense drought characteristics than that of the upstream stations during 1950 to 1990. After 1990, the three parameters of the station located upstream (R1) present a strong increasing trend and exceed the downstream stations in the severity and frequency, indicating this upstream station suffers from drought more severely and more frequently.

Tables 7-10 list the DD, AMD, ACD and ND of upstream and downstream stations in different levels of drought events. The statistical analysis is performed using the MIXED procedure and the paired *t*-test.

Tables 7-10 show that while strong trends are apparent in the drought parameters between upstream and downstream stations, many of the differences are not statistically significant. Table 7 shows that the difference in drought durations for upstream and downstream stations is significant only for Big Blue River (significant droughts) and for North Platte River (moderate droughts). For the other levels of droughts and for Niobrara River and Republican River, there are no differences between the upstream and downstream stations. Table 8 also shows that there are no differences in AMD between upstream and downstream stations for Niobrara River and Republican River. The differences for Big Blue appear only for mild droughts while those for North Platte are only for water shortage events. Table 9 shows that there no significant differences in ACD between up-

Table 7. Distribution of Drought Duration (DD) of different types for upstream and downstream stations along the four rivers. * denotes significant difference ($p<.05$).

River	Location	Extreme	Significant	Moderate	Mild	Water Shortage
Big Blue	**Up**	93	34*	65	55	42
	Down	37	27*	67	71	70
Niobrara	**Up**	14	4	17	47	133
	Down	15	4	19	49	124
North Platte	**Up**	14	11	38*	76	119
	Down	12	7	23*	61	133
Republican	**Up**	13	6	29	63	118
	Down	54	34	45	45	86

Table 8. Distribution of Annual Maximum Drought Duration (AMD) of different types for upstream and downstream stations along the four rivers. * denotes significant difference ($p<.05$).

River	Location	Extreme	Significant	Moderate	Mild	Water Shortage
Big Blue	**Up**	38	48	67	96*	126
	Down	10	18	37	59*	105
Niobrara	**Up**	5	7	12	25	68
	Down	4	5	9	20	50
North Platte	**Up**	4	8	22	60	143*
	Down	4	7	16	37	111*
Republican	**Up**	4	6	15	36	98
	Down	20	39	75	103	146

Table 9. Distribution Annual Accumulated Drought Duration (ACD) of different types for upstream and downstream stations along the four rivers. * denotes significant difference ($p<.05$).

River	Location	Extreme	Significant	Moderate	Mild	Water Shortage
Big Blue	**Up**	93	127	192	247	290
	Down	37	64	131	202	273
Niobrara	**Up**	14	18	35	82	214
	Down	15	19	38	87	211
North Platte	**Up**	15	25	63	139	258*
	Down	12	19	42	102	236*
Republican	**Up**	13	19	48	111	229
	Down	54	87	132	177	263

Table 10. Distribution Number of Drought events per year (ND) of different types for upstream and downstream stations along the four rivers. * denotes significant difference ($p<.05$).

River	Location	Extreme	Significant	Moderate	Mild	Water Shortage
Big Blue	**Up**	10	13	15	13	11
	Down	11	14	18	18	13
Niobrara	**Up**	5	6	9	15	18
	Down	9	7	11	17	23
North Platte	**Up**	3	4	6	9	6
	Down	3	3	6	10	9
Republican	**Up**	3	5	9	13	12
	Down	6	7	7	9	9

stream and downstream stations along any of the rivers for any of the drought types with the sole exception of North Platte River and only for water shortage events. Table 10 shows that in terms of number of drought events, there is no difference between upstream and downstream stations along any of the rivers.

4.2.6. Discussion on Upstream-Downstream Relationships of Severe Drought Events.

Based on the 5 × 5 matrix as shown in Tables 3-6 above, we tried to identify severe drought events in terms of drought level and duration. Since the entries near the lower right portion of the matrix usually have small values, those combinations were not an appropriate definition of severe droughts. If the drought level was set as water shortage, numerous drought events would be identified. Thus, the combination of the mild drought type and a threshold of 3 weeks can be a good definition of severe droughts. As shown in Tables 3-6, the number of 4-, 6-, and 8-week drought is the largest for the Blue River Basin. This is probably due to its small drainage area of the watershed, as well as a small baseflow from the weak hydrologic connection between the river and the principal aquifer. The combined effect of the two situations gives only small amount of water that sustains the streamflow between precipitation events and makes the streamflow highly correlated with precipitation patterns. Although the Platte River watershed has the largest drainage area, the number of 4-, 6-, and 8-week drought is larger than that for the Niobrara and Republican River basins. This is in part attributed to the fact that the streamflow records of the four stations in the North Platte River used in this analysis are about 30 years longer than those of other stations. In 1930's, a severe drought occurred in Nebraska.

Table 11 summarizes for each station 1) the number of streamflow droughts with duration of three weeks or longer, 2) the largest streamflow drought deficit and its time period, and 3) the longest streamflow drought duration and its time period during the period of record. As can be seen, the numbers of droughts with duration greater than three weeks occurring on each station are about the same for the Big Blue and North Platte Rivers. In contrast, the number of droughts on the Niobrara River increases downstream, indicating that severe drought becomes more frequent downstream. The Republican River shows an opposite pattern: the severe droughts occur at the upstream stations more frequently than the downstream stations.

According to Table 11, the time periods of the drought events with the largest deficit or the longest duration are not necessarily consistent among the upstream and downstream stations along the same river. Over the period 1964-1994 along the Big Blue River, the significant drought events with the largest deficit recorded by the 4 stations occurred in the1970s, while the events with the longest duration occurred in the 1970s, 1980s and 1990s. The largest deficit for stations BB3 and BB4 occurred in 1976 and 1977 (Table 11). This is apparently associated to the below normal precipitation in 1976. Along the Niobrara River during 1957-1991, the three downstream stations (N4-N6) recorded the same severe drought event with the largest deficit simultaneously, while the 3 upstream stations (N1-N3) recorded 3 different events. For the events with the longest duration, it seems that the drought events in recent years tend to last longer because all the 3 upstream stations indicate that the events lasting the longest happened in 1989-1990. The largest deficit at stations N4, N5, and N6 of the Niobrara River occurred in the same year (1976). The precipitation of 1976 measured from the rain gauge at Valentine near the middle stream of the Niobrara River was 32.4 cm, compared to the average annual rate of 55.6 cm from 1948 to 2001.

For the North Platte River in 1930-1991, the one upstream and two downstream stations (NP2-NP4) show the drought events with the largest deficit during 1934-1935, and with the longest duration during 1954-1955. Although the annual precipitation of 1976 in Scottsbluff of the North Platte River Valley was only 24.7 cm, well below the average of 39.1 cm, this below normal precipitation did not lead to the largest water deficit in the North Platte River. The drought of 1934-35 in Nebraska was apparently much worse.

It appears that 3 out of the 4 stations along the Republican River indicate the severe drought events occurred in 2000-2001 during the study period 1952-2001, suggesting that the significant streamflow drought events become more severe and last longer in recent years. Like other three basins, the Republican River Basin also suffered a drought in 1976. The precipitation was 28.7 cm at a rain gauge of Benkleman, below the average rate of 47.4 cm. It is interesting to note that the precipitation in 2000 was 45.8 cm, only slightly below the average precipitation rate. Yet, as shown in Table 11, the largest deficit and longest duration of drought for a couple of stations in the Republican River occurred in 2000.This might be caused by increasing water use and human activities on this river. Another possible reason is that the study periods of the other 3 rivers do not cover the very recent years due to the lack of records. So it is impossible to accurately show the drought situation in the very recent years. A severe drought started in 1999 and continued to 2006 in Nebraska and other High Plains region.

Table 11 also reveals the impacts of several major severe droughts in Nebraska history through the statistics of the largest deficit and the longest drought duration for each station. In the North Platte River, the drought of the 1930s was the longest dry period for Nebraska in recent history [16] and is often referred to as the Dust Bowl (see Stations NP2, NP3 and NP4 on the North Platte River).

Table 11. Statistics on drought events of duration of at least three weeks.

River (Study period)	Station	Number of drought		Largest deficit		Longest duration	
		Total	/Year	m^3	Time Period	Days	Time Period
Big Blue (1964 – 1994) 31 years	06879900 (BB1)	69	2.2	685	9/3/1974–4/27/1975	327	9/9/1980–8/1/1981
	06880500 (BB2)	71	2.3	374	6/26/1971–5/3/1972	313	6/26/1971–5/3/1972
	06881000 (BB3)	74	2.4	425	6/5/1976–5/23/1977	353	6/5/1976–5/23/1977
	06882000 (BB4)	69	2.2	381	8/2/1976–5/26/1977	305	7/25/1991–5/24/1992
Niobrara (1957 – 1991) 35 years	06454100 (N1)	70	2.0	125	5/3/1974–9/21/1974	240	4/9/1989–12/4/1989
	06454500 (N2)	70	2.0	196	5/17/1964–11/24/1964	253	4/25/1989–1/2/1990
	06457500 (N3)	90	2.6	078	2/26/1989–11/18/1989	266	2/26/1989–11/18/1989
	06461500 (N4)	73	2.1	072	5/4/1976–12/16/1976	227	5/4/1976–12/16/1976
	06465000 (N5)	96	2.7	070	5/29/1976–11/18/1976	187	4/23/1975–10/26/1975
	06465500 (N6)	98	2.8	068	5/29/1976–11/18/1976	178	4/23/1980–10/17/1980
North Platte (1930-1991) 62 years	06679500 (NP1)	119	1.9	496	11/19/1959–5/21/1962	915	11/19/1959–5/21/1962
	06682000 (NP2)	117	1.9	336	4/15/1934–1/8/1935	510	1/4/1954–5/28/1955
	06684500 (NP3)	113	1.8	318	4/10/1934–1/6/1935	457	3/29/1954–6/28/1955
	06686000 (NP4)	125	2.0	349	4/11/1934–12/12/1934	341	3/30/1954–3/5/1955
Republican (1952 – 2001) 50 years	06823000 (R1)	118	2.4	202	3/18/2000–12/23/2000	281	3/18/2000–12/23/2000
	06827500 (R2)	87	1.7	553	3/1/2000–1/27/2001	333	3/1/2000–1/27/2001
	06843500 (R3)	98	2.0	335	7/25/2000–3/3/2001	308	9/6/1998–7/10/1999
	06869500 (R4)	76	1.5	649	8/20/1991–7/2/1992	318	8/20/1991–7/2/1992

For the Big Blue River Basin and the Niobrara River Basin, a major drought within the study periods occurred in the mid-1970s. This drought resulted in loss of over $10 million in eight counties ([14]; see Stations BB1, BB3 and BB4 on the Big Blue; N1, N4, N5 and N6 on the Niobrara River). In addition, the year of 2000 was a severe drought year ([31]; see stations R1, R2 and R3 on the Republican River).

It is interesting to note that some severe droughts with the largest deficit or the longest duration indicated by some stations were not recorded as a major drought event in Nebraska history (e.g., station NP1 on the North Platte River during 1959-1962). Reasons for such omissions need to be investigated further.

Statistical analysis shows that the difference in the largest deficit between upstream and downstream stations along any of the four rivers is not statistically significant. The same is also true for the longest drought duration for all the rivers except the Niobrara River.

5. Summary

In this paper, the upstream-downstream association in terms of the basic statistical characteristics of annual flow discharge and the streamflow drought severity and frequency were explored on 18 stream gauge stations along 4 major rivers in Nebraska: the North Platte, Niobrara, Big Blue and Republican Rivers. We used the paired *t*-test and ANOVA with MIXED procedure to test whether there were any significant differences in terms of streamflow- and drought-related parameters between upstream and downstream stations. Overall, the statistical tests showed that there are not many significant differences between upstream and downstream stations along the four rivers.

Based on the results of the two comparative studies, the following upstream-downstream relationships are summarized for each river:

- For the Big Blue River, the four stations are consistent with respect to the coefficients of variation and positive slopes of the annual mean discharge, the distribution of the annual high- and low-flow seasons, and the total number of severe drought events occurring during the study period. The severity and frequency of drought events are also similar among the upstream and downstream stations during 1964-1985. After that period, the droughts at downstream stations become more intense, more frequent and last longer than the upstream droughts.
- For the North Platte River, the four stations show the consistency on the positive slopes of the annual mean discharge, the distribution of the high- and low-flow seasons, the severity of drought events and the number of severe droughts. On the other hand, the coefficients of variation of the annual mean discharge increase from downstream to upstream, and the downstream stations show a higher number of drought occurring each year than the upstream stations for the entire

study period. Because the stations studied are all located upstream of the lake and dam, the conclusions are not as reliable and can only be applied on the upstream segments.

- For the Niobrara River, the six stations only show consistency on the coefficients of variation of the annual mean discharge and the distribution of the annual high- and low-flow seasons. The stations demonstrate mixed signs of the annual discharge trend slope, either positive or negative. Furthermore, the upstream stations encounter more severe droughts in recent years, while the downstream stations encounter droughts more frequently. This complex upstream-downstream relationship on the Niobrara is attributed to its diverse nature and its journey through the Sandhills region.
- The relationships along the Republican River are also complex as expected. The only agreement among the four stations is the negative trend slope of the annual mean discharge. The stations exhibit inconsistencies in other statistical characteristics: increasing coefficients of variation from upstream to downstream, varying distributions of high- and low-flow seasons. In addition, the results suggest that the upstream stations suffer from drought more severely and more frequently in recent years. Obviously, the water use activities such as reservoir regulation, canal diversion, and groundwater pumping in the Republican River Basin influence the relationships.

The streamflow drought conditions and statistics differ in each of the four watersheds. They can be influenced by fluctuation of precipitation, the size of drainage area, soil types, hydrologic connection between river and groundwater systems, and the demand levels on surface and groundwater. Below-normal precipitation seems to be the most important factor contributing to the largest deficit of streamflow. Diversion of stream water to canals and reservoir regulation are probably other major factors resulting in different features of streamflow drought and statistics among individual rivers reaches within a watershed. Future work includes conducting the above analysis for the irrigation season (June-September) to identify the impact of streamflow diversion and groundwater pumping on the streamflow and drought events.

7. Acknowledgement

This work was sponsored by an NSF Information Technology Research (ITR) grant (*ITRF#IIS00219970*). The authors would like to thank Bill Waltman, the United States Geological Surveys (USGS), the United States Department of Agriculture (USDA), the High Plains Regional Climate Center (HPRCC), and the National Drought Mitigation Center (NDMC) for support in domain knowledge and expertise. The authors would also like to thank Lei Fu, Jing Zhang, Songjie Wei, Jeff Mahnke, and Fujiang Wen for their programming work.

8. References

[1] T. F. Homer-Dixon, "Strategies for studying causation in complex ecological political systems," Occasional Paper, The Myth of Global Water Wars.

[2] C. A. Flowerday, Ed., "Flat water: A history of nebraska and its water, conservation and survey division institute of agricultural and natural resources," University of Nebraska-Lincoln, Resource Report, No. 12.

[3] H. Hisdal and L. M. Tallaksen, Eds., "Assessment of the regional impact of droughts in Europe," Drought Event Definition,Technical Report, No. 6, pp. 41, 2002.

[4] M. P. Lawson, A. Reiss, R. Phillips, and K. Livingston, "Nebraska droughts: A study of their past chronological and spatial extent with implications for the future," Occasional Papers, Department of Geography, University of Nebraska- Lincoln, No. 1, pp. 147, 1971.

[5] L. B. Leopold, "A view of the river," Harvard University Press, Cambridge, MA, pp. 298, 1994.

[6] H. F. Lins and J. R. Slack, "Streamflow trends in the United States," Geophysical Research Letters, Vol. 26, No. 2, pp. 227−230, 1999.

[7] M. A. Miah, "Man-made climatic changes in the Ganges basin," International Journal of Climatology, Vol. 22, pp. 993−1016, 2002.

[8] R. Neff, H. Chang, C. G. Knight, R. G. Najjar, B. Yarnal, and H. A. Walker, "Impact of climate variation and change on Mid-Atlantic region hydrology and water resources," Climate Research, Vol. 14, pp. 207−218, 2000.

[9] C. Revenga, S. Murray, J. Abramovitz, and A. Hammond, "Watersheds of the world: Ecological value and vulnerability," World Resources Institute and Worldwatch Institute, Washington DC, 1998.

[10] D. A. Wilhite, "Government response to drought in the United States: With particular reference to the Great Plains," Journal of Climate and Applied Meteorology, Vol. 22, pp. 40−50, 1983.

[11] V. Yevjevich, "An objective approach to definition and investigation of continental hydrologic droughts," Hydrology Paper, Colorado State University, Fort Collins, Colorado, 1967.

[12] E. Zelenhasic and A. Salwai, "A method of streamflow drought analysis," Water Resources Research, Vol. 23, No. 1, pp. 156−168, 1987.

[13] Nebraska Agricultural Statistics Service, http://www.agr.state.ne.us/agstats/cropwthr.htm (accessed in 2009).

[14] F. J. Wen and X. H. Chen, "Evaluation of the impact of groundwater irrigation on streamflow depletion in Nebraska," Journal of Hydrology, Vol. 327, pp. 603−617, 2006.

[15] N. Peranginangin, R. Sakthivadivel, N. R. Scott, E. Kendy, and T. S. Steenhuis, "Water accounting for conjunctive groundwater/surface water management: Case of the Singkarak-Ombilin river basin, Indonesia," Journal of

Hydrology, Vol. 292, pp. 1−22, 2004.

[16] H. Hisdal, K. Stahl, L. M. Tallaksen, and S. Demuth, "Have streamflow droughts in Europe become more severe or frequent," International Journal of Climatology, Vol. 21, pp. 317−333, 2001.

[17] A. Bleed, "Groundwater in an atlas of the sand hills," A. Bleed and C. Flowerday (Editors), Conservation and Survey Division, University of Nebraska-Lincoln, Lincoln, Nebraska, Resource Atlas, No. 5b, pp. 67−92, 1989.

[18] SAS Institute Inc. SAS System Version 9.1, SAS Institute Inc. Cary, NC.

[19] J. A. Dracup, K. S. Lee, and E. G. Paulson, Jr., "On the definition of droughts," Water Resources Research, Vol. 16, pp. 297−302, 1980.

[20] L. M. Tallaksen, "Streamflow drought frequency analysis," in J. V. Vogt and F. Somma, Eds., "Drought and drought mitigation in Europe," Kluwer Academic Publishers, Derdrecht, pp. 103−117, 2000.

[21] J. Abaurrea and A. C. Cebrián, "Drought analysis based on a cluster Poisson model: Distribution of the most severe drought," Climate Research, Vol. 22, pp. 227−235, 2002.

[22] D. A. Wilhite, "Drought as a natural hazard: Concepts and definitions," Chapter 1, in D. A. Wilhite, Ed., "Drought: A global assessment," Natural Hazards and Disasters Series, Routledge Publishers, U. K., 2000.

[23] D. R. Helsel and R. M. Hirsch, "Statistical methods in water resources: Techniques of water resources investigations of the United States geological survey," Book 4, Chapter A3, Hydrologic Analysis and Interpretation, pp. 510, 2002.

[24] D. Yang, B. Ye, and D. L. Kane, "Streamflow changes over Siberian Yenisei river basin," Journal of Hydrology, Vol. 296, pp. 59−80, 2004.

[25] D. P. Lettenmaier, E. F. Wood, and J. R. Wallis, "Hydro-climatological trends in the continental United States: 1948-1988," Journal of Climate, Vol. 7, pp. 586−607, 1994.

[26] A. Tabidian and D. T. Pederson, "Impact of irrigation wells on baseflow of the big blue river, Nebraska," Water Resources Bulletin, Vol. 31, No. 2, pp. 295−306, 1995.

[27] S. Stefan, M. Ghioca, N. Rimbu, and C. Boroneant, "Study of meteorological and hydrological drought in southern Romania from observational data," International Journal of Climatology, Vol. 24, pp. 871−881, 2004.

[28] E. Kahya and S. Kalayci, "Trend analysis of streamflow in Turkey," Journal of Hydrology, Vol. 289, pp. 128−144, 2004.

[29] USGS, U. S., Geological Survey, http://water.usgs.gov/nsip (accessed in 2009).

[30] X. H. Chen and L. C. Shu, "Groundwater evapotranspiration captured by seasonally pumping wells in river valleys," Journal of Hydrology, Vol. 318, pp. 334−347, 2006.

[31] G. J. McCabe and D. M. Wolock, "Trends and temperature sensitivity of moisture conditions in the conterminous United States," Climate Research, Vol. 20, pp. 19−29, 2002.

J. Water Resource and Protection, **2009, 1, 316-324**
doi:10.4236/jwarp.2009.15038 Published Online November 2009 (http://www.scirp.org/journal/jwarp)

Watershed Characterization of Wadi Aurnah, Western Arabian Peninsula

Mashael AL SAUD
Space Research Institute, King Abdel Aziz City for Science and Technology, King Abdel Aziz, Kingdom of Saudi Arabia
E-mail: *geomm5.mashael@gmail.com*
Received July 2, 2009; *revised August* 18, 2009; *accepted August* 27, 2009

Abstract

The Western part of Arabian Peninsula constitutes a shield-like mega-structure, in which mountain chains are oriented in the NW-SE direction. Along this mountainous region, surface runoff is almost diverted towards the Red Sea in the west. Thus, several catchment topographic units exist to capture rainfall water among them. Even tough, the precipitation rate in the Western part of Arabian Peninsula is low (i.e. <200mm), yet a number of drainage systems occur and reveal empirical stream networking. However, studies belong to the watersheds located in the Western part of Arabian Peninsula are still rare and sometimes they show erroneous morphological characterization, notably in the catchments delineation. This is attributed mainly to the complicated drainage pattern, which is structurally-controlled. Thus, related morphological and hydrological studied obtained on these drainage systems reveal discreditable results and measures. This study aims to characterize Wadi Aurnah Watershed (~3113 km^2), which comprises a typical catchment in the Western part of Arabian Peninsula. In addition to topographic maps, remotely sensed data (ASTER and IKONOS satellite images) were utilized to delineate water divides with the most precision. Consequently, relevant morphological and hydrological characteristics of Aurnah watershed were obtained.

Keywords: Watershed, Topographic Maps, ASTER, Arabian Peninsula

1. Introduction

The Arabian Peninsula, as a part of the Dead Sea Rift System, is a semi-island that surrounded by Red Sea, Arabian Sea and the Arabian Gulf from the west, south and east; respectively (Figure 1). Therefore, water from rainfall flows along the mountainous regions towards the sea. The intensity and continuity of runoff differ from one region to another depending on precipitation rate and behavior, as well as the geologic and geomorphic characteristics of terrain are influencing. However, the precipitation rate in the whole Peninsula is low enough to create continues run-off, and often flow of water from surrounding mountains does not even reach the sea. Moreover, indicators of climate change are obviously noted through the diversity in sediments sequence as well as from the frequent existence of paleo-drainges [1].

The Western part of Arabian Peninsula, where Wadi Aurnah is located, encompasses a steep sloping terrain (the so-called Hijaz Escarpment), notably along the mountain chains of the Arabian Shield. This Shield comprises a mega-structure that spread into the middle part of the Peninsula. Therefore, the area constitutes the most elevated crests in the region, thus peaks of more than 2000 m frequently exist. Hence, several valley systems (Wadis in Arabic) are detaching from these peaks towards the Red Sea.

Wadi Aurnah Watershed is located between the following geographic coordinates: 39° 12′ 00" E; 40° 18′ 00" E and 21° 01′ 30"N; 21° 35′ 30"N. It is one of the major five catchments in the central part of the Tihamah-Hijaz (middle part of the Arabian Shield) region. It is surrounded from the east by a number of mountain chains. These are: Jabal Twayriq (1872 m), Jabal Al Amid (2135 m) and Jabal Bared (2337 m), Al Tarykah (2402 m) and Jabal Al-Adim (2476 m). The catchment of this wadi comprises about 3113 km^2. Within this catchment, the Holy Muslim city of Makka Al Mukaramah is located. This, in turn, increases the human activities, notably in Hajj pilgrimage.

The area of concern (Wadi Aurnah Watershed) is characterized by the Mediterranean climate in winter and of monsoonal rainfall during spring. However, Hijaz Escarpment serves as a climatic barrier that hinders air

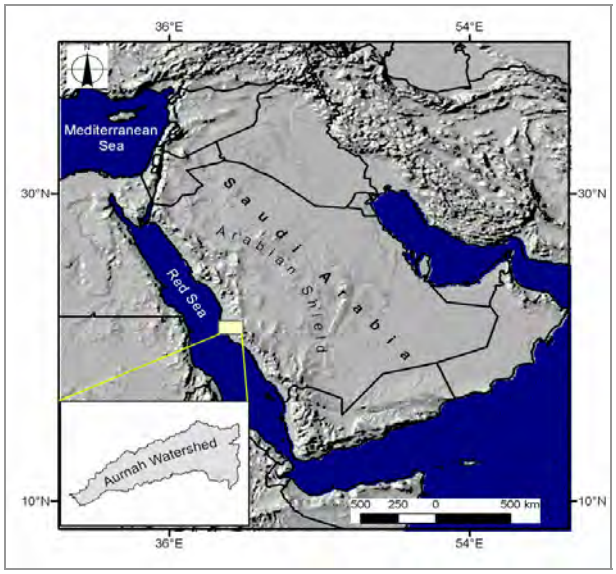

Figure 1. Location map of the study area.

masses derived from the west. Although some studies calculated the average rainfall in the area of concern as 350-400 mm such as in Italconsult [2] and [3], but recent records exhibit less amounts of annual rainfall. Thus, low rainfall rate dominates the area of concern, and it ranges between 50 and 200 mm a year. In addition, sand storms commonly exist, which makes the basin covered by about 880 km^2 of sand desert (~28% of the whole area).

According to Moor and Al-Rehaili [4] and Sahl [5], the geology of the area is dominant by Late Precambrian and plutonic rocks. In addition, Tertiary sedimentary rocks occur in the fault-bounded troughs near the Red Sea coast. The Cenozoic lavas form extensive fields in the north part of the area. The Quaternary surficial deposits are widespread on different, but they are mainly concentrated in the coastal plain.

The geomorphological features and catchment characteristics of Wadi Aurnah were included in a number of studies, such as those done by Es-Saeed *et al*. [6]; Merza and Baroudi [7] and Aawari [8]. However, obvious contradictory exists in these studies, notably in the cartography of the catchment boundary. This contradictory is attributed mainly to the complicated geological setting of the area, which is reflected in extensive geological structures and geomorphologic features. This, in turn, results errors in delineating the exact limits of water divides. As well as the frequent intermittency in stream networks added another problem in tracing the drainage system. In this respect, the accuracy in watershed delineation is important, since the area and perimeter of a watershed are used in climate interpolation and run-off calculations.

This study aims to reach an accurate delineation of Wadi Aurnah catchment boundary. This enables consequently characterizing its geomorphic and hydrologic measures, and help in calculating the relevant numerical relations. This was achieved through a detailed tracing approaches from topographic maps (1:50000) as well as from satellite images with high resolution.

2. Materials and Method

Delineation of catchment boundary can be done manually or automated. However, there is still disagreement on the reliability of drainage extraction by automated methods, notably in areas dominant with complicated geology and rugged topography. Almost all workers in this concern pointed out that manual extraction of appropriate scale is more reliable than the automated ones [9−14].

In this study, manual delineation was primarily carried out from topographic maps. It was achieved by tracing the drainage networks and this includes all appeared streams and reaches on topographic maps. However, remote sensing and Geographic Information System, GIS techniques were utilized whenever erroneous and obscure drainage behaviour exists. For this purpose, 17 map-sheets (1:50000 scale) were used to trace the drainage system of the whole Arunah Watershed area. The sampling of streams and reaches involved drawing lines connecting the slope or ridge tops. Assuming the water will drain away from those points, the watershed is delineated by enclosing a polygon (Figure 2). This delineation was achieved digitally in GIS (*Arc View*) system, and the satellite images were subjected to several digital and optical advantages including: band combination, colour slicing, edge detection, filtering, in addition measuring tools were used to calculate different dimensions (e.g. total length, perimeter, number of reaches for each stream order, etc).

Several cartographic problems existed during the manual tracing of drainage network from topographic maps, since the available topographic maps revealed erroneous aspects of drainage behaviour, and more certainly in stream connectivity. Hence, in the available maps, streams sometime disappear, notably where Quaternary deposits exist. This phenomenon is dominant in the coastal plain of the study area and can be attributed mainly to:

1) Low rainfall rate that results slow run-off, and low-level stream water,

2) High evaporation rate, which reduces the water flux in channels,

3) The dominant Quaternary deposits (sand dunes, alluvial, aeolian sediments, etc) characterize the terrain by high porosity and permeability, thus streams easily enter into these deposits and disappear.

In order to avoid this problem, remotely sensed data was utilized. ASTER satellite images were processed using *ERDAS Imagine* software. These images are characterized by 15m resolution in visible bands and 90m in

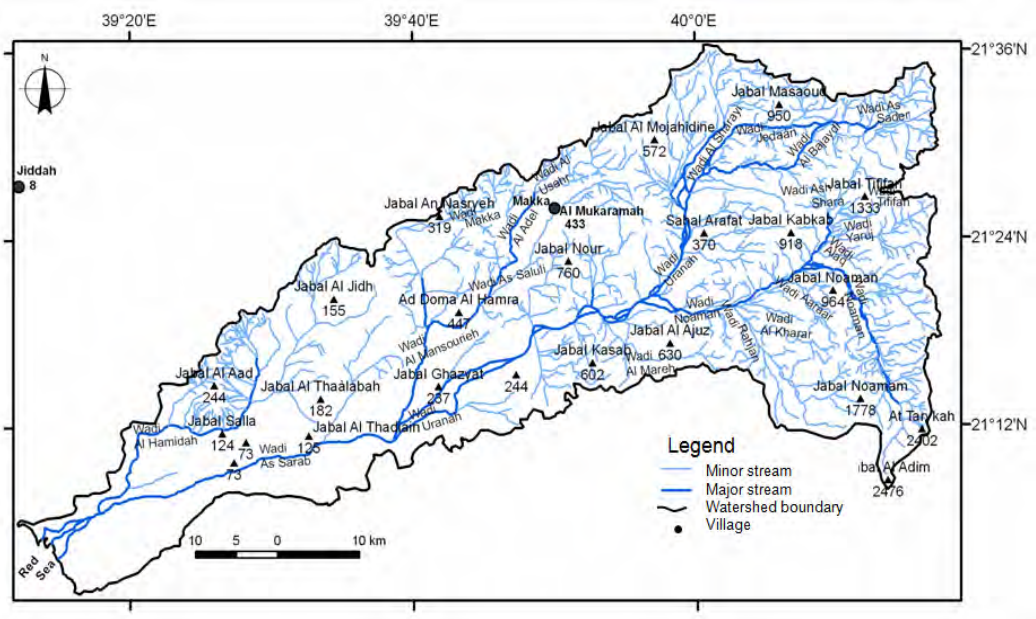

Figure 2. The catchment area of Wadi Aurnah.

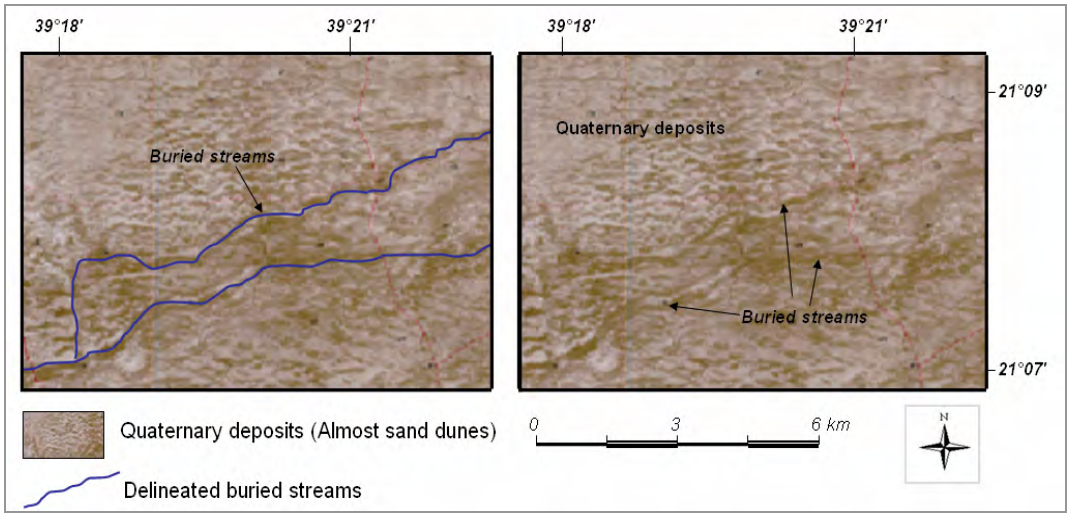

Figure 3. Example showing the tracing of buried streams in the coastal plain of Wadi Arunah, using thermal bands in ASTER images.

Thermal Infrared (TIR) bands. Accordingly, the thermal interpretation from the thermal bands was useful in this study. Bands 10-14 in ASTER images provided creditable information on porous sediments, which almost occupy wet horizons and buried streams. Figure 3 shows an example of using thermal bands in ASTER images to trace buried streams in the coastal plain of Wadi Arunah.

Another major problem existed during the delineation of stream network from the available maps is the connection between streams of opposite flow directions, which results errors in plotting water divides. This was common in the available maps, notably where terrain features overlap with stream routes, such as roads that exist among valleys. For this purpose, the available satellite images with high resolution (i.e. IKONOS, 1m resolution) were used. A clear example is shown in Figure 4.

3. Results and Data Analysis

More than 20 wadis exist in the studied catchment and compose complete network of drainage system. Ten of these wadis are major ones (i.e., cross-section area more than 40m^2). Some of these wadis are joined with each other, such as Aurnah and Wadi As Sarab where both are

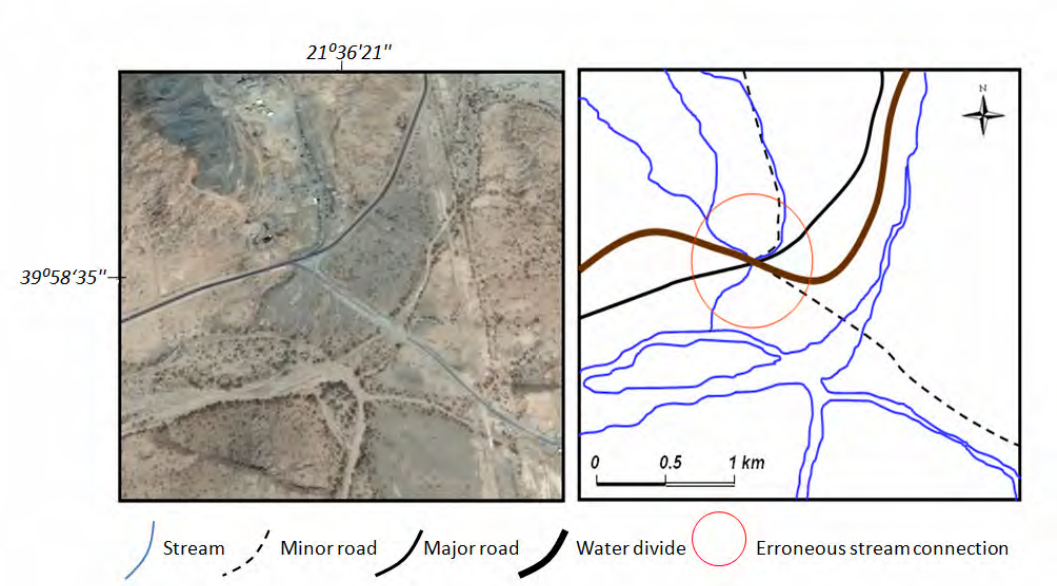

Figure 4. Example from the area of study showing the use of IKONOS images to discriminate the roads from streams, which observed in conflict behavior on topographic maps.

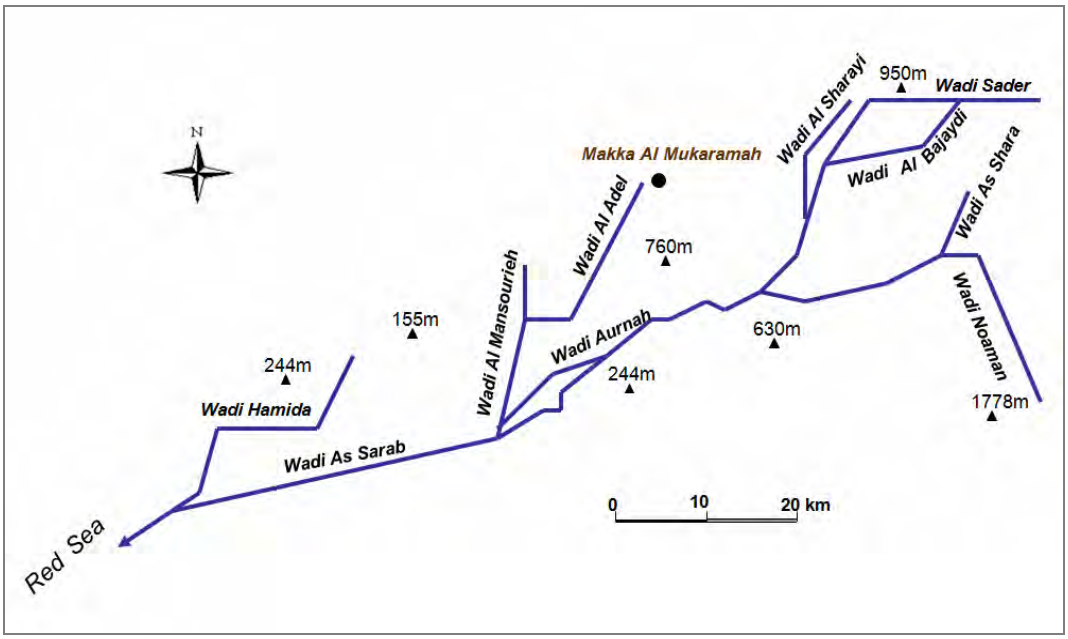

Figure 5. Schematic presentation of the major wadis in the Wadi Aurnah.

oriented in the NE-SW direction to compose one major wadi (Figure 5a). The resulting wadi is joined with another (unique) wadi from the south (i.e. Wadi Noaman). There are also other connecting wadis in the north. They appear in a parallelel to each other in the NE-SW direction with an angle of connection of about 30-40 degrees to the primary wadi (Figure 5b).

The accurate cartography of Wadi Aurnah Watershed (Figure 1) enables characterizing the relevant geomorphologic and hydrological measures. Usually, the selection of measures depends mainly on the purpose of the study (e.g., water harvesting, tanks construction, flood-prone areas, etc).

The production of data digitally in a GIS system gives chance to manipulate different measures and calculations. In addition, modifications and corrections can be regu-

larly applied in GIS system, especially those changes occurred with time (e.g., urban expansion on stream courses, excavation, etc). Therefore, the following are the obtained geomorphic and hydrologic measures on Wadi Aurnah Watershed.

3.1. Volume of Precipitated Water (P)

Usually, in watershed management studies, the volume of precipitated water (P) is primarily calculated. The main variables required for this volumetric measure are the area of the catchment (A_c) and the average precipitation rate (P_r).

According to Wadi Aurnah watershed, and since the determined area is 3113km^2; therefore, the average precipitation rate remains the variable to be measured. However, in the lack of accurate and updated climatic records, remotely sensed data can be utilized. Hence, TRMM (Tropical Rainfall Mapping Mission) rainfall data was used in this study. It is a space technique introduced by NASA to produce daily records of rainfall data (Figure 6). Several studies, related to rainfall, were successfully obtained relying on TRMM products [15−17].

The estimated average precipitation rate for Wadi Aurnah watershed as obtained from TRMM, for the years between 2004 and 2007 is 145mm. Therefore, the volume of precipitated water (P) can be calculated as follows:

$$P = A_c\,(\text{m}) \times P_r\,(\text{m})$$

$$= \frac{3113}{1000} \times 145 \times 10^6 = 451 \text{ Million m}^3\text{/year}$$

The calculated amount shows discrepancy with old measures, which were estimated as more than 900 Million m^3/year.

3.2. Hypsometric Curve

It is an empirical cumulative function of elevations in a catchment that can be made by measuring the area lying between successive pairs of contours. The percentage of the total that each of these areas constitute are then computed, and the percentage of the total area lying above or below each different contour is obtained by summation.

For Wadi Auranah Watershed, the obtained elevation/area data is plotted in Table 1, and it was graphically expressed in Figure 7. This data was derived from topographic maps (1:50000) with 20-meter contour interval. Therefore, the contour map of the area was digitally made by using GIS (Arc view software).

The obtained hypsometric curve (Figure 7) shows that about 30% of the catchment is characterized by steep slope terrain. While about 48% of the catchment owns gentle sloping terrain, in which the elevation is less than 1500m. In addition, the curve shows sharp signatures in elevation, which are attributed mainly to the existence of fault systems.

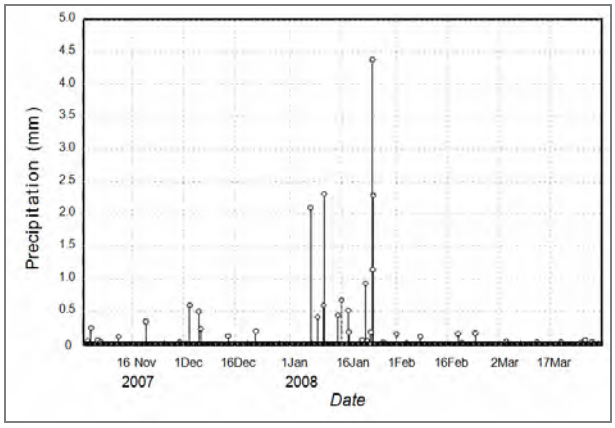

Figure 6. Example showing precipitation record from TRMM data for Wadi Aurnah watershed.

Table 1. Elevation/area measures of Wadi Aurnah Watershed.

Intervals of contour elevations (m)	Area between contours (km^2)	Accumulated area	% of area above elevation
<100	538.1	538.1	17.28
100-200	499.5	1037.6	16.04
200-300	455.6	1493.3	14.63
300-400	86.5	1579.9	2.77
400-500	610.2	2190.1	19.59
500-600	187.4	2377.5	6.01
600-700	135.3	2512.8	4.34
700-800	108.6	2621.5	3.48
800-900	86.4	2707.8	2.77
900-1000	69.5	2777.4	2.23
1000-1100	60.2	2837.7	1.93
1100-1200	53.6	2891.3	1.72
1200-1300	45.6	2936.9	1.46
1300-1400	38.2	2975.1	1.22
1400-1500	31.3	3006.4	1.00
1500-1600	24.7	3031.1	0.79
1600-1700	21.1	3052.2	0.67
1700-1800	15.3	3067.5	0.49
1800-1900	9.4	3076.9	0.30
1900-2000	10.2	3087.2	0.32
2000-2100	8.5	3095.7	0.27
2100-2200	5.4	3101.2	0.17
2200-2300	3.5	3104.7	0.11
2300-2400	6.7	3111.4	0.21
2300-2400	1.35	3112.7	0.04
>2400	0.65	3113.4	0.02

Accordingly, from the obtained data mean altitude (Ma) can be calculated in the following equation:

$$Ma = \frac{\sum A_c . E_d}{A_t}$$

where Ac is the area between each two adjacent contours, E_d is the difference between these contours and A_t is the total area of the catchment. Therefore, the mean altitude in Wadi Aurnah is estimated at 452m.

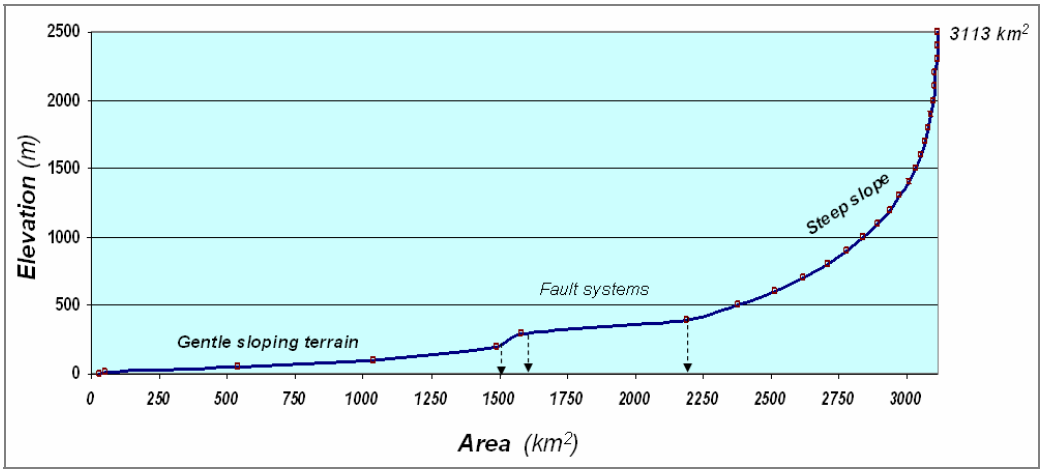

Figure 7. Hypsometric curve of Wadi Aurnah watershed.

3.3. Relief Ratio (R_r)

The relief ratio is a measure of basin average slope. It provides an approximate estimate on the topographic gradient affecting the lateral movement of groundwater in near-surface saturated areas on the scale of the entire basin. High values of R_r should be correlated with efficient lateral redistribution of moisture. It is also a function of infiltration, surface runoff, erosion and flow velocity [18]

$$R_r = \frac{\Delta A}{L_m}$$

where Δ A is the altitude difference and L_m is the maximum stream length.

For Wadi Aurnah catchment, R_r was calculated as follows:

$$R_r = \frac{2476 - 0}{146.11} = 17 \text{ m/km}$$

The resulting ratio indicates low to moderate relief slope, which hinders the erosional processes, except in they exist in torrential rainfall events.

3.4. Texture Topography (Tt)

This measure represents the degree of drainage dissection. It indicates the tendency of terrain to shrink water, which is influenced by lithology and structure as well. Accordingly, Smith [19] classified texture topography into three major classes. These are: soft, moderate and rough for the values < 4, 4-10 and > 10; respectively. The following equation expresses the texture topography:

$$Tt = \frac{\sum Nu}{Bc}$$

where Nu = number of tributaries (as obtained by digitally in GIS-*Arc View*), and Bc = basin perimeter.

For Wadi Aurnah catchment, the texture topography will be:

$$Tt = \frac{5499}{406} = 13.54 \text{ tributary/km}$$

The resulting value of texture topography indicates the existence of rough topographic terrain, which often retards the energy of run-off process due to the existence irregular surface features (e.g., massive rock boulders, depressions, etc.).

3.5. Relief Gradient (R_g)

It represents landmass maturity; therefore, a region in youth stage shows frequency distribution skewed towards the lower elevation. Whilst, an old stage region, shows distribution skewed towards the high elevation. Pike and Wilson [20] have suggested that degree of dissection can be characterized by a relief gradient, which expresses the ratio of upland to lowland elevations within the catchment area, and expressed as:

$$R_g = \frac{\text{Mean Elevation} - \text{Minimum Elevation}}{\text{Maximum Elevation} - \text{Minimum elevation}}$$

Therefore, the relief gradient of Wadi Aurnah Watershed i:

$$R_g = \frac{452 - 0}{2476 - 0} = 0.58$$

The resulting relief gradient exhibits low to moderate value, which indicates that Wadi Aurnah is still under a mature stage of development.

3.6. Mean Catchment Slope (C_s)

Mean catchment slope C_s is considered as an index to the general gradient of the catchment, which is tightly re-

lated to the geologic setting of the catchment. Thus, it influences the velocity of runoff and thus erosion processes. According to Gordon *et al.* [21], C_s is simply calculated by:

$$C_s = \frac{\text{(Elevation at 0.85 L) – (Elevation at 0.10L)}}{\text{Elevation at 0.75 L}}$$

where L is the maximum length of the basin, and measurements are taken along this line (0.01 L near the lower part of the catchment and 0.85 L towards the upper end).

For Wadi Aurnah Watershed, the mean catchment slope is:

$$C_s = \frac{1053 - 22}{602} = 1.71$$

Likewise the indicative results in relief ratio and gradient, the mean catchment slope also shows a low to moderate terrain slope for the whole catchment area.

3.7. Shape

There are several shapes of catchments that are supposedly reflecting run-off "bunch up" at the outlet. Certainly, the ultimate concentration of its peak flow can be used to help in studying the effects of basin shape on the hydrograph and on stream behaviour [22] (Black, 1991).

For example, a circular catchment would result in run-off from various parts of the watershed reaching the outlet at the same time. While, an elliptical watershed having the outlet at one end of the major axis and having the same area as the circular watershed, would cause the runoff to be spread out over time, thus producing a smaller flood peak than that of the circular watershed.

A number of watershed properties have been developed to reflect basin shape. The following are the major properties:

3.7.1. Width/Length Ration (WL)

The ratio between width (*W*) and length (*L)* in a drainage basin is a function of time that runoff effectively reaches the major watercourse. The higher the *WL* ratio, the higher the runoff duration is (i.e., adequate time lag for infiltration process).

For the catchment of Wadi Aurnah, the maximum width is 56.79 km and the maximum length is 123.5 km; therefore, *WL* ration will be:

$$WL = \frac{56.79}{123.5} = 0.46$$

This indicates that *WL* ration of Wadi Aurnah is almost moderate, since it represents a 1:2 proportion between both dimensions. This doubled ratio reveals that the basin of Wadi Aurnah has a uniform catchment shape (Figure 2).

3.7.2. Length to the Center of Area (L_{ca})

It is the distance measured along the main channel from the basin outlet to the point on the main channel opposite the center of area as shown in Figure 8). Hence, it considers the distance between the threshold and outlet of a basin and its orientation and does not express its area. An example is shown in Figure 8 for two basins with equal area, but different orientation and thus unequal L_{ca}.

The $L_{ca\ for}$ Wadi Aruanh Watershed is 64.88 km. Comparing L_{ca} for the total length of the catchment (123.5km), thus, it is nearly equal to half of the total length. This indicates regular flow of surface water run-off within the basin.

Shape factor (L_1)

$$L_1 = (LL_{ca})^{0.3}$$

where L is the maximum length of the watershed. Thus, the L_1 for Wadi Aruanh Watershed will be:

$$L_1 = (123.5 \times 64.88)^{0.3} = 14.83$$

3.7.3. Circularity Ration (R_c)

The circularity of shape measures the degree of similarity between the outer limits of the catchment with a circle [23]. According to Strahler [24] it can be expressed in the following equation:

$$R_c = A/A_0$$

where A_0 is the area of a circle having a perimeter equals to the perimeter of the basin. Since the perimeter of the area of Wadi Aurnah is known (406 km); thus to measure the area of the circle, the radius must be primarily calculated. Consequently, obtaining the perimeter/radius equation as follows:

$$P = 2\ \pi\ r$$

$$406 = 2 \times 3.14\ r$$

$$r = 64.64$$

Having the radius enables calculating the area of the circle as follows:

$$A = 2\pi\ r^2$$

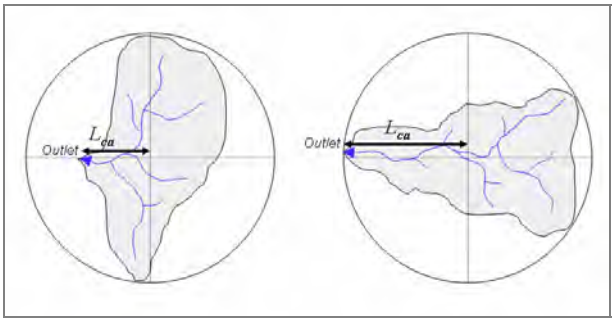

Figure 8. Example showing two basins with the same area, but different orientation, thus the influence of this shaping on water discharge.

$$A = 2 \times 3.14 \times 64.64 = 13124 \text{ km}^2$$

Therefore, the circularity ration will be:

$$R_c = \frac{3113}{13124} = 0.23$$

The circularity (R_c) of the studied basin is considered as moderate, and this confirms the previous resulting values of L_{ca} and L_1. Hence, regularity in discharge quite exists. This also indicates that the basin is in the mature stage of development.

3.7.4. Elongation Ration (R_e)

The elongation ration describes the degree of catchment stretching with respect to its area. Thus, it equals 1 for a circle and 0 for a straight line. Figure 9 presents a schematic example of two basins with different elongation ratio; thus the behavior of discharge is almost unequal in both cases.

According to Schumm [25], the elongation ration is expressed as:

$$R_e = 2/L_m (A/\pi)^{0.5}$$

where L_m is the maximum length of the catchment parallel to the principal drainage lines. Thus, the elongation ration for Wadi Aruanh Watershed is:

$$R_e = 2/146.11 (3113/3.14)^{0.5}$$
$$= 0.166$$

The resulted elongation ration also points out to a typical catchment area, where surface water is uniformly fed from the existing streams and then discharge in the outlet. This, in turn coincided with the width/length ration.

The above measures of the catchment shape are of significant, because they represent hydraulic parameters, which are often utilized in watershed management approaches and land use planning [26]. They are also essential to calculate a number of hydraulic coefficients for engineering and hydrologic practices.

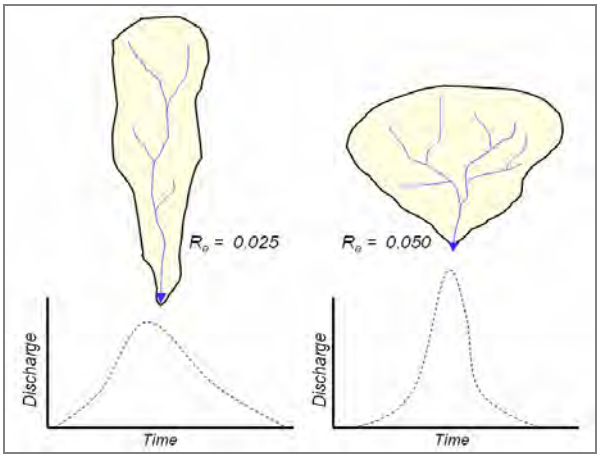

Figure 9. Example showing the relationship between basins of different elongation ratio and their discharges.

4. Discussions and Conclusions

The current study presents a method of watershed analysis for a typical catchment in the Western part of Arabian Peninsula. It provides detailed information on the geomorphologic setting of the catchment and its hydrologic characteristics.

The applied approach of catchment cartography was precisely implemented, not only by conventional method of drainage sampling, but also by using new techniques of remote sensing and GIS. This was a helpful tool to support the manual streams sampling directly from the topographic maps. Therefore, the obtained digital data set was the first of its type that made on Wadi Aurnah Watershed. If it would be utilized in hydrologic studies, then it can provide valuable information for watershed management and land use planning.

The fundamental output in this study is the new accurate approach of streams' sampling and catchment delineation and thus calculating the exact area of the catchment, which owned discrepancy in different previous studies. Also, it helped calculating the amount of water received from rainfall, which can be included as a principal variable in assessing water budged for the basin. It was found that the catchment receives a very amount of water from rainfall, since only 145.000 m^3 supplies each 1 km per year, which is not adequate to recharge the existing aquifers in the region.

The major hydrologic variables were calculated and their measures were obtained by the GIS system, which enables applying different measures and calculations in a simple approach of application. The established hypsometric curve was also essential to identify the elevation/area ratio. It was found that the average altitude in Aurnah catchment is 452 m, and only about 10% of the area extends above 1000m altitude, and around 50% of the area is located in altitude of less than 250m. In addition, a steep sloping terrain exists between the most elevated peaks (i.e. 2476m down to about 2200m) where gentle slopes occur. The later is interrupted by an acute regression trend, which is attributed to the existing fault blocks. These faults represent the transitional area between the elevated region and the coastal plain, and control the boundary of some sub-basins exists in the area.

The overall relief of the studied catchment is low to moderate as it was identified from the relief ratio (R_r), relief gradient ((R_g) and mean catchment slope (C_s), which were estimated as 17 m/km, 0.58 and 1.71 for each of them; respectively. This creates slow run-off with sufficient time lag for evaporation and infiltration as well. Moreover, the low-moderate relief reduces the impact of erosional processes, notably the channel erosion. Added to this, the effective relief properties, the rough texture topography, which may retard surface run-off, thus creates non-uniform flow regime and, likewise that in the relief properties, it helps giving enough time for

evaporation and infiltration rates, besides low effective erosion.

The shape characteristics of Wadi Aurnah exhibit typical shape type. It is a funnel-like shape with a uniform width/length ration. This ration (i.e., 0.46 or ~1: 2) helps an equal distribution of stream flow from mountain ranges towards the outlet into the primary watercourse. This fact was also supported by the resulting value of length to the center of the area (L_{ca}), which is almost half of the total stream length. In the other hand, the applied shape parameters (L_1, R_c and R_e) all are coincided and indicate that the overall shape of the catchment is regular with uniform boundary distribution. This is definitely considers the catchment shape, whilst other physical and anthropogenic factors (faults, land use.etc) may interfere and create irregular flow regime.

The above measures, in combination with site investigation, often are used by hydrologists and engineers, especially in constructing dams, water tanks, lakes, etc. Thus, combination of obtained measures would provide a comprehensive figure on the catchment characteristics, which can be used mainly in optimum watershed management approaches.

5. References

[1] M. Al Saud, "Using satellite imageries to study drainage pattern anomalies in Saudi Arabia," Environmental Hydrology Journal, Vol. 15, No. 30, pp. 1−15, 2007.

[2] Italconsult, "Water supply survey for Yeddah–Makkah −Taif area," Special Report, Geological Investigation, Ministry of Agriculture and Water, No. 3, 1967.

[3] M. Merza and A. Youssef, "Climate conditions in winter in Makka Al Mukaramah," Kuwait Geography Society, Vol. 253, 2001.

[4] A. Moor and M. Al-Rehaili, "Geological map of Makka Quadrangle sheet 21D," Kingdom of Saudi Arabia, Unpublished M.A. Thesis, University of Eastern Michigan, 1989.

[5] M. Sahl, "Geology of Makka Al Mukaramah City area," Saudi Arabian Deputy Ministry for Mineral Resources, Report DGMR, pp. 238, 1987.

[6] M. Es-Saeed, Z. Sen, A. Basamad, A. Dahlawi, and W. Al-Bardi, "Strategic groundwater storage in Wadi Naáman, Makka region, Saudi Arabia," Technical Report (in Arabic), Saudi Geological Survey-TR-2004-1, pp. 32, 2004.

[7] M. Merza and M. Baroudi, "Geological and geomorphological principles of Makka Al Mukaramah and their role in terrain topography," Unpublished Technical Report (in Arabic), pp. 102, 2005.

[8] I. Aawari, "Vegetation cover in Wadi Noaman with special emphasis on its tributary: Wadi El Majayrish," Unpublished MSc thesis (in Arabic), Department of Geography, Faculty of Arts, Jiddah, KSA, pp. 473, 2005.

[9] D. Mark. "Relations between field-surveyed channel networks and map-based geomorphometric measures," Inez, Kentucky, Ann. Assoc. Am. Geogr., Vol. 73, No. 30, pp. 358−372, 1983.

[10] J. O'Callagham and D. Mark, The extraction of drainage networks from digital elevation data," Computer Vision, Graphics Image Processing, Vol. 28, pp. 323−344, 1984.

[11] S. Jenson and J. Domingue, "Extracting topographic structure from digital elevation data for geographic information system analysis," Photogram. Eng. Sens., Vol. 54, No. 1, pp. 1593−1600, 1988.

[12] A. Tribe, "Automated recognition of valley heads from digital elevation models," Earth Surface Processes Landforms, Vol. 16, pp. 33−49, 1991.

[13] A. Ichoku, A. Meisels, and J. Chorowicz, "Detection of drainage channel networks on digital satellite images," International Journal of Remote Sensing, Vol. 17, pp. 1659−1678, 1996.

[14] J. Martinez-Casasnovas and H. Stuiver, "Automated delineation of drainage networks and elementary catchments from digital elevation models," ITC Journal, Vol. 3, pp. 198−208, 1998.

[15] Y. Ohsaki, A. Numata and T. Higashinwaatoko, Validation of rain/no-rain discrimination in the standard TRMM data products 1B21 and 1C21, IEEE., Vol. 2, pp. 875−877, 2000.

[16] L. Chiu, G. Serafino and W, Terg, "Applications of Tropical Rainfall Measuring Mission (TRMM) data," IEEE, Vol. 5, pp. 2118−2120, 2002.

[17] C. Scott, C. Thomas and L. Scott, "A comparison of TRMM to other basin-scale estimates of rainfall during the 1999 Hurricane Floyd flood," Natural Hazards, Accepted online, 2009.

[18] R. Chorley, S. Schumm, D. Sugden, and D. Geomorphology, Methuen, London, pp. 607, 1984.

[19] K. Smith, "Standards for grading texture of erosional topography," American Journal of Science, Vol. 248, pp. 655-668, 1950.

[20] R. Pike, S. Wilson, and S. Elevation-relief ratio, "Hypsometric integral and geomorphic area-altitude analysis," GSA Bull., Vol. 82, pp. 1079−1084, 1971.

[21] D. Gorden, A. McMahon, and L. Finalson, "Stream hydrology: John Wiley & Sons Ltd," Chichester, England, pp. 523, 1992.

[22] P. Black, Watershed Hydrology, Prentice Hall Advanced Reference Series, NJ, pp. 324, 1991.

[23] V. Miller, "A quantitive geomorphic study for drainage basin characteristics in the Clinch Mountain area," Virginia and Tennessee, Technical Report, Geology Depart., Colombia University, I-30, N6 ONR 271-30, No. 3, 1953.

[24] A. Strahler, "Dimensional analysis applied to fluvial eroded landforms," Geol.Soc.America. Bull., Vol. 69, pp. 279−300, 1958.

[25] S. Schumm, "The elevation of drainage systems and slopes in badlands at Perth Amboy," Geol. Soc. Amer. Bull., New Jersey, Vol. 67, pp. 597−646, 1956.

[26] M. Jane, "Geomorphological & land use planning for Dana watershed. GIS Development," 2008. Available on: http://www.gisdevelopment.net/application/nrm/water/watershed/watws0008pf.htm.

J. Water Resource and Protection, **2009, 1, 325-335**
doi:10.4236/jwarp.2009.15039 Published Online November 2009 (http://www.scirp.org/journal/jwarp)

Evapotranspiration Characteristics of a Lowland Dry Evergreen Forest in Central Cambodia Examined Using a Multilayer Model

Tatsuhiko NOBUHIRO[1*], Akira SHIMIZU[2], Katsunori TANAKA[3], Koji TAMAI[1], Naoki KABEYA[2], Eriko ITO[4], Takanori SHIMIZU[1], Makoto ARAKI[1], Sophal CHANN[5]

[1]*Forest Hydrology Laboratory, Forestry and Forest Products Research Institute, Tsukuba, Japan*
[2]*Kyushu Research Center, Forestry and Forest Products Research Institute, Kumamoto, Japan*
[3]*Research Institute for Global Change, Japan Agency for Marine-Earth Science and Technology, Yokohama, Japan*
[4]*Hokkaido Research Center, Forestry and Forest Products Research Institute, Hokkaido, Japan*
[5]*Forestry Administration, Forest and Wildlife Science Research Institute, PhnomPenh, Cambodia*
E-mail: *tatuhiko@ffpri.affrc.go.jp*

Received July 6, 2009; *revised September* 9, 2009; *accepted September* 15, 2009

Abstract

Development pressure has led to serious deforestation on the Indochina Peninsula. Particularly rapid deforestation has occurred in easily accessible lowland areas, and it is thus important to accumulate knowledge about these forests immediately. We measured evapotranspiration rates for a lowland dry evergreen forest in Kampong Thom Province, central Cambodia, using the energy balance Bowen ratio (EBBR) method based on meteorological data collected from a 60-m-high observation tower. Daily evapotranspiration was higher during the dry season than during the rainy season of the Asian monsoon climate. The seasonal variation in evapotranspiration generally corresponded to the seasonal difference in the vapor pressure deficit. A multilayer model was used to simulate the seasonal variation in evapotranspiration. The multilayer model also reproduced the larger evapotranspiration rate in the dry season than in the rainy season. However, observed values substantially exceeded model-calculated results during certain periods at the beginning of the dry season and in the late dry season. Moreover, during the rainy season, the model tended to overestimate evapotranspiration. The differences between these observed and simulated values may have been caused by seasonal characteristics of photosynthesis and transpiration in the lowland dry evergreen forest that were not considered in the model simulation.

Keywords: Cambodia, Energy Balance Bowen Ratio Method, Evapotranspiration, Lowland Dry Evergreen Forest, Multilayered Model

1. Introduction

The Indochina Peninsula, including Cambodia, belongs to the Asian monsoon climate zone characterized by distinct rainy and dry seasons. Pressures including increases in population, farmland development, and illegal logging have led to serious deforestation problems across the Indochina Peninsula. For example, the area covered by forest in Thailand decreased from 54% in 1960 to 25.3% in 1998 [1], and the forested area in Cambodia dropped from 73% in 1969 to 58% in 1997 [2].

Since artificial afforestation of commercial species such as teak has also been occurring in Indochina [3,4], very few forests exist in their natural state. To develop suitable forestry management practices for this region, a first urgent task is to assemble information on the various natural and artificial forest types, considering the climatic characteristics of the seasonal tropics.

Several studies have examined water cycles and resources in the Asian monsoon region, focusing on deforestation and certain regional climatic features. Using a gradient model, Pinker *et al*. [5] reported that evapotranspiration rates in the dry evergreen forest at the Sakaerat

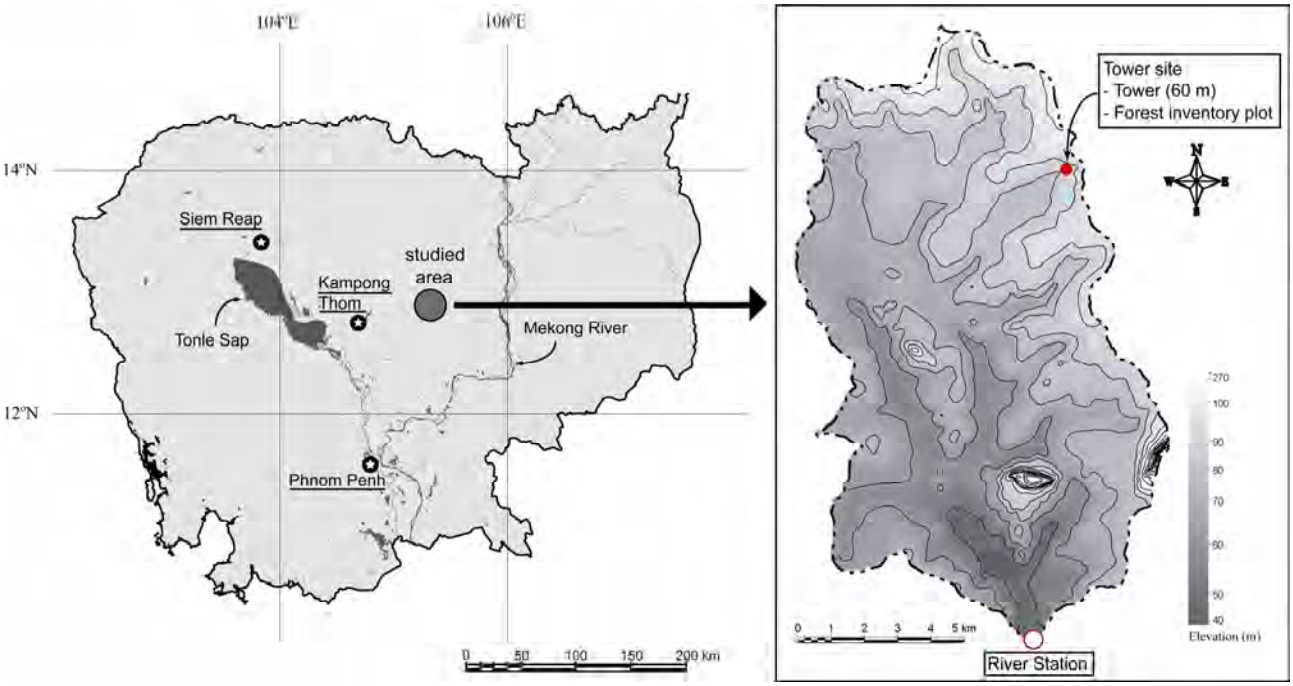

Figure 1. Location of the observation points in the O Thom I watershed.The contour interval of the topographic map is 10 m.

Environmental Research Station in Thailand was highest in June (rainy season; 3.3 mm day^{-1}) and lowest in January (dry season; 0.6 mm day^{-1}). Using the energy balance Bowen ratio (EBBR) method, Attarod *et al.* [6] also reported higher evapotranspiration rates during the rainy season (4.1 mm day^{-1}) than in the defoliated dry season (2.5 mm day^{-1}) for an artificial teak forest at Mae Moh in northern Thailand. However, Tanaka *et al.* [7], measuring evapotranspiration by the eddy correlation method for a hill evergreen forest in the Kog-Ma watershed of northern Thailand, reported that transpiration peaks appeared during the late dry season. At Kog-Ma, the water budget, canopy rainfall interception, sap flow, and soil water content were also measured, and both soil moisture and root system development were determined to be sufficient throughout the year that suppressed transpiration did not occur during the dry season [8,9].

As noted above, in the dry season of the Indochina Peninsula, transpiration decreases in some forests, whereas brisk transpiration continues in other forests. Differences in transpiration may be caused by differences in tree species and site environments such as soil depth or root system development. Thus, it is important to accumulate information on various forest types [10,11].

Lowland dry evergreen forest was once widely distributed over the Indochina Peninsula. Currently, however, this forest type is found only in limited areas, such as Kampong Thom Province in central Cambodia. Given the strong development pressures and lack of previous research on lowland forests, the need to gather information on lowland dry evergreen forest is particularly urgent.

This paper presents the results of evapotranspiration observations using the EBBR method in a lowland dry evergreen forest located in Kampong Thom Province. The characteristics of evapotranspiration are also described based on comparison with model simulations for the study forest; the simulations were conducted by a multilayer model that was previously applied to a hill evergreen forest of the Kog-Ma experimental watershed in Thailand [7].

2. Site Description and Observations

2.1. Site Description

The study was conducted at the O Thom I experimental watershed in Kampong Thom Province, Cambodia. The O Thom I River is a branch of the Stung Chinit River which feeds the Tonle Sap River, a major tributary of the Mekong River in central Cambodia. The O Thom I watershed covers an area of 137 km^2, with altitude ranging between 46 and 273 m. Kabeya *et al.* [12] reported that annual precipitation in 2004 was around 1500 mm at the Stung Chinit River, and monthly averaged temperature ranged from 26.8 to 30.2ºC.

We constructed a 60-m-high observation tower from which meteorological elements were measured in the northeast part of the O Thom I experimental watershed (12º44'N, 105º28'E, 88 m a.s.l.; Figure 1). The topography near the tower was rather flat.

Vegetation at the experimental watershed consisted of broad-leaved evergreen trees such as dipterocarp species.

Table 1. Parameters used in the simulation.

Parameter	Symbol	Value	Reference or Remarks
Physical Characteristics of an Individual Leaf			
Drag coefficient on both leaf surfaces	C_d	0.2	[24]
Bulk coefficient for sensible heat on both leaf surfaces	C_h	0.06	[26]
Optical Characteristics of an Individual Leaf			
Transmissivity of solar radiation and PAR	τ	0.2 and 0.06	[27]
Reflectivity of solar radiation and PAR	ρ	0.3 and 0.09	[27]
Biological Characteristics of an Individual Leaf			
Slope[a]	m	9	parameter tuning referred to Tanaka et al. [7]
Maximum rate of carboxylation at 25°C[b]	V_{cmax25}	20 μmol m^{-2} s^{-1}	parameter tuning referred to Tanaka et al. [7]
Other Characteristics of an Individual Leaf			
Surface emissivity	ε	1.0	
Capacity of water storage on the upper side	W_{Umax}	0.1 mm LAI^{-1}	parameter tuning referred to Tanaka [25]
Capacity of water storage on the lower side	W_{Lmax}	0.1 mm LAI^{-1}	Assumed equal to W_{UMAX}
Canopy Structure			
Number of canopy layers		50	
Canopy height	h	33 m	[13]
Leaf Area Index	LAI	3.87 - 4.49	see Tab. 2
Vertical profile of Leaf Area Density	a(z)	D-Type	a(z) is regarded as beta distribution [7,13]
Distribution of leaf inclination	g(α)	60° (SD=18°)	g(α) is regarded as normal distribution [7]
Characteristics of the Soil			
Reflectivity of solar radiation and PAR	α_{soil}	0.26 and 0.06	[26]
Roughness length	z_0	0.02 m	[26]
Moisture availability	β_{soil}	0	soil evaporation is assumed to be negligible
Other Characteristics of the Soil			
Surface emissivity	ε	1.0	[7]
Soil heat storage		0 W m^{-2}	[7]

[a]For stomatal model

[b]For net assimilation model

The vegetation near the meteorological observation tower was analyzed in great detail. The mean diameter at breast height and the mean tree height of overstory trees were 39.6 cm and 27.2 m, respectively. The maximum tree height was about 45 m. Although the upper canopy trees were low in density (512 stems ha^{-1}), they covered a large area of the canopy, with some secondary layer trees filling crown gaps between trees in the upper canopy [13]. Within the O Thom I watershed, the soil group was identified as acrisol [14] with a soft soil layer reaching to a depth of at least 7 m [15]. Ohnuki *et al*. [11] reported that the lowland dry evergreen forested area had a maximum water storage capacity of 1350 mm.

2.2. Observation Scheme

Our analysis of evapotranspiration and water balance in the O Thom I watershed parallels the study of Shimizu *et al.* [16], who also measured precipitation, runoff, shallow groundwater level, soil moisture, and meteorological factors in an experimental watershed of Kyusyu Island in southeastern Japan.

Pyranometers (CM3, Kipp & Zonen) were installed 60 m above the ground at the top of the observation tower to monitor solar radiation and reflected radiation. Two ventilated psychrometers (MH-020T, Eko) were installed above the forest canopy at 34 and 38 m. A net radiometer (Q7.1, REBS) and a cup anemometer (3301-5, Young) were placed at 36 m, and two heat flux plates (MF-180M, Eko) were installed 2 cm under the forest soil near the tower. Atmospheric pressure measurements (mini-TROLL, Air brown) were carried out at Kbal Domrey (12°54'N, 105°28'E) 20 km north of the tower site and recorded every hour. The leaf area index (LAI) was estimated using a LAI-2000 plant canopy analyzer (LI-COR) and hemispherical photography at the end of each month. A

rain gauge (RG-2M, Onset) was installed at 60 m height on 25 April 2004. Pyrgeometers (CGR-3, Kipp & Zonen) were temporarily placed at the top of the tower, and intensive observations of upward and downward longwave radiation were carried out from 27 February to 2 March 2006. Meteorological measurements, including of soil heat flux, were taken at 10-s intervals near the tower and recorded as 10-min averages (or cumulative values) using a data logger (CR10X, Campbell). The primary meteorological observations for this study were made throughout the year in 2004.

To confirm the instrumental accuracy of the ventilated psychrometers, which has a large effect on the Bowen ratio calculation, verifications were carried out every 3 months. The psychrometers were set at the same height, and inter-variation of the equipment was checked. At the same time, dry- and wet-bulb temperatures were also calibrated using an Asman psychrometer (Y-6005K, YOSHINO).

2.3. Estimation of Evapotranspiration by the Energy Balance Bowen Ratio Method

The energy balance Bowen ratio (EBBR) method, which measures the energy budget above the forest canopy from the profiles of potential temperature and water vapor pressure, was used to estimate evapotranspiration as described by Hattori [17] and Kaimal and Finnigan [18]. The method assumes that the diffusion coefficients of the latent and sensible heat fluxes are equal at the atmospheric surface layer. Therefore, the Bowen ratio (β) can be used to estimate latent heat flux as follows:

$$\beta = \frac{H}{\lambda E}, \tag{1}$$

$$\lambda E = \frac{Rn - G}{1 + \beta}, \tag{2}$$

where Rn is the net radiation (including net shortwave and longwave radiation), H is the sensible heat flux, λE is the latent heat flux, and G is the ground heat flux. The Bowen ratio can then be calculated by measuring the dry- and wet-bulb temperatures at the two levels and incorporating the psychrometric constant and the gradient of the saturation vapor pressure curve as follows:

$$\beta = \frac{\gamma(TD_1 - TD_2)}{(\delta + \gamma)(TW_1 - TW_2) - \gamma(TD_1 - TD_2)}, \tag{3}$$

where γ is the psychrometric constant, δ is the gradient of the saturated vapor pressure curve at the average value of the wet-bulb temperatures, and $TD_1 - TD_2$ and $TW_1 - TW_2$ are the differences between dry- and between wet-bulb temperatures at the two heights (34 and 38 m), respectively. All data required to solve these equations were collected using the instruments mentioned above.

When applying the EBBR method, atmospheric stability is preferable in a nearly neutral condition [19]. Tamai *et al*. [20] reported that the degree of atmospheric stability in O Thom I experimental watershed is generally suitable for tower flux measurements, including by the EBBR method. Moreover, as described above, we paid careful attention to maintaining the instrumental accuracy of the psychrometers; therefore, we expect that our observational results obtained by the EBBR method are highly reliable.

3. Multilayer Model for Evapotranspiration

The multilayer model that had been previously applied to the hill evergreen forest at Kog-Ma experimental watershed [7,9] was applied to the lowland dry evergreen forest at O Thom I experimental watershed. In this chapter, we explain the required input data and the parameters used to apply the multilayer model to our experimental watershed.

3.1. Model Structure

The multilayer model consists of distinct physical processes and contains five sub-models that incorporate the following: 1) Reynolds stress and temperature, CO_2, and H_2O exchanges on leaves; 2) radiation transfer within the forest canopy; 3) atmospheric diffusion within and above the forest canopy; 4) energy balance on leaves and the ground surface; and 5) rainfall interception and water budget on the leaf surface.

The details of each sub-model are described below.

1) The Farquhar-type photosynthesis model [21] and Ball's stomatal conductance model [22] are used for the CO_2 and H_2O exchanges of leaves.

2) The vertical profiles of leaf area density a(z) and the distribution of the leaf inclination angle g(α) are used to determine radiation transfer.

3) A second-order closure sub-model [23] is used to simulate atmospheric transfer within and above the forest canopy. This sub-model predicts the effect of a(z) on atmospheric diffusion from the soil surface to twice the canopy height [24].

4) For the energy balance sub-model, the heat storage in the leaves and the energy stored by photosynthesis are assumed to be negligible, and the radiation energy in each divided layer is estimated from the transmissivity and reflectivity of shortwave and longwave radiation apportioned into sensible and latent fluxes. The energy balance on the ground surface is estimated from the input radiation energy from the lowest layer and the soil heat flux [25].

5) The rainfall interception sub-model assumes that rainfall wets only the upper sides of leaves, whereas condensation wets both the upper and lower sides of leaves, and transpiration and CO_2 exchange occur only at dry lower-leaf stomata. Moreover, this sub-model captures the effects of a(z) and g(α) on rainfall interception,

which are important during the rainy season.

The multilayer model also assumes that wind velocity, air and leaf temperatures, humidity, and CO_2 concentration are horizontally uniform, although it does consider the difference in photosynthetically active radiation (PAR) in sunlit and shaded areas [7].

3.2. Model Input

The data input to the multilayer model are solar elevation (*SE*), downward shortwave radiation ($S\downarrow$), downward longwave radiation ($L\downarrow$), horizontal wind velocity (u), air temperature (T), vapor pressure (e), CO_2 partial pressure (c), and rainfall over the forest (P). The outputs are upward shortwave radiation ($S\uparrow$), upward longwave radiation ($L\uparrow$), net radiation (Rn), sensible heat flux (H), latent heat flux (λE), CO_2 flux (Fc), and their respective vertical profiles. The multilayer model separates the latent heat flux into transpiration and evaporation components. Canopy structure, the characteristics of individual leaves, and information on soil characteristics are treated as the model parameters.

3.3. Model Parameters

To apply the multilayer model, we used the parameters shown in Table 1. The forests at the Kog-Ma experimental watershed in Thailand and the O Thom I experimental watershed in Cambodia differ. Therefore, we used parameters that are relevant to the canopy structure and leaf characteristics of Cambodian lowland dry evergreen forest.

Seasonal variations in the LAI were measured near the tower site (Table 2). The canopy was divided into 50 equal layers. Vertical profiles of the nondimensional leaf area density (a(z)h/LAI) were determined as a D-type beta distribution, defined as when the upper part of the canopy is denser [7], based on the vegetation structure inventory [13]. Meanwhile, the physical and optical characteristics of individual leaves, such as the drag and bulk coefficients for sensible heat, transmissivity and reflectivity of solar radiation, and photosynthetically active radiation were assumed to be the same as those reported by Tanaka *et al.* [7] for their hill evergreen forest site in Thailand.

The parameters relating to individual leaves or the canopy structure, such as slope (m), maximum rate of carboxylation at 25ºC (V_{cmax25}), and water storage capacity on the upper side of an individual leaf (W_{Umax}), tended to have a large effect on the simulation results in the parameter-tuning analysis of Tanaka *et al.* [7]. However, the characteristics of these parameters at the Cambodian lowland dry evergreen forest are obscure. Therefore, in this research, these three parameters were fixed throughout the observation period at values at which the annual amount of simulated evapotranspiration became approximately equivalent to the observed result (see Table 1).

Table 2. Seasonal variation in the leaf area index obtained near the observation tower.

	Month												Annual
	1	2	3	4	5	6	7	8	9	10	11	12	
average (3 years)*	3.95	4.01	3.96	3.89	4.06	4.32	4.39	4.26	4.10	3.98	3.87	3.85	4.05
2004	4.18	4.21	4.07	3.91	3.99	4.26	4.49	4.37	4.03	3.87	3.93	3.94	4.10

*Apr 2003- Mar 2006

Because the soil water content at 100 cm depth maintained a wet soil condition during the dry season [28], and the ground water level was approximately 3 m below the ground surface even at the end of the dry season [29], we assumed that drying within the soil did not occur during the analysis period. Evaporation from the forest floor was considered to be negligible because the forest canopy was very dense, and thus radiation transfer to the soil surface was assumed to be very small.

Rainfall at the tower site was measured from 25 April 2004. Generally, the period from January to April corresponds to the dry season [13,30]; because we did not record rainfall for this period, we used input values of zero rainfall for our multilayer model during this period. We do not consider this assumption to contradict because the ground water level gradually decreased during the period in 2004 for which data are lacking [28]. The time interval for our multilayer model simulation was 10 min, corresponding to the interval between individual meteorological measurements.

4. Results and Discussions

4.1. Seasonal Variation in Each Meteorological Component

Figure 2 shows the seasonal variations in observed and estimated components averaged (or integrated) every three days. The seasonal variations in solar elevation at noon calculated from the latitude and longitude of the tower site (*SE*), and observed $S\downarrow$ and S↑, are shown in Figure 2 (a). The solar elevation was maximal in April and August, corresponding to the late dry season and the middle of the rainy season, respectively. The downward shortwave radiation during the rainy season was almost the same as that during the dry season. The integrated values of downward and upward shortwave radiation in 2004 were 6.84 and 0.76 GJ m^{-2} $year^{-1}$, respectively. The mean value of albedo during the observation period was 0.111. Figure 2(b) shows the seasonal variation in $L\downarrow$ and $L\uparrow$ estimated from the meteorological elements (see Appendix). Figure 2(c) presents the seasonal variation in air temperature observed at a height of 34 m (TD_1). The lowest air temperature was during the early dry season (<25ºC), and the highest was during the late dry season (>30ºC). In contrast, temperatures did not fluctuate much during the rainy season, with an average value of approximately 27ºC. Figure 2(d) gives the vapor pressure

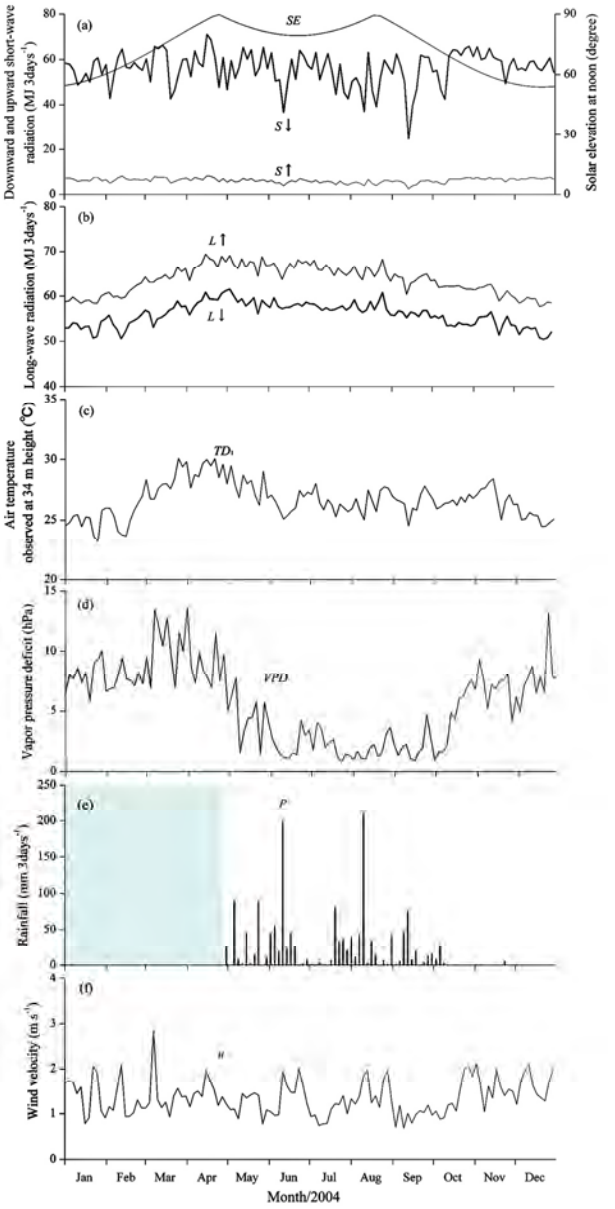

Figure 2. Seasonal variation in (a) solar elevation at noon (*SE*), downward shortwave radiation (*S*↓), and upward shortwave radiation (*S*↑); (b) downward longwave radiation (*L*↓) and upward longwave radiation (*L*↑); (c) air temperature (TD_1); (d) vapor pressure deficit (*VPD*); (e) rainfall (*P*), shading indicates a period lacking data; and (f) wind velocity (*u*). All values were averaged or integrated every three days.

deficit (*VPD*) at a height of 34 m, which indicates the dryness of the air. The figure shows a clear tendency of high *VPD* during the dry season (>5 hPa) and low *VPD* throughout the rainy season (<5 hPa). Figure 2 (e) illustrates the seasonal variation in rainfall (*P*) from 25 April onward. Rainfall exceeded 200 mm over 3 days^{-1} twice during the rainy season. In addition, a short dry season, namely a period with little rain during the rainy season [31], was clearly observed between the end of June and the middle of July. The dry season commenced in the middle of October with very little subsequent rainfall. Figure 2 (f) shows the seasonal variation in wind velocity observed at a height of 36 m (*u*). Although we expected that wind velocity would be high during the rainy season, we did not observe any clear seasonal variation in wind velocity.

From these results, we roughly classified three seasons for the study watershed: 1) an early dry season with cool, dry air and little rain; 2) a late dry season with hot, dry air and little rain; and 3) a rainy season with much rain. Each period corresponded to January to the middle of February and the end of October to December, the end of February to the beginning of May, and the middle of May to the middle of October, respectively.

4.2. Observational Results for Evapotranspiration by the EBBR Method

Figure 3 shows the seasonal variation in evapotranspiration calculated by the EBBR method. The vertical bars show the standard deviations in each period. When seasonal variation in evapotranspiration in 2004 was considered, the average value of evapotranspiration during the rainy season (middle of May to middle of October) was 2.3 mm day^{-1}, which was less than the average value during the dry season (3.5 mm day^{-1}). Additionally, peaks in the evapotranspiration rate were also observed at the late dry season (7 March 2004: 5.7 mm day^{-1}) and the beginning of the dry season (29 October 2004: 5.5 mm day^{-1}).

As shown in Figures 2(a) and (b), no large seasonal variations in *S*↓, S↑, *L*↓, and *L*↑ between the dry season and rainy season were found at this site. The highest temperature was found in the first half of the dry season, followed by the rainy season, and then the latter half of the dry season; this seasonal order differed from the seasonal variation in observed evapotranspiration. On the other hand, as shown in Figure 2(d), we found a clear difference in *VPD* between the dry and rainy seasons. These results suggest that larger evapotranspiration in the dry season than in the rainy season originated from the seasonal variation in the *VPD*.

Stomatal aperture at the leaf level is modeled as the increase in *VPD* leading to stomatal closure [32]. Based on this concept, increasing *VPD* seems to lead to decreasing evapotranspiration. Meanwhile, transpiration at the community level is composed of equilibrium evaporation and imposed evaporation, defined by the proportionality relation to effective radiation, and multiplication of *VPD* and stomatal conductance, respectively [33]. Based on this definition, the increment of *VPD* may cause an increase in transpiration. Furthermore, even in

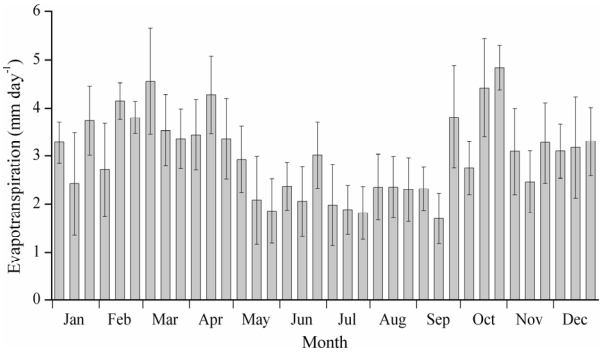

Figure 3. Daily amount of evapotranspiration by the EBBR method in 2004 shown as monthly based 10-day averages. Vertical bars indicate standard deviations for each observation period.

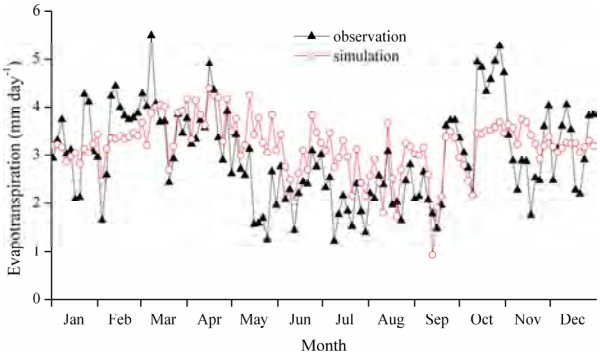

Figure 4. Comparison between observed (closed triangles) and simulated (open circles) daily amounts of evapotranspiration in 2004 averaged every three days.

the dry season, deeper soil remained wet in our experimental watershed [11,28,29]. Therefore, trees could obtain sufficient water even during the dry season with high *VPD*; thus, little stomatal closure may have occurred at the study site. Therefore, the depression rate of stomatal conductance accompanying the increment in *VPD* would not be so large, and as a result, the imposed evaporation may increase with the high *VPD*.

4.3. Comparison Between Observed and Simulated Evapotranspiration

Figure 4 presents the evapotranspiration rates obtained from the observations through EBBR method and from the multilayer model. Each point shows the observed and simulated daily evapotranspiration rates averaged over three days.

In this study, we used the following types of parameters in the multilayer model: 1) those obtained from direct measurement of a lowland dry evergreen forest in Cambodia (e.g., LAI, canopy height); 2) those identified in the hill evergreen forest at Kog-Ma, Thailand (e.g., physical and optical characteristics of an individual leaf); and 3) those determined based on the annual amount of simulated evapotranspiration's becoming approximately the same as the observed result (m, V_{cmax25}, and W_{Umax}). Therefore, the model did not necessarily represent the present condition of the lowland dry evergreen forest in O Thom I. However, the model substantially reproduced the observed result of larger evapotranspiration in the dry season by the EBBR method. Therefore, many of the parameters assumed in this research may have roughly expressed the characteristics of the Cambodian lowland dry evergreen forest.

Because some parameter values were determined by the simulated total amount of evapotranspiration nearing the observation result, the values estimated by the multilayer model were sometimes more or less than observed values. The observed evapotranspiration exceeded the simulated values during the late dry season (middle of February to the beginning of March) and at the beginning of the dry season (beginning of October), as noted in the first paragraph of Section 4.2. These periods coincided mostly with the peak of seasonal variation in evapotranspiration. Furthermore, during the rainy season, the model results overall tended to exceed the observed evapotranspiration.

Seasonal variation in the physiological characteristics of individual leaves may be one explanation for why the model did not reproduce the two peaks of observed evapotranspiration during the dry season and overestimated evapotranspiration in the rainy season. In the model simulation conducted in this study, parameters such as the photosynthetic rate and stomatal aperture of each leaf were assumed to be fixed values. However, the photosynthetic rate is known to reach maximum values at the time of foliation and then decline with advancing leaf age [34−36]. Such a phenological feature has also been recognized in photosynthesis observations of evergreens in other tropical regions [37,38]. The stomatal conductance of evergreen trees has also been demonstrated to fluctuate seasonally due to variation in environmental factors such as meteorological conditions and soil aridity in the seasonal tropics [39−43]. Therefore, the parameters concerning the assimilation rate and stomatal aperture at our study site might also change with the maturity and senescence of leaves.

Leaf dynamics clearly display seasonal changes in the evergreen forests of the study area. Investigations of litter fall and the LAI showed that leaf abscission and foliation became active at the beginning and late parts of the dry season (E. Ito, unpublished data). Therefore these phenological characteristics thus probably did not agree with fixed assumptions for parameters of photosynthesis and evapotranspiration throughout the year. However, many tree species with various phenologies intermingle with the evergreen forest neighboring the meteorological observation site; on the whole, the seasonal variation in physiological characteristics for the various species has

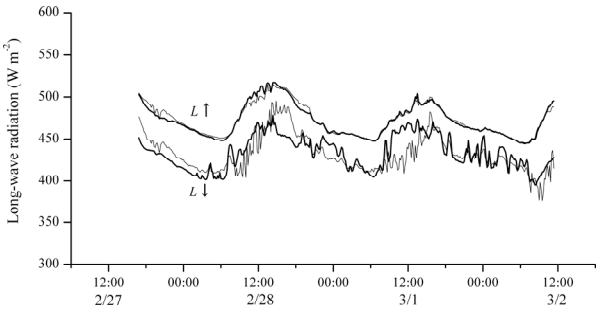

Figure 5. Time series of longwave radiation from 27 February to 2 March 2006. $L\downarrow$ and $L\uparrow$ indicate downward and upward longwave radiation, respectively, and the thick and thin lines indicate observed and estimated values, respectively.

not yet been clarified quantitatively. Therefore, we presently do not have enough information to explain the peaks of evapotranspiration during the dry season by the physiology of individual leaves alone or to reflect this issue in the model simulation. However, on the basis of the above discussion, we suggest that seasonal variation in the physiological characteristics of individual leaves of various tree types in the surrounding forest had a large effect on the evapotranspiration in the O Thom I experimental watershed. The observational findings of the transpiration peak during the dry season and the higher daily amount of evapotranspiration in the dry season than in the rainy season would be strongly affected by those seasonal variations.

A next research step will be to further investigate the characteristics of tree physiology postulated on the basis of the model simulation in this study.

5. Conclusions

This study confirmed the following findings. From meteorological observations, we could roughly classify three seasons for a lowland dry evergreen forest in central Cambodia: an early dry season, a late dry season, and a rainy season. We then used the energy balance Bowen ratio (EBBR) method to observe the evapotranspiration rate. The daily evapotranspiration amount was higher in the dry season (3.5 mm day^{-1}) than in the rainy season (2.3 mm day^{-1}). The high vapor pressure deficit during the dry season likely had a large effect on the higher evapotranspiration during the dry season. The finding of higher evapotranspiration in the dry season than in the rainy season was also reproduced by the multilayer model of Tanaka *et al*. [7].

However, our results also showed differences between the simulation and observation. During the beginning and late parts of the dry season, observed evapotranspiration was greater than simulated evapotranspiration. In contrast to the dry season, simulated evapotranspiration during the rainy season tended to be larger than observed evapotranspiration. The above results suggest that one cause of the quantitative difference in observed and simulated evapotranspiration in some periods was the seasonal variation in physiological characteristics such as photosynthesis and/or transpiration, which we treated as constant parameters in the multilayer model simulation.

Further investigation of physiological and phenological features accompanied by continuous observation of evapotranspiration in lowland dry evergreen forest of Cambodia would help clarify the above suggestions.

6. Acknowledgments

This study was partly funded by the Ministry of the Environment, Japan (Global Environment Research Coordination System). We also thank Mr. Ty Sokhun, Director General of the Forestry Administration of Cambodia, and our Cambodian colleagues of the Forest and Wildlife Science Research Institute, Cambodia.

7. Appendixes

7.1. Estimation of Downward Longwave Radiation

Downward longwave radiation was a necessary input for the multilayer model. However, only short-term observations of upward longwave radiation ($L\uparrow$) and downward longwave radiation ($L\downarrow$) were carried out in this study. For this reason, it was necessary to presume downward longwave radiation ($L\downarrow$) throughout the period. We explain the method that we used to presume $L\downarrow$ in this section.

Net radiation (Rn) is composed of shortwave and longwave radiation, as given in Equation (4):

$$Rn = S\downarrow + S\uparrow + L\downarrow + L\uparrow . \quad (4)$$

Here, with radiation energy from the black body proportionate to the fourth power of the absolute temperature, the following equation is approved at the canopy surface:

$$L\uparrow = \sigma \times K^4 , \quad (5)$$

where σ is the proportionality constant value and K is the absolute temperature of the canopy surface. The temperature of the canopy surface was not measured; therefore the temperature observed at 34 m height was substituted into Equation (5) instead of the canopy surface temperature. Equation (6) was then rearranged as follows:

$$L\uparrow = \sigma \times (TD_1 + 273.15)^4 , \quad (6)$$

where TD_1 is the temperature observed at a height of 34 m. Then the following Equation (7) was obtained with reference to Equations (4) and (6):

$$L\downarrow = Rn - S\uparrow - S\downarrow - \sigma(TD_1 + 273.15)^4 . \quad (7)$$

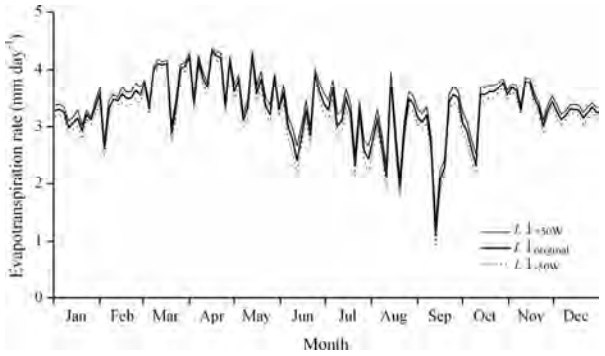

Figure 6. The effect of downward longwave radiation ($L\downarrow$) on evapotranspiration during the daytime. The legends show the calculated evapotranspiration rate using $L\downarrow$ ($L\downarrow_{original}$) estimated from Equations (7), with 50 W m^{-2} added to $L\downarrow$ ($L\downarrow_{+50W}$), and with 50 W m^{-2} subtracted from $L\downarrow$ ($L\downarrow_{-50W}$), respectively.

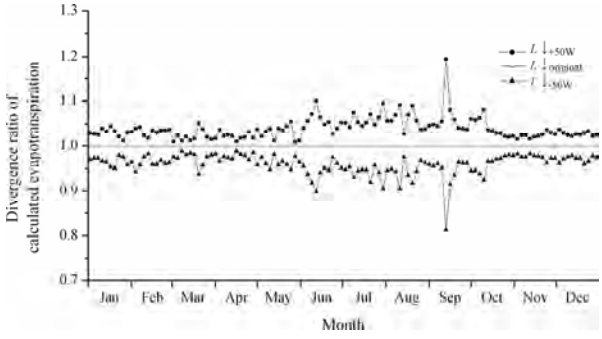

Figure 7. The divergence ratio, calculated by the divergence of the evapotranspiration with $L\downarrow_{+50W}$ and $L\downarrow_{-50W}$ from the evapotranspiration with the original $L\downarrow$. The legends are the same as in Figure 6.

The estimated $L\uparrow$ and $L\downarrow$ obtained from Equations (6) and (7) were verified by observed $L\uparrow$ and $L\downarrow$ obtained during the intensive observation period from 27 February to 2 March 2006 (Figure 5). When σ was defined as 5.61×10^{-8} (W m^{-2} K^{-4}), the coefficient of determination between observed and estimated $L\downarrow$ was 0.54. Maximum estimation error in $L\downarrow$ was about ±50 W m^{-2}, and the difference between integral values of observed and estimated $L\downarrow$ during the daytime was about 3%.

7.2. Effect of L↓ Error on Simulated Evapotranspiration

As mentioned above, the maximum estimation error in $L\downarrow$ was approximately ±50 W m^{-2}. To verify that the effect of the $L\downarrow$ estimation error on the calculated evapotranspiration rate changed between –50 and +50 W m^{-2}, numerical simulation was performed. Figure 6 shows the seasonal variations in evapotranspiration obtained from the simulation results by using (1) $L\downarrow$ estimated from $\sigma = 5.61 \times 10^{-8}$ ($L\downarrow_{original}$), (2) an increase of 50 W m^{-2} from $L\downarrow_{original}$ ($L\downarrow_{+50W}$), and (3) a decrease of 50 W m^{-2} from $L\downarrow_{original}$ ($L\downarrow_{-50W}$). The three simulations resulted in the same tendency of seasonal patterns of evapotranspiration.

Figure 7 shows the ratio of divergence in evapotranspiration obtained by the cases of $L\downarrow_{+50W}$ and $L\downarrow_{-50W}$ from the basic simulation result ($L\downarrow_{original}$). During the period when the net radiation was small, the estimation error of $L\downarrow$ had a relatively large effect on the simulated radiation output, but during the other periods, the estimation error contributed less than 5%. However, when the accuracy of daily-integrated $L\downarrow$ was considered, very little difference was observed between the numerical simulations illustrated in Figure 7. From the above, we concluded that the estimation method of $L\downarrow$ used in this study was appropriate.

8. References

[1] A. Nalampoon, "National forest policy review, Thailand," in P. B. Durst Ed., "An overview of forest policies in Asia," FAO, Bangkok, pp. 293–311, 2003.

[2] E. Savet and T. Sokhun, "National forest policy review, Cambodia," in P. B. Durst Ed., "An overview of forest policies in Asia," FAO, Bangkok, pp. 93–108, 2003.

[3] B. Krishnapillay, "Silviculture and management of teak plantations," Unasylva, Vol. 201, pp. 14–21, 2000.

[4] A. Mittelman, "Teak planting by smallholders in Nakhon Sawan, Thailand," Unasylva, Vol. 201, pp. 62–65, 2000.

[5] R. T. Pinker, O. E. Thompson, and T. F. Eck, "The energy balance of a tropical evergreen forest," Journal of Applied Meteorology, Vol. 19, pp. 1341–1350, 1980.

[6] P. Attarod, M. Aoki, D. Komori, T. Ishida, K. Fukumura, S. Boonyawat, P. Tongdeenok, M. Yokoya, S. Punkngum, and T. Pakoktom, "Estimation of crop coefficients and evapotranspiration by meteorological parameters in a rain-fed paddy rice field, cassava and teak plantations in Thailand," Journal of Agricultural Meteorology, Vol. 62, pp. 93–102, 2006.

[7] K. Tanaka, H. Takizawa, N. Tanaka, I. Kosaka, N. Yoshifuji, C. Tantasirin, S. Piman, M. Suzuki, and N. Tangtham, "Transpiration peak over a hill evergreen forest in northern Thailand in the late dry season: Assessing the seasonal changes in evapotranspiration using a multilayer model," Journal of Geophysical Research, Vol. 108 (D17), pp. 4533, 2003.

[8] T. Kume, H. Takizawa, N. Yoshifuji, K. Tanaka, C. Tantasirin, N. Tanaka, and M. Suzuki, "Impact of soil drought on sap flow and water status of evergreen trees in a tropical monsoon forest in northern Thailand," Forest Ecology and Management, Vol. 238, pp. 220–230, 2007.

[9] K. Tanaka, H. Takizawa, T. Kume, J. Xu, C. Tantasirin, and M. Suzuki, "Impact of rooting depth and soil hydraulic properties on the transpiration peak of an evergreen forest in northern Thailand in the late dry season," Journal of Geophysical Research, Vol. 109, D23107, 2004.

[10] N. Tanaka, T. Kume, N. Yoshifuji, K. Tanaka, H. Taki-

zawa, K. Shiraki, C. Tantasirin, N. Tangtham, and M. Suzuki, "A review of evapotranspiration estimates from tropical forests in Thailand and adjacent regions," Agricultural and Forest Meteorology, Vol. 148, pp. 807–819, 2008.

[11] Y. Ohnuki, C. Kimhean, Y. Shinomiya, and J. Toriyama, "Distribution and characteristics of soil thickness and effects upon water storage in forested areas of Cambodia," Hydrological Processes, Vol. 22, pp. 1272–1280, 2008.

[12] N. Kabeya, A. Shimizu, T, Nobuhiro, and K. Tamai, "Preliminary study of flow regimes and stream water residence times in multi-scale forested watersheds of central Cambodia," Paddy and Water Environment, Vol. 6, pp. 25–35, 2008.

[13] A. Shimizu, N. Kabeya, T. Nobuhiro, T. Kubota, Y. Tsuboyama, E. Ito, M. Sano, S. Chann, and N. Keth, "Runoff characteristics and observations on evapotranspiration in forest watersheds, central Cambodia," in H. Sawada *et al*. Ed., "Forest Environments in the Mekong River Basins," Springer, Tokyo, pp. 135–146, 2007.

[14] J. Toriyama, S. Ohta, M. Araki, M. Kanzaki, S. Khorn, P. Pith, S. Lim, and S. Pol, "Soils under different forest types in the dry evergreen forest zone of Cambodia: Morphology, physicochemical properties, and classification," in H. Sawada *et al*. Ed., Forest Environments in the Mekong River Basins," Springer, Tokyo, pp. 241–253, 2007.

[15] Y. Ohnuki, C. Kimhean, Y. Shinomiya, S. Sor, J. Toriyama, and S. Ohta, "Apparent change in soil depth and soil hardness in forest areas in Kampong Thom province, Cambodia," in H. Sawada *et al*. Ed., "Forest Environments in the Mekong River Basins," Springer, Tokyo, pp. 263–272, 2007.

[16] A. Shimizu, T. Shimizu, Y. Miyabuchi, and Y. Ogawa, "Evapotranspiration and runoff in a forested watershed, western Japan," Hydrological Processes, Vol. 17, pp. 3125–3139, 2003.

[17] S. Hattori, "Explanation on derivation process of equations to estimate evapotranspiration and problems on the application to forest stand," Bulletin of the Forestry and Forest Products Research Institute, Japan, Vol. 332, pp. 139–165, 1985.

[18] J. C. Kaimal and J. J. Finnigan, "Atmospheric boundary layer flows: Their structure and measurement," Oxford University Press, New York, 1994.

[19] W. Brutsaert, Ed., "Evaporation into the atmosphere: theory, history, and applications," D. Reidel Publishing Company, 1982.

[20] K. Tamai, T. Nobuhiro, A. Shimizu, N. Kabeya, S. Chann, and K. Nang, "Characteristics of atmospheric stability above an evergreen forest in central Cambodia," Hydrological Processes, Vol. 22, pp. 1267–1271, 2008.

[21] G. D. Farquhar, S. V. Caemmerer, and J. A. Berry, "A biochemical model of photosynthetic CO_2 assimilation in leaves of C_3 species," Planta, Vol. 149, pp. 78–90, 1980.

[22] J. T. Ball, "An analysis of stomatal conductance," Ph.D thesis, Stanford University, Stanford, California, 1988.

[23] T. Watanabe, "The bulk transfer coefficients over a vegetated surface based on K-theory and 2nd-order closure model," Journal of the Meteorological Society of Japan, Vol. 71, pp. 33–42, 1993.

[24] N. R. Wilson and E. H. Shaw, "A higher order closure model for canopy flow," Journal of Applied Meteorology, Vol. 16, pp. 1197–1205, 1977.

[25] K. Tanaka, "Multi-layer model of CO_2 exchange in a plant community coupled with the water budged of leaf surfaces," Ecological Modelling, Vol. 147, pp. 85–104, 2002.

[26] K. Tanaka, Y. Kosugi, N. Ohte, S. Kobashi, and A. Nakamura, "Model of CO_2 flux between a plant community and the atmosphere, and simulation of CO_2 flux over a planted forest," (in Japanese with an English abstract) Japanese Journal of Ecology, Vol. 48, pp. 265–286, 1998.

[27] J. Ross, "Radiative transfer in plant communities," in J. L. Monteith Ed., "Vegetation and the atmosphere," Vol. 1, Academic Press, California, pp. 13–55, 1975.

[28] M. Araki, J. Toriyama, S. Ohta, M. Kanzaki, E. Ito, B. Tith, S. Pol, S. Lim, S. Khorn, P. Pith, and S. Det, "Soil moisture conditions in four types of forests in Kampong Thom, Cambodia," in H. Sawada *et al*. Ed., "Forest environments in the Mekong river basins," Springer, Tokyo, pp. 254–262, 2007.

[29] M. Araki, A. Shimizu, J. Toriyama, E. Ito, N. Kabeya, T. Nobuhiro, B. Tith, S. Pol, S. Lim, S. Khorn, P. Pith, S. Det, S. Ohta, and M. Kanzaki, "Changes of vertical soil moisture conditions of a dry evergreen forest in Kampong Thom, Cambodia," in H. Sawada *et al*. Ed., "Forest environments in the Mekong river basins," Springer, Tokyo, pp. 112–124, 2007.

[30] N. Kabeya, A. Shimizu, S. Chann, Y. Tsuboyama, T. Nobuhiro, N. Keth, and K. Tamai, "Stable isotope studies of rainfall and stream water in forest watersheds in Kampong Thom, Cambodia," in H. Sawada *et al*. Ed., "Forest environments in the Mekong river basins," Springer, Tokyo, pp. 125–134, 2007.

[31] J. Matsumoto, "Seasonal transition of summer rainy season over Indochina and adjacent monsoon region," Advances in Atmospheric Sciences, Vol. 14, pp. 231–245, 1997.

[32] J. B. Stewart, "Modelling surface conductance of pine forest," Agricultural and Forest Meteorology, Vol. 43, pp. 19–35, 1988.

[33] K. G. McNaughton and P. G. Jarvis, "Predicting effects of vegetation changes on transpiration and evaporation," in T. T. Kozlowski Ed., "Water deficits and plant growth," Academic Press, New York, Vol. 7, pp. 1–47, 1983.

[34] D. S. Ellsworth, "Seasonal CO_2 assimilation and stomatal limitations in a *Pinus taeda* canopy," Tree Physiology, Vol. 20, pp. 435–445, 2000.

[35] S. Mediavilla and A. Escudero, "Photosynthetic capacity, integrated over the lifetime of a leaf, is predicted to be independent of leaf longevity in some tree species," New Phytologist, Vol. 159, pp. 203–211, 2003.

[36] Q. Han, T. Kawasaki, T. Nakano, and Y. Chiba, "Spatial

and seasonal variability of temperature responses of biochemical photosynthesis parameters and leaf nitrogen content within a *Pinus densiflora* crown," Tree Physiology, Vol. 24, pp. 737–744, 2004.

[37] K. Kitajima, S. S. Mulkey, and S. J. Wright, "Seasonal leaf phenotypes in the canopy of a tropical dry forest: Photosynthetic characteristics and associated traits," Oecologia, Vol. 109, pp. 490–498, 1997.

[38] K. Kitajima, S. S. Mulkey, and S. J. Wright, "Decline of photosynthetic capacity with leaf age in relation to leaf longevities for five tropical canopy tree species," American Journal of Botany, Vol. 84, pp. 702–708, 1997.

[39] F. C. Meinzer, G. Golostein, N. M. Holbrook, P. Jackson, and J. Cavelier, "Stomatal and environmental control of transpiration in a lowland tropical forest tree," Plant, Cell and Environment, Vol. 16, pp. 429–436, 1993.

[40] P. B. Reich, "Phenology of tropical forests: Patterns, causes, and consequences," Canadian Journal of Botany, Vol. 73, pp. 164–174, 1994.

[41] J. I. Pitman, "Ecophysiology of tropical dry evergreen forest, Thailand: measured and modelled stomatal conductance of *Hopea ferrea*, a dominant canopy emergent," Journal of Applied Ecology, Vol. 33, pp. 1366–1378, 1996.

[42] D. S. Thomas, D. Eamus, and S. Shanahan, "Influence of season, drought and xylem ABA on stomatal responses to leaf-to-air vapour pressure difference of trees of the Australian wet-dry tropics," Australian Journal of Botany, Vol. 48, pp. 143–151, 2000.

[43] K. Kitajima, S. S. Mulkey, M. Samaniego, and S. J. Wright, "Decline of photosynthetic capacity with leaf age and position in two tropical pioneer tree species," American Journal of Botany, Vol. 89, pp. 1925–1932, 2002.

J. Water Resource and Protection, **2009, 1, 336-344**
doi:10.4236/jwarp.2009.15040 Published Online November 2009 (http://www.scirp.org/journal/jwarp)

Effects of Estrogen Contamination on Human Cells: Modeling and Prediction Based on Michaelis-Menten Kinetics[1]

F. IBRAHIM[1], B. HUANG[1], J. Z. XING[2], W. ROA[3], Stephan GABOS[4]
[1]*Chemical and Materials Engineering University of Alberta, Edmonton, Alberta, Canada*
[2]*Department of Laboratory Medicine and Pathology, University of Alberta, Edmonton, Canada*
[3]*Department of Oncology, Cross Cancer Institute, Edmonton, Canada*
[4]*Alberta Health and Wellness, Edmonton, Alberta, Canada*
E-mail: *stephan.gabos@gov.ab.ca*
Received July 12, 2009; *revised August* 8, 2009; *accepted August* 17, 2009

Abstract

In this paper, we propose a novel prevention strategy to alert citizens when water is contaminated by estrogen. Epidemiological studies have shown that chronic exposure to high blood level of estrogen is associated with the development of breast cancer. The preventive strategy proposed in this paper is based on the prediction of estrogen effects on human living cells. Based on first principle insights, we develop in this work, a mathematical model for this prediction purpose. Dynamic measurements of cell proliferation response to estrogen stimulation were continuously monitored by a real-time cell electronic sensor (RT-CES) and used in order to estimate the parameters of the model developed.

Keywords: Water Protection, Early Warning, Estrogen, Mathematical Modeling, Parameter Estimation, Prediction

1. Introduction

Some chemicals, both natural and man-made, can interfere with endocrine glands and their hormones where the hormones act on the target tissues. These chemicals are called endocrine disruptors or endocrine disrupting chemicals (EDCs) [1]. EDCs induce harmful effects that have been observed on reproduction, growth and development in certain species of wildlife and it has been proven that there are increases in some human reproductive disorders and some cancers which could be related to disturbance of the endocrine system. Estrogen and estrogen-like chemicals are a major part of EDCs.

Estrogen is essential for life and its major biological function is modulating a woman's reproductive process. Estrogen affects the reproductive tract, the urinary tract, the heart and blood vessels, bones, breasts, skin, hair, mucous membranes, pelvic muscles and the brain. Secondary sexual characteristics, such as pubic and armpit hair also begin to grow when estrogen levels rise. Many organ systems including the musculoskeletal and cardiovascular systems and the brain are affected by estrogen [2]. In addition to its positive effects, however, unregulated quantity of estrogen may lead to health disaster due to its capacity to stimulate some tumors to grow. The epidemiological and in vitro studies have shown that chronic exposure to higher blood level of Estrogen is associated with the development of breast cancer [3].

While estrogen is present in both men and women, it is usually present at significantly higher levels in women of reproductive age [4]. Thus, the likelihood of women having a serious excess of estrogen-like substances in the body is much greater than for men. In addition to the natural presence of estrogen in human body, a number of EDCs including estrogen have been detected in environmental sources particularly in drinking water and food. Estrogen may exist accidentally in water due to rejection of detergents and birth control pills in water system and by adding pesticides [5].

The water contamination of EDCs is becoming highly publicized concerns. Therefore, we study in this paper the case where water is the source of estrogen and we develop a prevention strategy related to water protection. The ultimate objective is to develop an early warning system such that citizens are alerted as early as possible when water is contaminated by an excess of estrogen.

[1] The short version of this paper was presented in EPPH2009.

More precisely, an alarm is triggered when the concentration of estrogen exceeds certain value. This value is determined by studying a predicted human cells response to estrogen stimulation. This prediction is then used by medical experts in order to assess the biological consequences of estrogen in water contamination. In order to achieve this goal, an analytical system must be developed to accurately measure estrogen at very low levels and to identify its biological effects. The system should also provide dynamic information about biological effects that can be used to predict the biological consequences of the contamination in longer period. This analytical system is based on the predicted human cells response using mathematical modeling. The parameters of the proposed model are estimated using dynamic measurements. Theses measurements represent cell proliferation dynamic response to estrogen stimulation and have been accurately measured with a real-time cell electronic sensor (RT-CES) in our recent work. The RT-CES is widely used for many cell-based toxicity and stimulation assay in clinical laboratory and other related applications [7,8].

The prevention strategy proposed in this paper is based on mathematical modeling of cell population dynamic response to estrogen stimulation rather than modeling of contaminant molecules transport in water canalization system as usually done in other water prevention strategies such as in [9].

1.1. The Proposed Prevention Strategy

As mentioned previously, the goal of our proposed prevention strategy is to protect citizens as early as possible when water is contaminated by estrogen. This goal is achieved by building a prediction strategy which gives us early information about the effect of estrogen on human cells in a dynamic fashion. The early information includes the following three prediction features:

1.1.1. Prediction of Cell Response to Estrogen Stimulation of Different Doses

The dynamic cell response to estrogen stimulation shows different patterns when changing the estrogen concentration. The prediction of cell response to different estrogen doses stimulation helps the medical experts to decide whether the concentration level of estrogen exceeds the allowed limit. For this prediction purpose, we develop a mathematical model for describing the estrogen effect on human cell. To obtain a dynamic model, one usually needs to determine the model structure using fundamental principles and then estimate the model parameters. The parameter estimation procedure is evolved using the least squares approach which looks for parameters that minimize the integral of the squared prediction error. The prediction error is the difference between the mathematical model output and the dynamic measurements which may be provided by a suitable sensor such as the Real-Time Cell Electronic Sensor (RT-CES).

1.1.2. Fast Determination of Estrogen Concentration

Using modeling strategy, we provide the possibility of determining the concentration of estrogen using only small part of cell response measurements. This allows medical experts to determine an estrogen concentration without waiting for collecting all possible measurements responses. This feature helps in the case where an early determination of the concentration is needed.

1.1.3. Future Prediction of Cell Dynamic Response to Different Estrogen Doses Stimulation

This feature helps medical experts to decide early whether an alert needs to be triggered using only short time measurements. Using only initial data, a local (intermediate) model is identified on-line to predict future evolution of cell response under different estrogen doses stimulation. We refer to this model as local (intermediate) because it is identified from specific initial dynamic response and used to predict its future evolution.

The model developed for the first prediction feature is considered as a universal or global one because it is identified off-line from complete time-history data and validated for predicting cell proliferation response to different estrogen concentrations as well as being used in the second prediction feature for rapid determination of estrogen concentration. The model determined from the third feature is considered as a local model.

Due to the fact that our prevention strategy is based on mathematical modeling framework, it is necessary to discover the related existing modeling strategies. We look for methods to describe estrogen effects on cells population dynamics. Unregulated exposure of cells to estrogen may lead to uncontrolled cells proliferation which is strongly related to cancer development. The description of estrogen effects on cells population dynamics belongs to tumor growth description area. Mathematical modeling of uncontrolled cells proliferation (tumor growth) has a long history [10]. One of the main objectives of such modeling is to find a way to optimize the antitumor therapy. At least three different phenomenological models have been proposed in the literature namely: the Logistic model, the Bertalanffy model and the Gompertz model [11]. The synthesis of these models is purely mathematical so that no biological insights are considered and there were several proposals to provide a biological rationale for these functions, as in [12] for instance, where the theory of cellular energy is used. In addition to the mathematical models mentioned above, the so-called two compartments cell dynamic model is proposed for tumor growth [13]. This model is based on knowledge about the cell cycle [14].

While our proposed prevention strategy is based on prediction of the effects of estrogen concentrations on

cell proliferation response, we need a mathematical model which includes a term that reflects estrogen concentration. None of the models proposed above has considered it. To the best of our knowledge, there exist no mathematical models in the literature that have this characteristic. As a result, we develop in this paper a mathematical modeling strategy that is able to reflect the effect of the concentration on cell proliferation response. This modeling strategy is based on some biological insights about the estrogen effects on the human cells as shown in Section 3.

The organization of this paper is as follows. The experiments procedure and the developed mathematical modeling approaches are presented in Section 2 and Section 3 respectively. Section 4 shows simulation results including model prediction validations. Discussion and concluding remarks are given in Section 5 and Section 6 respectively.

2. Material and Method

2.1. Experiment Setup

Equipments: The RT-CES system (ACEA Biosciences, CA, U.S.A.) used for this study is set up in Alberta Laboratory for Environment and Cancer Risk Assessment (ALECRA) and was described previously in [7]. Briefly, it consists of a 16x microelectronic sensor devices having 16 plastic wells in microtiter plate format, a device station and an electronic sensor analyzer. Cells are grown onto the surfaces of microelectronic sensors. In operation, the sensor devices with cultured cells are mounted to a device station placed inside a CO2 incubator. Electrical cables connect the device station to the sensor analyzer. Under the control of RT-CES software, the sensor analyzer automatically selects wells to be measured and continuously conducts measurements on wells. The electronic impedance can then be transferred to a computer and recorded. A schematic diagram of the instrument (RT-CES) is shown in Figure 1.

A parameter termed cell index (CI) is derived to represent cell status based on the measured electrical impedance. The frequency dependent electrode impedance (resistance) without or with cells present in the wells is represented as $R_b(f)$ and $R_{cell}(f)$, respectively. The *CI* is calculated by:

$$CI = \max_{i=1,\ldots,N}\left[\frac{R_{cell}(f_i)}{R_b(f_i)} - 1\right] \quad (1)$$

where *N* is the number of the frequency points at which the impedance is measured. Several features of the *CI* can be derived: 1) Under the same physiological conditions, if more cells attach onto the electrodes, the impedance value becomes higher, leading to a larger CI. If no cells are present on the electrodes or if the cells are not well-attached onto the electrodes, $R_{cell}(f)$ is the same as $R_b(f)$, leading to *CI*=0; Thus, *CI* is a quantitative measure of the number of cells attached to the sensors; 2) For the same number of cells attached to the sensors, changes in cell status, such as morphological change, may also lead to a change in *CI* .

In addition to cell numbers, the impedance also depends on the extent to which cells attach to the electrodes. For example, if cells spread, there will be a greater cell/electrode contact area, resulting in larger impedance. Thus, the cell biological status including cell viability, cell number, cell morphology and cell adhesion may all affect the measurements of electrode impedance that is reflected by CI on the RT-CES system. Therefore, a dynamic pattern of a given CI curve can indicate sophisticated physiological and pathological responses of the living cells to a given toxic compound [7].

Chemicals and Cell Cultures: Human glioma GH3 cell line (ATCC, USA) was maintained in F-12 Kaighhn's (F12K) media containing 10 % FCS, 100 $\mu g/mL$ penicillin and 100 units/mL streptomycin. The cells were culture at 37 C^o and 5 % CO2. Beta- Estrogen 17 acetate was purchased from Sigma-Aldrich Inc. (St Louis, USA).

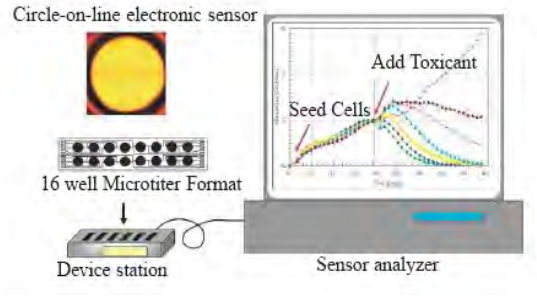

Figure 1. The real-time cell electronic sensor (RT-CES).

2.2. Experiment Method and Dynamic Growth with Estrogen Stimulation

GH3 was plated onto 16x sensor device at density of 8000/well in triplicate in F12K with 10 % FBS and cultured for 24 hours. Then the culture media was replaced with F12K without FBS. After 24 (hrs), two μl estrogen solutions with different concentrations were added into cell culture. The concentrations of estrogen at culture media were at range of 0.005 (nM) -1 (nM).
Figure 2 shows that the dynamic cell proliferation response to estrogen stimulation is dose dependant and increasing dose leads to increasing cell index (*CI*).

3. Model Development

As we mentioned in the introduction, the prevention strategy we develop is based on the predicted human

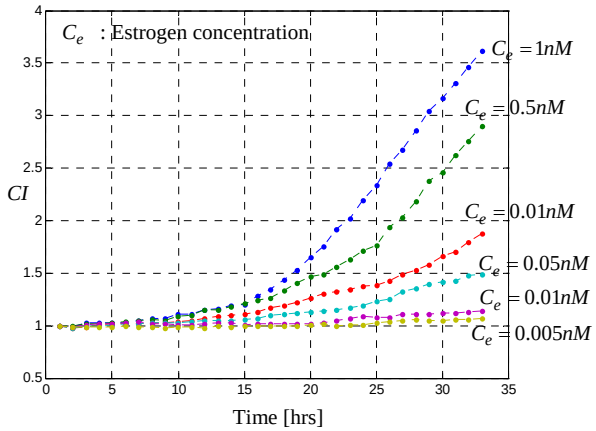

Figure 2. Dynamic proliferation response of GH3 cells to different doses of estrogen: 0.005; 0.01; 0.05; 0.1; 0.5; 1 [nM]. These data are measured by the real-time cell electronic sensor (RT-CES).

cells response to estrogen stimulation. A mathematical model which is able to predict this response is then needed. In order to build this mathematical model, we explore in the next section some biological insights which describe the estrogen transport mechanism from outside to inside the cell and which quantify the estrogen stimulative effects on cells. With biological insights, following the approach of [6] the model structures can then be determined. Experiment data from RT-CES such as the ones shown in Figure 2 can be used to fit the model parameters.

3.1. Estrogen Transport and Stimulative Effects

Estrogen circulates in the bloodstream and enters target cells by a non-energy-dependant process and the cell membrane provides a favourable lipid-rich environment for passage of estrogen by passive diffusion [15]. When estrogen enters a cell, it binds to high-affinity intracellular receptors (Figure 3). An estrogen receptor is a protein molecule found inside those cells that are targets for estrogen action. Estrogen receptors contain a specific site to which only estrogens (or closely related molecules) can bind [15]. The target tissues affected by estrogen molecules all contain estrogen receptors; other organs and tissues in the body do not. Therefore, when estrogen molecules circulate in the bloodstream and move throughout the body, they exert stimulative effects (cell proliferation) only on cells that contain estrogen receptors. From this introduction, we can hypothesize that a mathematical modeling strategy which reflects the effect of the estrogen concentration on cell proliferation response may consider two mechanisms, namely, the mechanism of estrogen transport into cell and the stimulative mechanism of estrogen inside the cell. Mathematical modeling of both mechanisms is presented next.

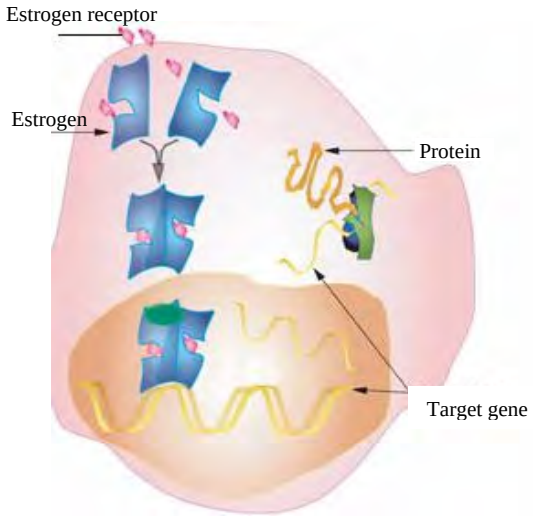

Figure 3. A schematic [16] of an estrogen target cell (breast, uterine, liver, etc).

3.1.1. Mathematical Modeling for Estrogen Transport Mechanism

The cell membrane functions as a semi-permeable barrier, allowing some molecules to cross it while fencing others outside the cell. This means that estrogen concentration outside the cell (refereed to as extracellular concentration c_e) is not at immediate equilibrium with estrogen concentration inside the cell (refereed to as intracellular concentration c_i) and a passive diffusion process takes place [15].

On the other hand, in a related area of pharmacokinetics and pharmacodynamics where the effect of drug is of main interest, it was accepted that passive diffusion transport of a toxicant (Doxorubicin) is described by relating the extracellular and the intracellular concentration by the following pharmacokinetic model [17]:

$$\frac{dc_i}{dt} = k_1\left(k_2 c_e + \frac{k_3 c_e}{k_4 + c_e} - c_i\right) \qquad (2)$$

In this equation, the dynamics of the intracellular concentration are a combination of a linear diffusive component and a saturable, carrier-mediated component (Michaelis-Menten like kinetics). The parameters k_1, k_2, k_3, k_4, are positive and constant. Due to the fact that estrogen enters cell by passive diffusion, we can assume that estrogen transport mechanism into the cell may be described by Equation (2).

3.1.2. Mathematical Modeling for Estrogen Stimulative Effects

As mentioned previously, when estrogen enters a cell, it binds to intracellular receptors and then starts exerting stimulative effects leading to cell proliferation. By observing the related experiment shown in Figure 2, we can conclude that the proliferation rate is proportional to es-

trogen concentration. In addition, due to the presence of the receptors inside the cell, the intracellular concentration c_i stimulates cell proliferation rather than the extracellular concentration. Mathematically, the proportionality of the cell proliferation rate to the intracellular concentration of estrogen can be expressed as follows:

$$\frac{dN}{dt} = kN + f(c_i) \tag{3}$$

This equation is inspired from cell population dynamics under toxicity effect given by [18]:

$$\frac{dN}{dt} = k_1 N - k_2 N c_i \tag{4}$$

where N is cell population, kN is proliferation rate and $k_2 N c_i$ is cell killing rate which we replace by the function $f(c_i)$ in the Equation (3). The function $f(c_i)$ represents a term which reflects the effect of intracellular estrogen concentration on cell proliferation rate.

3.1.3. Mathematical Modeling for Cell Proliferation Dynamic under Estrogen Stimulation

As mentioned above, we aim to develop a prevention strategy when water is contaminated by estrogen. This prevention straggly is based on predicted cell proliferation response to estrogen stimulation. A mathematical model which reflects the extracellular concentration of estrogen in water and relates it to cell population dynamics is needed. Putting together the transport equation (Equation (2)) and the cell population dynamic equation (Equation (3)), we obtain the desired model:

$$\frac{dc_i}{dt} = k_1\left(k_2 c_e + \frac{k_3 c_e}{k_4 + c_e} - c_i\right)$$

$$\frac{dN}{dt} = k_5 N + f(c_i) \tag{5}$$

The remaining step is to know in which manner the intracellular concentration affects the proliferation rate, i.e. how to choose the function $f(c_i)$? We may consider that this function is an unknown non-linear function. As a second order approximation, it is found the following structure is appropriate:

$$f(c_i) = k_6(c_i^2 + c_i + 1)$$

where the parameter k_6 must be constant and set to be positive in order to ensure the proportionality between cell proliferation dynamics and the intracellular concentration as observed from the related experiments (Figure 2). This approximation is chosen after several structure search steps based on experiment data and we concluded that using this approximation provides better results than using other general functions such as $f(c_i) = k_6 c_i^{k_7}$ or $f(c_i) = k_6 c_i^2 + k_7 c_i + k_8$ for instance. The criterion of the structure search is based on the confidence intervals of the parameters determined from the experiment data. Simulation results will demonstrate the success of this choice. The calculation of the confidence intervals of the model parameters is necessary in order to have an idea on the quality of the estimation. The derivation of the confidence interval is presented in the next section.

3.1.4. The Confidence Interval

In order to have a measure of the overall quality of the estimation and the uncertainty associated with a specific estimate, one needs to calculate the confidence intervals of the estimated parameters. A confidence interval is a region around an estimated value, and the true value of the parameters will be in this region with a confidence or probability of $100*(1-\alpha)$ (α is the significance level).

Consider the model (5). Let a state vector be expressed as $X = [x_1 \quad x_2]^T = [c_i \quad N]^T \in R^{2\times 1}$ and let the parameters vector be expressed as $\Theta = [k_1, ..., k_6] \in R^{6\times 1}$. The model (5) may be written in a compact form as:

$$\dot{X} = G(X,\Theta) \quad where \quad G(X,\Theta) = \begin{bmatrix} g_1(X,\Theta) \\ g_2(X,\Theta) \end{bmatrix} = \begin{bmatrix} k_1\left(k_2 c_e + \frac{k_3 c_e}{k_4 + c_e} - x_1\right) \\ k_5 N + f(c_i) \end{bmatrix} \tag{6}$$

with the observation equation :

$$y = f(X,\Theta) \quad where \quad f(X,\Theta) = N \tag{7}$$

The confidence interval for a parameter k_j is given by:

$\hat{k}_j - t_{\alpha/2}\sqrt{\sigma^2 C_{jj}} \le \hat{k}_j \le \hat{k}_j + t_{\alpha/2}\sqrt{\sigma^2 C_{jj}}$ where $j \in \{1, ..., 6\}$ is the parameter index and $t_{\alpha/2}$ is the critical value which equal to 1.960 for a 95% confidence interval [19].

The variance matrix C and the standard error σ are given by:

$$C = (J^T J)^{-1}; \quad \sigma^2 = \frac{\sum_{i=1}^{n}(y_i - \hat{y}_i)^2}{n - p}$$

where n is the number of data points and p is the number of the parameters.

J is the sensitivity matrix which is given by :

$$J = \frac{\partial y}{\partial \Theta} = \left[\frac{\partial y}{\partial k_1} \quad ... \quad \frac{\partial y}{\partial k_6}\right] \quad \text{where} \quad \frac{\partial y}{\partial k_j} = \frac{\partial f(X,\Theta)}{\partial k_j} + \frac{\partial f(X,\Theta)}{\partial X}\frac{\partial X}{\partial k_j}; \; j \in \{1, ..., 6\} \tag{8}$$

$$\frac{\partial f(X,\Theta)}{\partial k_j} = 0; \quad \frac{\partial f(X,\Theta)}{\partial X} = \left[\frac{\partial f(X,\Theta)}{\partial x_1} \; \frac{\partial f(X,\Theta)}{\partial x_2}\right] = [0 \quad 1]; \; j \in \{1, ..., 6\}$$

$$\frac{\partial X}{\partial k_j} = \begin{bmatrix} \frac{\partial x_1}{\partial k_j} \\ \frac{\partial x_2}{\partial k_j} \end{bmatrix} = \begin{bmatrix} s_{1_j} \\ s_{2_j} \end{bmatrix} \Rightarrow \quad \frac{\partial y}{\partial k_j} = 0 + [0 \quad 1]\begin{bmatrix} s_{1_j} \\ s_{2_j} \end{bmatrix}$$

$$= s_{2_j}; \; j \in \{1, ..., 6\}$$

The term $\frac{\partial X}{\partial k_j}$ represents the sensitivities of the state to the parameter k_j. The sensitivity matrix can be expressed by:

$$J = [s_{2_1}, ..., s_{2_6}] \quad (9)$$

On the other hand,

$$\frac{\partial \dot{X}}{\partial k_j} = \frac{\partial G}{\partial k_j} + \frac{\partial G}{\partial X}\frac{\partial X}{\partial k_j} \Rightarrow \frac{d}{dt}\left(\frac{\partial X}{\partial k_j}\right) = \frac{\partial G}{\partial k_j} + \frac{\partial G}{\partial X}\frac{\partial X}{\partial k_j} \Rightarrow \begin{bmatrix} \dot{s}_{1_j} \\ \dot{s}_{2_j} \end{bmatrix} = \frac{\partial G}{\partial k_j} + \frac{\partial G}{\partial X}\begin{bmatrix} s_1 \\ s_2 \end{bmatrix}$$

$$\dot{s}_{1_j} = \frac{\partial g_1}{\partial k_j} + \frac{\partial g_1}{\partial x_1} s_{1_j} + \frac{\partial g_1}{\partial x_2} s_{2_j} \; ; \quad s_{1_j}(0) = \frac{\partial x_1(0)}{\partial k_j} = 0 \quad (10)$$

$$\dot{s}_{2_j} = \frac{\partial g_2}{\partial k_j} + \frac{\partial g_2}{\partial x_1} s_{1_j} + \frac{\partial g_2}{\partial x_2} s_{2_j} \; ; \quad s_{2_j}(0) = \frac{\partial x_2(0)}{\partial k_j} = 0 \quad (11)$$

In order to calculate the sensitivities s_{2j}, which is necessary for calculation of the sensitivity matrix J, we solve the system equations (Equation (5)) together with the sensitivity equations (Equation (10)) and (Equation (11)).

4. Results

The results presented in this section demonstrate the ability of our proposed prevention strategy to meet the features mentioned in the introduction. For this purpose, we need to estimate the parameters of the proposed model (Equation (5)) from the experiments data provided by the RT-CES. These measurements represent cell population dynamics in response to different input concentrations of estrogen as shown in Figure 2. In our model identification procedure, part of these data is used for estimating the model parameters (for fitting) and the other part is compared to the predicted output of the proposed model for validation. The choice and the number of the data points used in the estimation procedure is done according to the requested biomedical scenario as mentioned in the introduction.

4.1. Prediction of Cell Response to Estrogen Stimulation of Different Doses

As we mentioned previously, the first feature of our proposed preventive strategy is the ability to predict cell response to different estrogen concentrations. The objective of this scenario is to validate the model developed as shown in Equation (5). This validation is also a demonstration of the first feature for the preventive strategy.

We use three sets of data shown in Figure 2 which correspond to [1 0.1 0.01] (nM) estrogen concentration for estimating the model parameters. Using three sets of measurements is equivalent to using 99 data points. The remaining three sets of data corresponding to [0.5 0.05 0.005] (nM) estrogen concentration are used to validate the model. The parameter estimation procedure results in the parameters values and their confidence intervals which are presented in Table 1.

It was noticed during the parameter estimation procedure that the optimizer sets the parameter k_5 to zero. This adds to our biological insights about the process that the

Table 1. The model estimated parameters.

95% confidence interval lower bound	$\hat{k}$	95% confidence interval upper bound
0.00417	0.0088	0.01343
6.16294	16.8546	27.54626
13.90592	26.5167	39.12747
0.00778	0.02575	0.04372
-0.00019	0.0003	0.00079

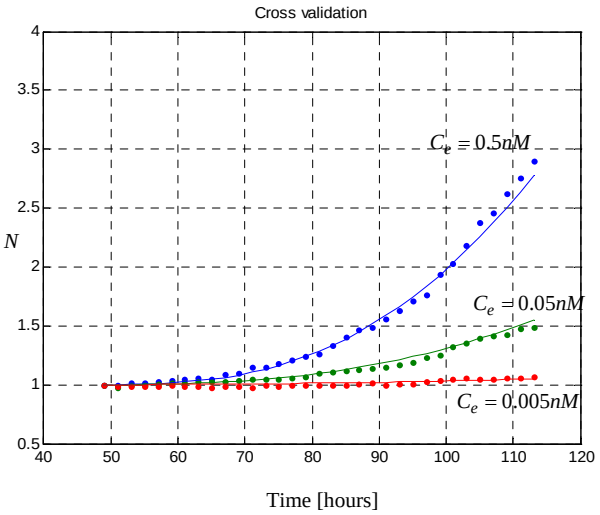

Figure 4. The model (5) with the estimated parameters (Table 1) predicts three sets of data corresponding to [0.5 0.05 0.005] (nM) estrogen concentrations. These data were not used in parameter estimation procedure. This demonstrates the ability of the model to predict cell proliferation response when concentration varies.

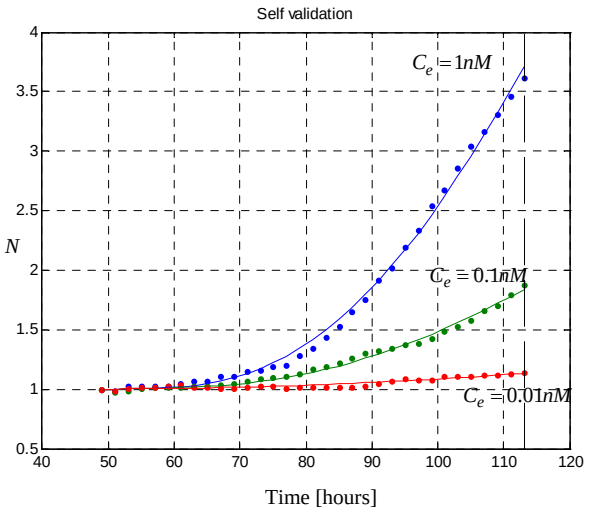

Figure 5. The model (5) fits the three sets of data corresponding to [1 0.1 0.01] (nM) estrogen concentration. These data are provided by the real-time cell electronic sensor RT-CES and used to estimate the model parameters presented in Table 1.

cell proliferation rate depends only on the intracellular concentration and not on the population variable N itself. This leads us to consider that the estrogen stimulation effect should be represented by the following model instead:

$$\frac{dc_i}{dt} = k_1\left(k_2 c_e + \frac{k_3 c_e}{k_4 + c_e} - c_i\right)$$

$$\frac{dN}{dt} = k_6(c_i^2 + c_i + 1) \qquad (12)$$

The prediction performance of the proposed model using the estimated parameters in Table 1 is presented in Figure 4 and Figure 5. In Figure 5 the proposed model fits the data which is used in parameter estimation phase. In Figure 4 the model predicts the remaining data which does not participate in model fitting. These validations demonstrate the ability of the model to predict cell proliferation response when concentration varies.

4.2. Rapid Determination of Estrogen Concentration

In this scenario, we use the model (5) with the estimated parameters presented in Table 1 to estimate estrogen concentration from short term measurements. The concentration is treated as an unknown parameter for the model and is estimated from a short period of response. Examples of these concentrations correspond to 0.5 (nM) and 0.005 (nM).

As shown in Figure 6, the proposed model is able to provide an estimation of the concentration that equals to 0.512, which is close to the real value 0.5 (nM), within 88 hours. Figure 7 shows that the model is also able to provide an estimation of the concentration that equals to 0.047 (nM) within 84 hours, which is close to the real value 0.05 (nM). This scenario provides the second feature of our preventive strategy which helps in the case where an early determination of the concentration is needed.

4.3. Future Prediction of Cell Response to Different Estrogen Doses Stimulation

In this scenario, we identify a set of parameters for the model (5) using short time measurements. The objective is to predict the future evolutions of cell responses based on the initial response. The purpose of this scenario is to provide the third feature of the proposed prevention strategy which helps medical experts to decide early whether an alert needs to be triggered using only short time measurements. We refer to this model as local or intermediate model and it is identified on-line after collecting some initial response data and then the model is used to predict the future evolution. This model is only

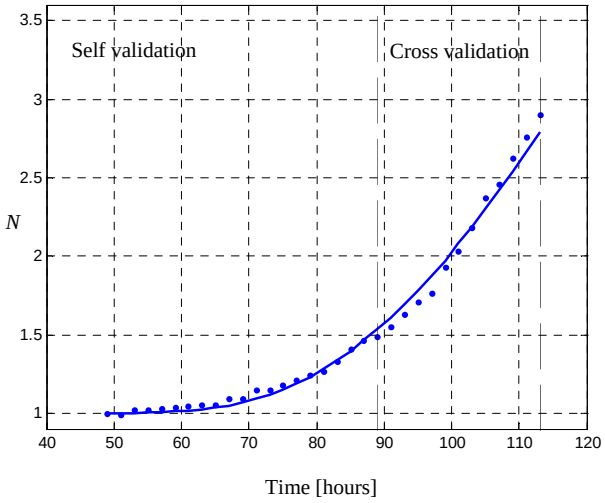

Figure 6. The model (5) is able to provide a close estimation of the concentration using short time data (up to 88 [hr]). The real concentration value equals to 0.5 (nM) and the estimated value equals to 0.512 (nM).

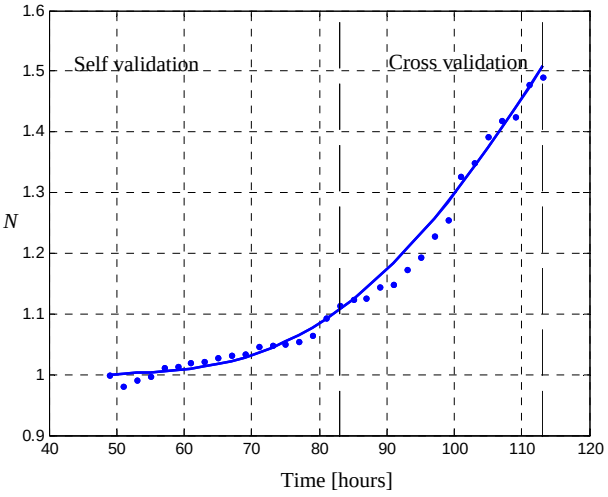

Figure 7. The model (5) is able to provide a close estimation of the concentration using short time data (up to 84 [hr]). The real concentration value equals to 0.05 (nM) and the estimated value equals to 0.047 (nM).

Table 2. The model estimated parameters.

95% confidence interval lower bound	$\hat{k}$	95% confidence interval upper bound
0.00006	0.00732	0.01458
6.38188	20.42131	34.46075
14.87463	45.89356	76.91249
0.02363	0.0334	0.04317
-0.00002	0.00017	0.00037

for prediction purpose and the values of the estimated parameters vary with different length of data used, also

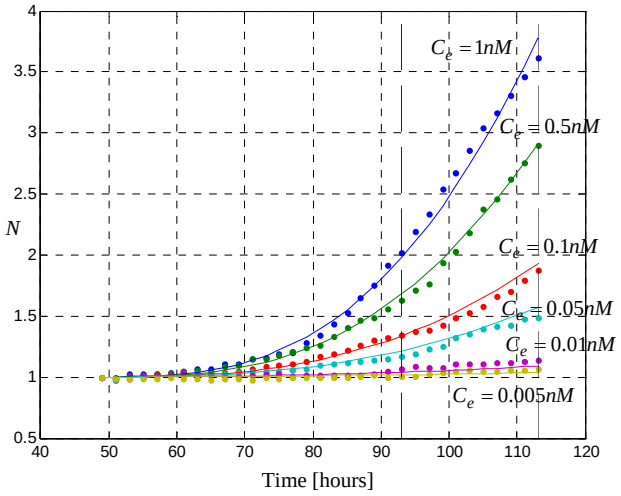

Figure 8. Using only a part of history data (up to 92 [hr]); a set of parameters is estimation (Table 2). Using this set of parameters, the model (5) is able to predict the future evolution.

known as adaptive estimation. As an example, using short time data (up to 92 [hr], which is equivalent to 138 data points) in parameter estimation procedure, we obtain the parameters values and their confidence intervals shown in Table 2.

Figure 8 shows that, using the set of estimated parameters presented in Table (2) for the model (5), the model is able to predict the future evolution of the data starting from $t = 92$ (hrs).

5. Discussions

The strategy presented in this paper has three main features which represent real scenarios in an early warning context. We have successfully achieved the objective through mathematical modeling and prediction based on data obtained from RT-CES experiments.

The heart of our prevention strategy is the mathematical modeling and prediction. Therefore the success of this strategy depends on the quality of the used model. The model we developed (Equation (5)) is able to provide a good cross validation with several choices of $f(c_i)$. However only the structure $f(c_i) = k_6(c_i^2 + c_i + 1)$ provides a reasonable confidence interval as shown in Tables [1,2]. Therefore in Section 3 we pointed out that this approximation is chosen after several structure search steps and the criterion for this structure search is based on the confidence intervals of the parameters determined from the experimental data. All other terms of the model are derived directly from fundamental biological insights. More understanding of the cell stimulation mechanism by estrogen doses will lead to a more precise expression of $f(c_i)$. However, in absence of such deep knowledge so far, data-based structure search is the best choice.

6. Conclusions

The main contribution of this work is the development of a prevention strategy composed of three prediction features for water protection area. This strategy is based on mathematical models. Theses models are able to describe estrogen effects on human cell dynamic response and they are cross validated using data which is not used in the model identification phase. The calculated confidence intervals of the parameters for the developed models show a good estimation quality.

The ultimate objective of our prevention strategy is to protect citizens as early as possible when water is contaminated by estrogen. This strategy is composed of three prediction features, namely, prediction of cell response to different stimulations of estrogen concentration, early determination of estrogen concentration and prediction of future evolution of cell response using short time measurements.

It is important to mention that the proposed strategy is not limited to the case when water is contaminated by estrogen. The same methodology may be adopted when water is contaminated with other toxins. The work presented here is our first step toward building a high performance early warning system for water protection.

7. Acknowledgment

The authors gratefully acknowledge the support of the Natural Sciences and Engineering Research Council of Canada (NSERC), Alberta Health (Water for Life Project) and Alberta Laboratory for Environment and Cancer Risk Assessment (ALECRA).

8. References

[1] J. S. Patrick, J. A. Franklin, and J. J. C. James, "The environmental science of drinking water," ISBN-13: 978−0−7506−7876−6, 2005.

[2] K. N. Rajesh, "Endocrine disruptors: Effects on male and female reproductive systems," CRC Press, 1st Edition ISBN-10: 0849331641, 1999.

[3] P. Lemieux and S. Fuqua, "The role of the estrogen receptor in tumor progression," The Journal of Steroid Biochemistry and Molecular Biology, Vol. 56, No. 87−91, 1996.

[4] R. A. Hess and K. Carnes, "The role of estrogen in testis and the male reproductive tract: A review and species comparison," Animal Reproduction, Vol. 1, pp. 5−30. 2004.

[5] M. L. Johnson, A. Salveson, L. Holmes, M. S. Denison, and D. M. Fry, "Environmental estrogens in agricultural drain water from the central valley of California," Journal Bulletin of Environmental Contamination and Toxicology, Vol. 60, pp. 609−614, 1998.

[6] B. Huang and J. Z. Xing, "Dynamic modeling and

prediction of cytotoxicity on microelectronic cell sensor array," Canadian Journal of Chemical Engineering, Vol. 86, pp. 393−405, 2006.

[7] J. Z. Xing, L. Zhu, J. A. Jackson, S.Gabos, X. J. Sun, X. B. Wang, and X. Xu, "Dynamic monitoring of cytotoxicity on microelectronic sensors," Chemical Research in Toxicology, Vol. 18, pp. 154−161, 2005.

[8] J. Z. Xing, L. Zhu, S. Gabos, and L. Xie, "Microelectronic cell sensor assay for detection of cytotoxicity and prediction of acute toxicity," Toxicology in Vitro, Vol. 20, pp. 995−1004, 2006.

[9] T. M. Brosnan, "Early warning monitoring to detect hazardous events in water supplies," In An ILSI Risk Science Institute Workshop Report, 1999.

[10] R. P. Araujo and D. L. S. McElwain, "A history of the study of solid tumour growth: The contribution of mathematical modeling," Bulletin of Mathematical Biology, Vol. 66, pp. 1039−1091, 2004.

[11] F. Kozusko and M. Bourdeau, "A unified model of sigmoid tumour growth based on cell proliferation and quiescence," Cell Proliferation, Vol. 40, pp. 824−834, 2007.

[12] P. Castorina and D. Zappala, "Tumor gompertzian growth by cellular energetic balance," Physica A, Vol. 365, pp. 473−480, 2006.

[13] J. C. Panetta, "A mathematical model of breast and ovarian cancer treated with paclitaxel," Mathematical Bioscience, Vol. 146, pp. 89−113, 1997.

[14] M. Eisen, "Mathematical models in cell biology and cancer chemotherapy," Springer 30, New York, 1979.

[15] P. F. Lebowitz and S. M. Swain, "Cancer chemotherapy and biotherapy: Principles and practice," Fourth Edition, Hormonal Therapy for Brest Cancer, Lippincott Williams and Wilkins, New York, pp. 809−838, 2006.

[16] "Lawrence livermore national laboratory exploring the link between diet and cancer," https:// www.llnl.gov/ str/ December05/ Kulp.html.

[17] A. W. El-Kareh and T. W. Secomby, "Two-mechanism Peak concentration model for cellular pharmacodynamics of doxorubicin," Neoplasia, Vol. 7, pp. 705−713, 2005.

[18] R. E. Eliaz, S. Nir, C. Marty, and F. C. Szoka, "Determination and modeling of kinetics of cancer cell killing by doxorubicin and doxorubicin encapsulated in targeted liposomes," Cancer Research, Vol. 64, pp. 711−718, 2004.

[19] K. D. Bird, "Analysis of variance via confidence interval," ISBN 0 76196357, SAGE Publication, 2004.

J. Water Resource and Protection, **2009, 1, 345-350**
doi:10.4236/jwarp.2009.15041 Published Online November 2009 (http://www.scirp.org/journal/jwarp)

Discussion on Role of Forest to Control Agricultural Non-Point Source Pollution in Taihu Lake Basin-Based on Source-Sink Analysis

Jianfeng ZHANG[1], Jingmin JIANG[1*], Zhijian ZHANG[2], Qihua SHAN[1], Guangcai CHEN[1], Ying WANG[1], Yonghui XU[3], Harry WU[4], Aljoy ABARQUEZ[4]

[1]*Institute of Subtropical Forestry, Chinese Academy of Forestry, Fuyang, China*
[2]*International Centers for Bamboo & Rattan, Beijing, China*
[3]*Yixing Forestry Technology Extension Station, Yixing, China*
[4]*CSIRO Plant Industry, Canberra, Australia*
E-mail: *jmjiang*6001@126.*com*
Received August 21, 2009; *revised September* 4, 2009; *accepted September* 12, 2009

Abstract

Taihu Lake is located at the center of Changjiang delta region, the Lake and its effluent rivers are important water sources for 40 million around inhabitants and rapidly increasing industrial factories in Shanghai, Jiangsu and Zhejiang. The pollutants originate mainly from acidy rain, home sewage of the vast number of inhabitants, livestock manure, agricultural fertilizers & pesticides applied over fields in the drainage basin, and the industrial sewage. Due to the kinds of pollutants, the Lake water is getting highly eutrophic, with frequent blooms of blue-green algae. Compared with point-source pollutants, diffuse pollution is much complicated and difficult to control. Thus combating non-point pollution (NPP) is paid much great attention. Based on analysis on source-sink of NPP in Taihu Lake basin, it is concluded that the function of forests on NPP control is multiple and important by both source reduction and sink expansion. The primary objective of planting trees through constructing forested wetlands and establishing riparian forest buffers is to control soil & water erosion, decrease agrochemicals application, and improve farming conditions in the region of Taihu Lake basin. Moreover forests help to intercept acidy rain, protect streambanks, uptake nutrients, hold up pollutants and provide habitat for wildlife.

Keywords: Non-Point Source Pollution, Riparian Forest Buffer Zone, Source-Sink, Taihu Lake

1. Introduction

The Taihu Lake basin has an area of 36 500 km^2, located in three provinces and one municipality. The percentage in Jiangsu, Zhejiang, Anhui provinces and Shanghai is 52%, 33.4%, 13.5% and 0.1% respectively. The water area in the lake basin accounts for 17.5% of the entire lake area [1]. The Lake has the multifunction of flood-water storage, irrigation, navigation, water supply, aquaculture, and tourism. It is the main drinking water source for 40 million residents for areas such as Wuxi and Suzhou and people in neighboring Shanghai and Zhejiang. The Lake also is famous for its abundant production of fishes and crabs, and the aquaculture farms on the coast that apply skillful techniques [2].

The region along Taihu basin was developed very earlier owing to the kind natural conditions (Table 1), which was called "Kingdom of fishing & farming".

Also the vegetation resources were abundant there. Types of important forest (main species of trees): Pine forest (*Pinus massoniana*); bamboo forest (*Phyllostachys pubescens*); mixed evergreen-deciduous scrub. Types of important herbaceous vegetation: Swampy grassland of reeds and other emerged water plants on the lake shore and along water courses. Main kinds of crops: Rice (single or double cropping), wheat, rapeseed, tea, mulberry, fruit trees (peach, orange, loquat, myrica, plum, Japanese apricot (*Prunus mume*), jujube) [3].

In addition to supporting heavy boat traffic, Taihu provides some of the best known water-side scenery in China for domestic and foreign sightseeing visitors. Hence the urbanization level of the lake basin ranks the first in the entire country.

However, due to the excess consumption of resources

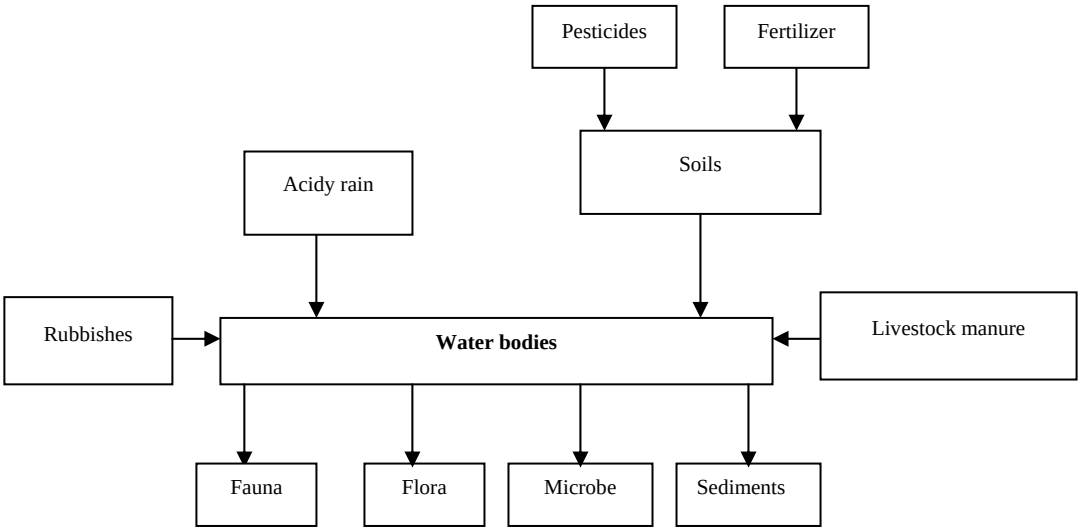

Figure 1. Source-sink of non-point agricultural pollution in Taihu lake basin.

Table 1. Natural conditions in Taihu basin.

Longitude: E 116°28'--123° Latitude: N 23°33'--32°08'	
Elevation (meters above sea level): 3.1-4.5 m above sea level	
Rainfall:	
	Mean annual Rainfall (mm): 974mm
	Months of Highest Rainfall: June 156mm
	Months of Lowest Rainfall: January 38mm
	Other notes on Rainfall (re: fog, snow, and/or other forms of precipitation): few snow; sometimes storm in summer
Temperature:	
	Mean Annual Temperature: 15.6^0C
	Months of Highest Temperature: July 29.9^0C
	Months of Lowest Temperature: January $2.9\ ^0$C
	Other notes on Temperature: hot summer(June, July and August)
Soil:	
	Depth to parent material:1-5m
	pH:6.2-8.0
	Colour: brown
	Texture: sand-loam
	Geological Origin: flooding
	Other notes on Soil: in some parts paddy soil
Exposure to Sunlight:	2000hr annually
Terrain:	
	Slope Steepness (% or degrees): plain area, $0\text{-}5^0$
	Drainage: not so heavy
	Depth of water table: 0.5-3m

for the regional socioeconomic development, forest coverage fell from 17% in 1950s to 13% 1980s, wetland area reduced more than 40% with land transition, averagely decreased 1469 ha annually among 1950-1985. With forest felling, soil erosion got worsen, and farm ecosystem was damaged. While wetland reduced, buffer zone disappeared, and pollutants went into rivers & lakes directly. Consequently the eco-environment has been drastically deteriorated. In the period of 1981-2000, TP increased 25.0% annually in the Lake, TN was 11.7%, and COD was 4%-6%. From 80's in last century, the water quality of Taihu Lake has descended one grade every 10 years, and now, it has become a typical area where is lacking qualified water [4]. According to Chinese General Station of Water Environmental Monitoring, water quality state was shown as Table 2.

Although the government attached importance to the water pollution treatment and takes many measures,

Table 2. Water quality state in Taihu (August 17-23).

Location	Profile	pH	DO (mg/l)	COD (mg/l)	NH3-N (mg/l)	Water quality grading
Shazhu, Wuxi	Lake body	8.14	6.46	2.80	0.28	Ⅱ
Lanshanzui, Yixing	Lake body	8.23	6.52	3.70	0.30	Ⅱ
Xishan, Suzhou	Lake body	7.44	4.69	4.90	0.23	Ⅳ

mainly focusing on point source pollution such as industrial waste water decontaminating, lake water clearing, and the water quality of Taihu Lake was still exasperate and the situation of water pollution was still austere. Especially the affair of blue-green algae bloom occurred in May 2007 sounded the alarm for the people and the government. It was really recognized that the risk and hazards of eutrophication. Therefore much more attempts should be put into the struggle. No doubt, the function of forests was significant in controlling non-point source agricultural pollution (NPP) in Taihu Lake basin.

2. Analysis on Source and Sink of Non-Point Agricultural Pollution

2.1. Framework of Source and Sink of NPP

For Taihu Lake basin the inflowing water comes mainly from mountains to the west and southwest of the lake, while the draining rivers start mostly from the east coast of the lake. Several rivers and channels connect the lake with Changjiang, but the water flux is controlled by dams to maintain the lake water level within a range of fluctuation of 2-3 m [1].

According to the source-sink theory, here source means inputs of pollutants, and sink indicates outputs of pollutants. In this basin source-sink of non-point agricultural pollution could be described as Figure 1.

It could be concluded from Figure 1 that the causes of water body pollution and eutrophication problem were complicated and multiple.

2.2. Components of the Source

According to the framework of source-sink of NPP as Figure 1 shown, the major agricultural NPP that resulting from these activities were acidy rain, livestock manure, fertilizers & pesticides, rubbishes & garbage. For these sources, to some extent acidy rain naturally occurred, while the others were concerned with human activities.

Located upstream of the Lake basin, Xitiaoxi river and Dongtiaoxi river both lied in Zhejiang province are recognized as the headwaters of the Lake. In the region local people live on the mountain range, planting bamboo and/or tea trees, cultivating grain or cash crops. During these farming activities, agrochemicals were applied, usually overused in order to have a good harvest and get much higher incomes. Moreover soils were often disturbed naturally. Thus when heavy raining or storm happening, water & soil erosion had to occur, and these soil nutrients finally flowed into the Lake passing through linked waters [3].

In a word, with rapid development of industry and the excess consumption of pesticides for agriculture, large amount of pollutants and nutrients like nitrogen and phosphorus were drained into surrounding channels and finally into the Lake, these materials caused an overgrowth of algae and further deterioration, including oxygen depletion, which resulted in the severe pollution.

2.3. Distribution of the Sink

As Figure 1 shown that the nutrients leading to eutrophication could be uptaken and/or digested by aquatic animals such as plankton, fishes, shrimps, aquatic plants or riparian forests which were naturally grown or planted. Nowadays some fries such as grass carp, chub, etc. often are put in rivers, lakes and reservoirs to purify water. On the other hand, around the watershed usually wetlands were established including aquatic plants such as duckweeds, buttercup, water lily, which were harvested annually to reduce nutrition content in water bodies. Sometimes a certain woody species were chosen and planted such as Nyssa aquatica, Liquidambar styraciflua, Quercus nuttallii, Carya illinoinensis Koch, Phyllostachys nigra, etc.

Meanwhile the microbe played an important role to consume nutrients and prevent alga from blooming [5]. Some compounds and elements, especially heavy metals, sinked into river bed or lake bottom and became sediments.

3. Function of Forests on NPP Controlling

3.1. Source Reduction

As discussed above for NPP controlling forests functioned actually on both source reduction and sink expansion.

3.1.1. Intercept Acidy Rain

With industry development and urbanization speeding up, acidy rain occurred widely and frequently on the earth, hurt waters and soils as well as forests and understory plants, became one of the important sources of NPP [5,6].

When acidy rain fell on a forest, a complex process began. Firstly, the tree canopy sheltered and nullified the impact effect of raindrops, reducing the rain to a thin mist below the canopy, even in the most torrential showers. There was slight measurable silt loss from mature forests, exceeded by the creation of soils by forests. If the rain was light, little of it penetrated beyond the can-

opy, but a film of water spread across the leaves and stems, and was trapped there by surface tension [7]. The cells of the tree absorbed what was needed, and the remainder evaporated to air.

In the stem bases of palms, plantains, and many epiphytes, or the flanged roots of figs, water was held as aerial ponds, often rich in algae and mosquitoes. Stem mosses and epiphytes absorbed many times their bulk of water, and the tree itself directed water via insloping branches and fissured bark to its tap roots, with spiders catching their share on webs, and fungi soaking up what they needed. Some trees trailed weeping branches to direct throughfall to their fibrous peripheral roots [8]. Through the interception of forests harmful effect of acidy rain on waters and soils were alleviated to some extent. In fact the degree of interception was most influenced by these factors: tree species, stand age, crown thickness, crown density, season, intensity of acidy rain, evaporation after rain [9].

3.1.2. Reduce Water & Soil Erosion

It was widely understood that water flow from rain and irrigation, as well as, clean cultivation and vacant field borders could increase erosion potential. However forests provided a barrier that could slow water flow and trap soil particles [10]. In forested land below the humus lies the tree roots, each clothed in fungal hyphae and the gels secreted by bacterial colonies. 30-40% of the bulk of the tree itself lied in the soil; most of this extends over many hectares, with thousands of kilometers of root hairs lying mat-like in the upper 60 cm of soil (only 10-12% of the root mass lied below this depth but the remaining roots penetrate as much as 40 m into the rocks below). The root mat actively absorbed the solution that water had become, transporting it up the tree again to transpire to air. This was especially useful along waterways, especially in slop fields [11]. In the context, trees could be planned in combination with other practices in order to develop complete conservation systems that enhanced landscape aesthetics, improve water quality and provided wildlife habitat. Well planned forest shelterbelts retain water and reduce evaporation by blocking drying winds in summer.

3.1.3. Decrease Chemical Fertilizer Application

Intercropping is a feasible and practical land use system in the basin region. Through long-term practice, it was found that many trees could harmoniously grow together with crops in the same field and at the same time, of which some could fix nitrogen, e.g. leguminous trees, enrich the soil when their residues decompose [12]. Trees also improved the soil conditions in other ways. Leaf litter decomposed and added tilth as well as nutrients to the soil. Even the root system, with its rhizobia and related communities of organisms, released nutrients and improved soil structure when it decomposed. Moreover some trees captured nutrients too deep in the soil for crops to reach, and brought these nutrients up to the surface and back to the soil as litter, where the crops could utilize them when the litter decomposed [13]. Furthermore, these deep roots could reduce the leaching of nutrients from soil following heavy rains and could conserve soil moisture by adding mulch and litters. By all the means, soil fertility could be maintained and generated naturally to help crops growing, less chemical fertilizers were applied to the fields [14].

3.2. Sink Expansion

As mentioned formerly there were different ways for pollutants output when eutrophication occurred in the water body. During the procedure of NPP combating constructing forested wetland and riparian forest buffer zone was significant for sink expansion.

3.2.1. Construct Forested Wetlands

The ecotones between lakes and terrestrial ecosystems were crucial for protection of the lake ecosystem against anthropogenic impact [15]. In view of the situation faced in Taihu Lake basin: population growing fast, surrounding lands mostly using for agriculture, construction of artificial wetlands was an attractive and cost-moderate solution to pollution by diffuse sources and even wastewater.

As Table 3 indicated, compared with the other type of wetland, forested wetlands were able to cope with the nitrogen and heavy metal pollution from these sources. It prevented, to a certain extent, penetration of undesirable components into the lake and protected the most vulnerable ecosystems, which were often lakes and reservoirs. The denitrification potential of wetlands was often surprisingly high. As much as 2,000 to 3,000 kg of nitrate-nitrogen could be denitrified per hectare of wetlands per year, depending on the hydraulic conditions [16]. This was of great importance for the protection of lakes, because a significant amount of nitrate was released by agricultural activities. As much as 100kg nitrate-nitrogen per hectare may be found in the drainage water from intensive agriculture.

It was essential to properly plan where to place the forested wetlands, as their effects were dependent on the hydrology (i.e., they should be covered by water most of the year and had a sufficient retention time to allow them to solve the considered and specific pollution problems), and on the landscape pattern.

As Jinlin Chen (2002) [17] did, the effect of forest on water environment protection was vital. When the width ratio of farmland to forest belt was 100 to 40, the purification effect on the losing nutrients was the best and 50.05% losing N, 29.37% losing P could be absorbed by forest under rape-rice rotation and 30.98% N, 86.73% P could be absorbed by forest under wheat-rice rotation.

Table 3. Characteristics of different type of wetlands adjacent to lakes.

Type of wetland	Characteristics	Ability to retain diffuse pollutants
Wet meadows	Grassland with waterlogged soil. Standing water for a part of the year.	Denitrification only in standing water. Removal of nitrogen and phosphorus by harvest.
Fresh water marshes	Reed-grass dominated, often with peat accumulation.	High potential for denitrification, which is limited by the hydraulic conductivity.
Forested wetlands	Dominated by trees, shrubs. Standing water not always for the entire year.	High potential for denitrification and accumulation of pollutants, provided that standing water is present.

Under this circumstance the purifying ability of water is very satisfactory. When the width ratio of farmland to forest belt was 150 to 40, 33.37% lost N, 19.58% lost P could be absorbed by the forest under rape-rice rotation, while under wheat-rice rotation 20.65%lost N and 57.82 % lost P could be absorbed. There was only some purification effect when the width ratio of farmland to forest belt was 200 to 40. According to the analysis, it was suitable when the width ratio of farmland to forest between 100 to 40 and 150 to 40, because it not only could purify water, but also occupy less farmland.

For species selection, besides trees such as *Nyssa aquatica*, *Liquidambar styraciflua*, *Quercus nuttallii*, the following emergent macrophyte species were proposed to be used in constructed forested wetlands: cattails, bulrush, reeds, rushes, papyrus, and sedges. Submerged species could be applied in deep-water zones [3]. Species that had been used for this purpose include coon tail or horn wart, redhead grass, widegeon grass, wild celery, and water milfoil.

3.2.2. Establish Riparian Forest Buffers

Generally speaking, riparian forest buffers were typically a band of trees, shrubs, herbaceous cover or grasses with a certain width along a stream bank. Such a band of vegetation could trap sediment and bacteria, and absorb nutrients from both polluted runoff and sub-surface flow.

Riparian forest buffers were typically on sites with fine soils because of their position on the landscape [5]. So that the riparian forest buffer design needed to not only provide environmental protection but also economic benefits such as mid to long-term products as farmers rely on the fields to live. For example some of the products that could be harvested following the end of the conservation incentives at age 10 or 15; included decorative woody floras or short rotation crops for fuel, fodder or paper pulp.

Certain combinations of trees, shrubs, and grasses could function effectively as nutrient and sediment sinked for NPP pollutants [17]. As a special land use system, the woodlot must be intentionally integrated with crops and/or livestock. It was ideal if the woodlot management included active management of both the overstory trees and some type of understory crop simultaneously to produce non-timber products. This was not just wild harvesting of some understory plants such as mushrooms, but was a very intentional management system. Many high-value non-timber forest crops e.g., ginseng, goldenseal, mushrooms, and decorative ferns were cultivated under the protection of a forest canopy that had been modified to provide appropriate microclimate and light conditions [13]. Meanwhile, the timber stand improvement activities were carried out to develop the appropriate understory conditions. For Example, thinning less desirable stems and pruning lower branches on the eventual crop trees could result in the production of clean, knot-free wood that would eventually bring a higher economic return [12].

Hence streamside buffer strips were an effective best management practice that would help make the agricultural landscape sustainable, and reduce non-point source inputs into surface waters, which in turn should produce improvements in surface water quality, aquatic habitat, and aquatic communities [18].

It was concluded that similar buffer strips should be established along both sides of any perennial or intermit tent stream, as well as around lakes and ponds in and near farming activities, to reduce the adverse effects of NPP on surface water quality and aquatic life.

4. Conclusions and Discussions

Located at the center of Changjiang delta region, the Taihu Lake and its effluent rivers are important sources of water for the inhabitants and rapidly increasing industrial factories in Shanghai, Wuxi, Suzhou and other neighboring cities, so that the pollution of the Lake is a serious social concern.

The pollutants originated mainly from acidy rain, home sewage of the vast number of inhabitants, livestock manure, agricultural fertilizers & pesticides applied over fields in the drainage basin, and the industrial sewage of more than 700 factories and mines. Due to the kinds of pollutants, the Lake water was getting highly eutrophic, with frequent blooms of blue-green algae even in early summer or late autumn annually. Compared with point-source pollutants, diffuse pollution was much complicated and difficult to control. Thus combating NPP was paid much great attention.

Based on analysis on source-sink of NPP in Taihu Lake basin, it was concluded that the function of forests on NPP control was multiple and significant.

In view of the fact in the area: more population, less land, approaching reasonable land use system was crucial to maintain regional socioeconomic sustainable development. It was proved intercropping was favorable for controlling soil erosion, increasing soil fertility and gaining higher benefit of the slope field by relatively low input [19]. Besides of this art, building riparian forest buffers along rivers around Taihu Lake also was significant to tackle agricultural NPS pollution in headwater region.

Widely applied forested wetlands had acted mainly as sources of a variety of wood and non-wood products, in addition to a kind of landscape. At present, the importance of wetlands for agricultural sustainability and environmental protection was becoming increasingly emphasized.

5. Acknowledgement

This research is one part of Jiangsu provincial Key Scientific & Technological Project (BE2009603 and BE2008636), National Scientific & Technological Project (No.2006BAD03A15), RISF6803 and AusAID project "Capacity building for riverhead forest conservation and integrated water resource management in China". We are grateful to all the supports.

6. References

[1] B. Q. Qin, "Hydrodynamics on Lake Taihu, China," Ambio, Vol. 26, No. 8, pp. 45−48, 1999.

[2] S. W. Chai, X. M. Pei, Y. L. Zhang, J. H. Li, and J. F. Zhao, "Research on agricultural diffuse pollution and controlling technology," Journal of Soil and Water Conservation, Vol. 20, No. 6, pp. 191−194, 2006.

[3] J. F. Zhang, M. Y. Fang, and S. Li, "Developing agroforestry in slopelands to combat non-point pollution in China," Chinese Forestry Science and Technology, Vol. 6, No. 4, pp. 67−72, 2007a.

[4] J. F. Zhang, **"**Agroforestry and its application in amelioration of saline soils in eastern China coastal region," Forestry Study in China, Vol. 6, No. 2, pp. 27−33, 2004.

[5] T. C. Daniel, A. N. Sharpley, and J. L. Lemunyou, "Agricultural phosphorus and eutrophication: A symposium overview," Journal of Environmental Quality, Vol. 27, No. 1, pp. 251−257, 1998.

[6] C, Gao, "Environmental management options practiced in Europe to mitigate agricultural nutrient pollution of ground and surface water," Agricultural Eco-environment, Vol. 51, No. 2, pp. 50−53, 1999.

[7] M. A. Altieri, "The ecological role of biodiversity in agroecosystems," Agriculture, Ecosystems and Environment, No. 74, pp. 19−31, 1999.

[8] J. Baudry, R. G. H. Bunce, and F. Burel, "Hedgerows: An international perspective on their origin, function and management," Journal of Environmental Management, No. 60, pp. 7−22, 2000.

[9] B. Deckers, M. Hermy, and B. Muys, "Factors affecting plant species composition of hedgerows: Relative importance and hierarchy," Acta Oecologica, No. 26, pp. 23−37, 2004.

[10] J. R. Archer and M. J. Marks, "Control of nutrient losses to water from agriculture in Europe," Proceeding of Fertilizer Society, Vol. 6, No. 5, pp. 405−409, 1997.

[11] J. F. Zhang and Q. X. Sun, **"**Review on agroforestry systems in China," Chinese Forestry Science and Technology, Vol. 4, No. 3, pp. 80−84, 2005.

[12] W. L. Zhang, S. X. Wu, H. J. Ji, and H. Kolbe, "Estimation of agricultural non-point source pollution in China and the alleviating strategies I: Estimation of agricultural non-point source pollution in China in early 21 century," Chinese Science of Agriculture, Vol. 37, No. 7, pp. 1008−1017, 2004.

[13] R. C. Schultz, "Agroforestry opportunities for the United States of America," Agroforestry Systems, No. 31, pp. 117−132, 1995.

[14] J. F. Zhang and G. H. Qin, "Poplar-based agro-forestry in China and its economic analysis," Shandong Science and Technology Press, 2007b.

[15] R. A. Young, "A non-point source pollution model for evaluating agricultural watershed," Journal of Soil and Water Conservation, Vol. 44, No. 2, pp. 168−173, 1989.

[16] J. L. Chen, L. L. Shi, and A. G. Zhang, "Controlling effects of forest belts on non-point source pollution of agricultural lands in Taihu Lake area, China," Journal of Forestry Research, Vol. 13, No. 3, pp. 213−216, 2002.

[17] S. de Blois, G. Domon, and A. Bouchard, "Factors affecting plant species distribution in hedgerows of southern Quebec," Biological Conservation, No. 105, pp. 355−367, 2002.

[18] D. Kleijn and M. Verbeek, "Factors affecting the species composition of arable field boundary vegetation," Journal of Applied Ecology, No. 37, pp. 256−266, 2000.

[19] A. G. Busck, "Hedgerow planting analyzed as a social system–Interaction between farmers and other actors in Denmark," Journal of Environmental Management, No. 68, pp. 161−171, 2003.

J. Water Resource and Protection, **2009, 1, 351-361**
doi:10.4236/jwarp.2009.15042 Published Online November 2009 (http://www.scirp.org/journal/jwarp)

ArcGIS-Based Rural Drinking Water Quality Health Risk Assessment

Fuquan NI[1,2], Guodong LIU[1], Jian YE[2], Huazhun REN[3], Shangchun YANG[2]
[1]*College of Hydraulic & Hydroelectric Engineering, Sichuan University, Chengdu, China*
[2]*College of Information & Engineering, Sichuan Agricultural University, Ya'an, China*
[3]*College of Hydrology & Water Resources, Hohai University, Nanjing, China*
E-mail: *nfq*1965@163.*com*
Received August 14, 2009; *revised September* 8, 2009; *accepted September* 14, 2009

Abstract

Aiming at the unsafe of water quality which is the core problem in rural drinking water safety, the study collected 221 water samples of rural drinking water sources in Ya'an and detected the concentrations of the carcinogen and the non-carcinogen. Based on the analysis of water environment characteristics and the identification of water environment health risk source of Sichuan Ya'an City, which includes seven counties and a district and is the typical region of the western margin of Sichuan Basin, this study calculated and analyzed the carcinogenic risk (R) and non-carcinogenic risk (hazard index, HI) by applying the health risk model recommended by the US National Research Council of National Academy of Science. Then, taking advantage of the geo-statistic spatial analysis function of ArcGIS, this study analyzed the assessment result data (R and HI), selected the proper interpolation approach and educed R and HI spatial distribution maps of the study area. R and HI of the single factor and integrate factors were evaluated and thus obtained the following conclusions: For one thing, the cancerous risk indexes of the vast majority of water sources (about 94%) is the level of 10^{-7} and it belong to the safety extension. The main carcinogen in the water sources are As, Cr^{6+} and Pb, their concentrations are in the ranges of 0.004-0.01, 0.005, 0.01mg/l respectively and such water source mainly distributed in Yucheng district and Mingshan county. For another, the non-cancerous hazard indexes of the vast majority of water sources (about 98%) is also less than the limit value 1 and will not harm the local residents. The health risk of non-carcinogen comes mainly from As and fluoride, their concentrations are in the ranges of 0.004-0.01 and 0.1-4.2mg/l respectively. The results of the integrate factors health risk assessment showed that the total cancerous risk were still at the level of 10^{-6}, only 12 drinking water source investigation sites (5%) exceeded the drinking water management standard value of EPA (the limit value is 10^{-6}); the total non-cancerous hazard indexes are still in the range of 10^{-2}-10^{-1}, and will not harm the local residents either, only 18 drinking water source investigation sites (8%) exceeded the drinking water management standard value of EPA(the limit value is 1).The densely populated areas such as Yucheng District, Tianquan County, Yingjing County and Shimian County are where the four contaminating materials, i.e., As, Cr^{6+}, Pb and fluoride should be monitored with emphasis. Study results disclosed the health risk control indexes of source water quality of the studied area and thus provided the scientific basis for the water quality control of water sources. This study had worked efficiently in practice. Compared with the same kind of methods which had been found, the paper had the outstanding results for the health risk assessment of the rural drinking water safety.

Keywords: Water Sources, Water Environment, Water Quality, Health Risk Assessment, Arcgis, Geo-Statistical Analysis, Ya'an City

1. Introduction

Nowadays, 90% of the cancer sufferers are caused by chemical carcinogens [1] and 80% of the diseases are attribute to the unsafe of drinking water in poverty-stricken areas. Nearly 25,000 people died of such water pollution problems everyday [2], and 1/3 of urban inhabitants in developing countries can not get safe drinking water [3]. In

China, over 70% rivers and lakes are suffering pollution in various degrees. Due to the high fluoride water, the high arsenic water, the brackish water, the water polluted by organic compounds, schistosome, etc, 36 million people could not get safe water. Among them, the toxic substances content of the drinking water of 19 million residents exceed standard [2].

The pollutants in the water can be classified into contaminants of biological origin, physical origin and chemical origin according to their properties [4]. The threat of drinking water quality safety comes mainly from chemical pollution [5]. The chemical pollutants can be divided into carcinogenic pollutants and non-carcinogenic pollutants according to their different perniciousness to human. U. S. EPA (United States Environmental Protection Agency), IARC (The International Agency for Research on Cancer) and USDOE（U. S. Department of Energy） provide a great many data about the perniciousness of chemical pollutants to human health [6−8].

It is essential to carry out total health risk assessment in the safety management of drinking water quality. Through the health risk degree assessment of drinking water source, the comprehensive conclusion of water source quality which is represented by the risk degree of health hazard can be got directly. So, the primary and secondary of the pollutants in waters and priority setting of governance can be determined [9]. Currently these studies are necessary and helpful to understand the problems of drinking water risk and their status, and then the priority in next step can be appropriately set. Clean drinking water is fundamental to the health and welfare of the world people. It is very important to prevent water any quality deterioration. Prevention of water pollution is more important and practical than the remediation of contaminated water. Water quality protection should start from the source, at catchments or watershed scale.

Diseases are closely related to the following factors, such as climate, environment, water quality and management, education, air pollution, natural disease, society and so on. It is extremely essential for the understanding and further study of human health and the spatial distribution of its influencing factors, and it is so helpful for health decision-making departments to adopt corresponding preplan and countermeasures that social stability can be ensured. Therefore, the application research of Geographic Information System (GIS) in health risk assessment has got more and more attention and application, especially from overseas [10−17]. Meanwhile, the majority of domestic researches are focused on the study of health risk analysis for urban water sources, rural water sources, sewage recharge, groundwater and so on. Most of these researches are uncomplicated application of the formula of health risk recommended by U.S.EPA, and the effect of uncertainly factors or the further research based on GIS are considered rarely [18−21].

This study took the seven counties and one district of Ya'an City as an example. Based on the analysis of testing result of 221 rural water sources and through the selection, source identification, pollution load monitoring of the pollutants which affect water source quality mostly and the epidemiological survey, the health risk assessment model recommended by U.S. National Research Council of National Academy of Science was applied to calculate and study the carcinogenic risk and non-carcinogenic risk of the items exceeding the standard value in the source water, such as fluoride, nitrate, Fe, Mn, As, Cr^{6+}, Pb, Cd, Hg, etc. By applying ArcGIS of ESRI（Environmental Systems Research Institute, any GIS that allows vector and raster processing would work) and this study also did the spatial interpolation analysis in accordance with the various calculated carcinogenic risk（R）and non- carcinogenic risk (hazard index, HI) of each water quality monitoring sites and formed a series of thematic maps about R and HI. The above mentioned research results provided reliable guarantee for the water quality risk prediction and assessment in Ya'an.

2. Material and Methods

2.1. Overview of the Study Area

Ya'an City locates in the western part of Sichuan Province and belongs to mountainous region of western margin in Sichuan Basin. It is transitional area between Sichuan Basin and Qinghai-Tibetan Plateau and has seven counties and one district. With the development of industry and agriculture and the effect of mankind's activity, the water pollution of Qingyi Valley in Ya'an City was getting worse day by day. There were two types of water pollution in rural area of Ya'an: the first type was the schistosome-affected areas of Lushan County and Tianquan County where the water source is polluted by oncomelania; the other one was the river pollution caused by the aggravation of mankind's activities, by the forest devastation and by the fertilizer and pesticide abuse in agricultural production, which affected human life and drinking water production. According to the investigation and statistics, 580,200 residents didn't get safe drinking water, accounting for 46.77% of agricultural population. Among them, about 321,600 residents drink the water that didn't reach quality standard, 23,800 residents lived with water exceeded the standard fluoride content, 15,700 residents suffered from brackish water, 31,100 residents lived with IV or super IV untreated surface water, 171,400 residents took untreated surface water that the bacteriological index seriously exceeded the standard, 10,400 residents suffered from the untreated underground water with heavy pollution and 69,600 residents who took the water with other quality index exceeded the standard (mainly includes Glauber's salt, Fe,

Mn and mineral), 551,000 residents suffered from water shortage, and 142,800 residents suffered from the inconvenience of water supply, and the water source guaranteed rate that didn't reach the standard affecting 61,000 residents [22].

2.2. Models, Parameters and Criteria

The health risk assessment process recommended by U.S.EPA mainly includes: Data collecting and evaluating; Exposure assessment; Toxicity assessment; Risk characterization [23]. Health risk management of water environment is a neonatal management philosophy that further developed from water environment management. It is the concretized management which focuses on the actual situation of regional water environment and carries out risk management to ensure the health and safety of regional water environment on the basis of regional water environmental risk analysis and assessment [24−30]. In this study, models and parameters were used as following:

2.2.1. Carcinogenic Risk Assessment

It is generally agreed that the exposure dose rate has a linear relationship with human carcinogenic risk when people are under exposure condition of low chemical carcinogen dose. When high dose leads to high carcinogenic risk, there is an exponential relationship between the exposed dose rate and human carcinogenic risk, which can be calculated with the following formula:

$$R = SF \times E, \quad R < 0.01$$
$$R = 1 - \exp(-SF \times E), \quad R \geq 0.01 \tag{1}$$

where, R is the carcinogenic risk representing the excessive cancer probability in people's lifetime; SF is the chemical carcinogenic slope coefficient ($(mg \cdot kg^{-1} \cdot d^{-1})^{-1}$) representing the lifelong excessive cancer risk of people when they always exposed to chemical carcinogen at the dose of 1mg per kg everyday; E is the exposure dose rate ($mg \cdot kg \cdot d^{-1}$) representing the daily intake of assessed pollutant per kg.

E can be calculated with the following formula:

$$E = (C \times IR \times EF \times ED)/(BW \times AT) \tag{2}$$

where, C is the consistency of the chemical pollutants in source water ($mg \cdot L^{-1}$); IR is drinking rate ($L \cdot d^{-1}$, the suggested value of U.S.EPA is $2L \cdot d^{-1}$) representing daily amount of drinking water people take; EF is the exposure frequency ($d \cdot a^{-1}$) representing the days of assessed pollutants intake per year in evaluation period; ED is the exposure duration (a, the value recommend by U.S.EPA

Table 1. SF values $[mg/(kg \cdot d)]^{-1}$.

As	Cr^{6+}	Pb
1.50	0.0073	0.055

Table 2. RfD values [mg/(kg·d)].

Fe	Mn	fluoride	nitrate	As	Cr^{6+}	Hg	Cd	Pb
0.3	0.14	0.06	1.6	0.0003	0.003	0.0003	0.0005	0.055

is 30a) representing the years of lifelong assessed pollutants intake; BW is the average weight (kg, the optimum weight in China is 60kg); AT is the average time (d, average carcinogenic time and non-carcinogenic time are $70a \times 365d \cdot a^{-1}$, $ED \times 365d \cdot a^{-1}$ respectively).

2.2.2. Non-Carcinogenic Risk Assessment

The non-carcinogenic chronic toxic property of chemical pollutants to human body takes the reference dose as yardstick: people whose exposure level is higher than the reference dose are probable risk takers; and those whose exposure level is equal or lower than the reference dose are less probable risk takers.

HI is commonly used to represent the non-carcinogenic chronic toxic property:

$$HI = E/RfD \tag{3}$$

where, RfD is the reference dose ($mg \cdot kg^{-1} \cdot d^{-1}$).

2.2.3. Health Risk Assessment Parameters

The carcinogenic slope coefficients of the three kinds of pollutants which have carcinogenic effect on human body through drinking water are showed in Table 1. The reference dose (RfD) of the nine kinds of pollutants are showed in Table 2 [29].

2.2.4. Total Health Risk

For the total health risk caused by all kinds of toxic substance in the drinking water, given that the toxic effects of various kinds of poisonous substance to human body are having an additive relationship rather than cooperative or antagonistic relationship, the total health risk of drinking water R_T can be calculated by the following formula:

$$R_T = HI + R \tag{4}$$

The Formula (4) mentioned above is the total health risk assessment model of the pollutants in drinking water.

2.2.5. Risk Assessment Criteria

Non-carcinogenic risk evaluation criteria: according to the definition of hazard index, "1" was determined as risk control criteria of non-carcinogenic, chronic and poisoning effects to evaluate.

Carcinogenic risk evaluation criteria: risk management practices of foreign countries over the years had shown that carcinogenic risks of chemical contaminants, accor-

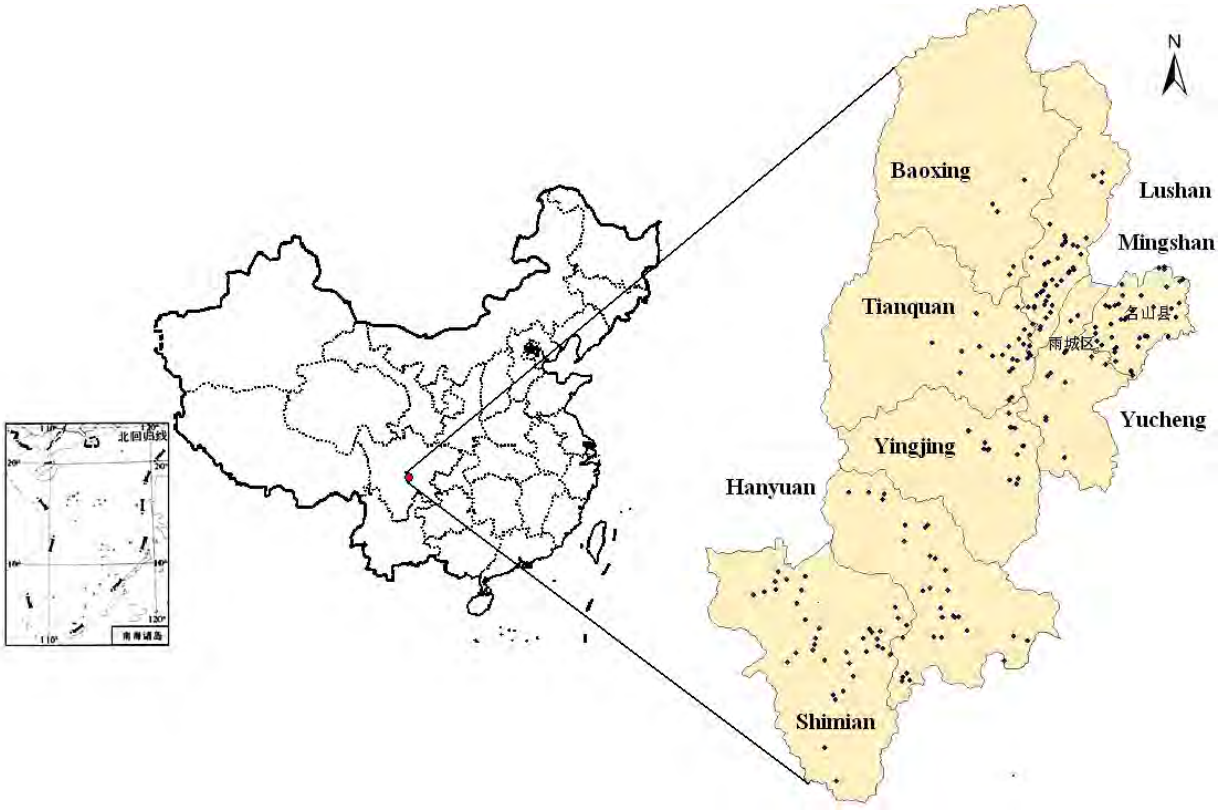

Figure 1. The sampling sites and the location of Ya'an city.

ding to the full extent of the evidence of its carcinogenicity, per million (1.00×10^{-6}) to ten thousandth (1.00×10^{-4}) are all acceptable. This study used the most stringent acceptable risk degree per million (1.00×10^{-6}) as the evaluation criteria to evaluate.

2.3. Samples Investigation

According to U. S. EPA, the methods of health risk assessment process included as follows: collecting and analyzing relevant data, recognizing potential harmful chemicals; analyzing releasing mode of pollutants, identifying exposed population and exposure pathway, assessing exposure concentration and intake concentration by different ways; collecting qualitative and quantitative toxicity data, determining toxicity data; characterization of potential adverse effect to health, carcinogenic risk assessment, non-carcinogenic risk assessment and so on.

In 2005, on basis of investigation about fundamental state and making fully use of recent two years' rural water quality census data by health department, sampling inspection of water system was divided into two parts according to topography, geomorphology, geology, hydrology, water systems and drinking water sources, distribution of water-borne diseases and water supply project type. Health department acted in concert with water resources units to collect samples of source water and peripheral water of central water supply project, well water, reservoir water and pond water and to carry out laboratory test and detection on water quality in related townships. And then, the distribution areas where the water quality was below the standard and the numbers of people living in those areas were obtained according to the different qualities of water. 221 water samples were collected (see in Figure 1) and 21 indexes were under detection, including physical water quality index (color, turbidity degree, offensive odor, visible materials by bare eye), hydrochemical index(PH, COD, total hardness, total dissolved solid, chloride, sulfate), toxicology index (Fe, Mn, Fluoride, As, Hg, Cd, Cr, Pb, Nitrate) and bacteriology index (faecal coliforms, total coliforms), etc. Depending on whether the water quality indexes of the detected water were harmful to human body or not, 9 chemical toxicology indexes of health risk assessment, i.e., Fe, Mn, Fluoride, As, Hg, Cd, Cr, Pb and Nitrate, were then selected and assured.

2.4. Arc-GIS Tools

Spatial analysis capability makes GIS different from other mapping system. GIS has been widely used in water and environment applications and many efforts have been made for applying GIS to resource and environ- ment management [31−34]. Health risk assessment for water quality of the rural water sources involves multi-sphere factors, hydrosphere, atmosphere, geo-

Figure 2. As risk thematic map.

sphere and biosphere, which are ideal spatial activities being handled by GIS [35−37]. The spatial data management, analysis and visualization of GIS have greatly facilitated health risk assessment studies. GIS as a general spatial modelling, is the best option for health risk assessment for water quality of rural water sources approach which can potentially allow users to inter actively carry out assessment manipulations and to facilitate easier decision making for risk control. This study adopted ESRI's ArcGIS platform, one of the most powerful GIS software.

2.5. GIS Spatial Database

Before the interior data analysis, relevant maps, data, text material of the studied area were collected at first. Then, digitize the relevant maps by using ArcGIS and set up a unified coordinate system (Beijing geodetic coordinate system 1984) to integrate these data through editing and registration. After that, the structure of thematic layer and the data of the storage area of GIS system were applied to establish the basal spatial database of the studied area, meanwhile the pertinent attribute data were stored and necessary notes were added, such as mountains, rivers, villages and so on. When detecting the water quality in the fields, it is necessary to note down the geodetic coordinates (by using the Global Positioning System, GPS), so that the sampling point layers will automatically generate by means of ArcGIS and according to the coordinate of monitoring points, and at the same time to match the unified coordinate.

2.6. Geo-Statistical Analysis and Model Fitting

The core of geo-statistical Analysis is to select the appropriate spatial interpolation method to create the surface through the analysis of the sample data and the awareness of the geographical features of sampling area. Interpolation method can be divided into two kinds according to the mathematical principle implementing it, one is the deterministic interpolation method and the other is the geo-statistical interpolation which is also called the Kriging interpolation. The Kriging method is the core content of geo-statistic that based on the spatial autocorrelation. It carries out the unbiased estimation on the unknown sampling points of the regionalization variables, applying the original data and the structural properties of the semi-variance function. Based on the spatial statistics analysis and the theoretical model of the semi-variation function, this study carried out the universal Kriging interpolation in risk value of the water quality of rural water sources in studied areas.

3. Results

3.1. Single Factor Assessment of the Carcinogenic Risk

According to the assessment models of carcinogenic risk (Formula (1) and (2)), the data about water quality of Ya'an were analyzed in ArcGIS, and then the thematic maps of single factor risk values of various types of carcinogen were made (shown in Figure 2, 3, 4). The result indicated that the distribution of arsenic, chromium (6+), lead were mainly in Yucheng District. In addition, there were also small quantity of arsenic and lead distributes in Liaochang village in Ming Shan County. Obtained results tallied with the practical situation that there was a higher density of population and there were more chemical plants and more chemical pollutant discharged in Yucheng District.

3.2. Single Factor Assessment of the Non-Carcinogenic Risk

Due to the observation precision of the detection equipments, none of the targeted value in original database that are below the detection precision can be detected, and this lead to the problem of mutilated data. Such defect is just made up, owing to one important function of Geo-statistical Analysis based on ESRI's ArcGIS which may implement the interpolation in the non-sample spatial areas.

In this study, 9 kinds of pollutants (including three carcinogenic pollutants) in Ya'an City were analyzed respectively by using kriging spatial interpolation meth-

Figure 3. Cr (6+) risk thematic map.

Figure 5. Flouride hazard index.

Figure 4. Pb risk thematic map.

Figure 6. As hazard index.

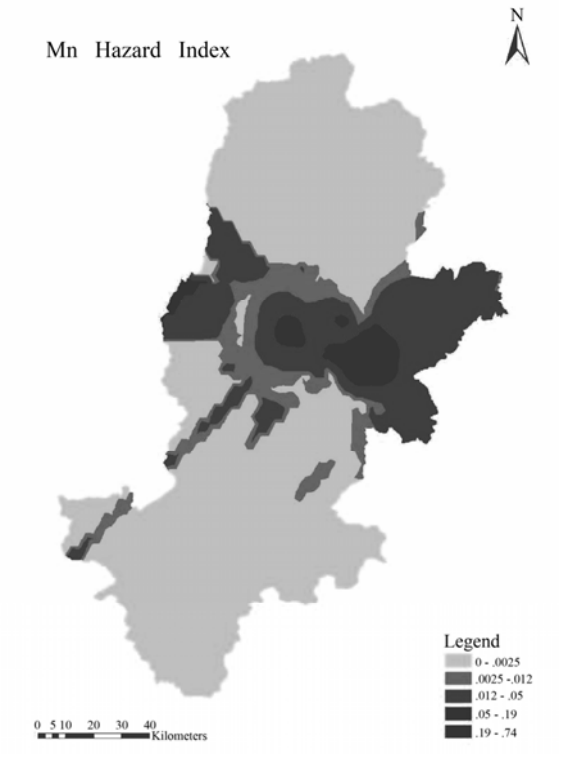

Figure 7. Mn hazard index.

Figure 8. Cr (6+) hazard index.

od. And the thematic maps were formed, they were distribution maps of hazard index of Iron, manganese, fluoride, mercury, nitrate, arsenic, cadmium, chromium (6+), lead respectively. Obtained result indicated that: Fe mainly distributes in Mingshan County, while some areas of Tianquan County and Yingjing County also had a small quantity of distribution, and the distribution gradually decreased from north-east to south-west. Observing from the topographic map, series of vertical mountains could be seen on the contiguous areas of Mingshang County and Yucheng District, thus this coincided with the lay of the land and the stream direction. While, manganese distributed mainly in Yucheng District and some areas of Tianquan County, Mingshan County and Baoxing County. In a similar way, it could be found that the spatial analysis maps of the risk value of several other kinds of pollutants were also reasonable. The maximum of HI values of fluoride, arsenic, manganese, chromium (6+) greater than 0.5, hence their HI thematic maps were also shown in Figure 5, 6, 7, 8 respectively.

3.3. Total Risk Assessment of Water Quality of the Integrate Factors

Summed up the carcinogenic risk (R) and the non-carcinogenic risk (HI) of single factor of each water source respectively, the total risk of integrate factors of carcinogen and non-carcinogen of these water sources obtained respectively (shown in Figure 9 and 10). Then, summed up the total risk of integrate factors of carcinogen and non-carcinogen, and the total risk thematic map got (shown in Figure 11).

4. Analysis and Discussions

4.1. Single Factor Assessment of the Carcinogenic Risk

From Figure 2, 3 and 4, most of the cancerous risk indexes of the vast majority of water sources (about 94%) were the level of 10^{-7} and it belong to the safety extension. The main carcinogen in water sources were As, Cr^{6+} and Pb, their concentrations are in the ranges of 0.004-0.01, 0.05, 0.01mg/l respectively and such water source mainly distributed in Yucheng District and Mingshan County. According to Guidelines for Drinking Water Quality of WHO (Third Edition, 2008), the limit values of As, Cr^{6+} and Pb are 0.01, 0.05 and 0.01mg/l respectively, the measured values of As and Pb of 12 water sources in Yucheng District exceeded the limits, the measured value of Cr^{6+} of 7 water sources in Yucheng District exceeded the limit, the measured value of As of 1 water sources in Mingshan County exceeded the limit. About 149458 residents are exposed to concentration of As, Cr^{6+} and Pb exceeding 0.01, 0.05 and 0.01mg/l.

The cancerous risk indexes of As, Cr and Pb were in the range of 10^{-6}-10^{-4}, 10^{-7}-10^{-6}, 10^{-6} respectively and the indexes of some rural drinking water sources had ex

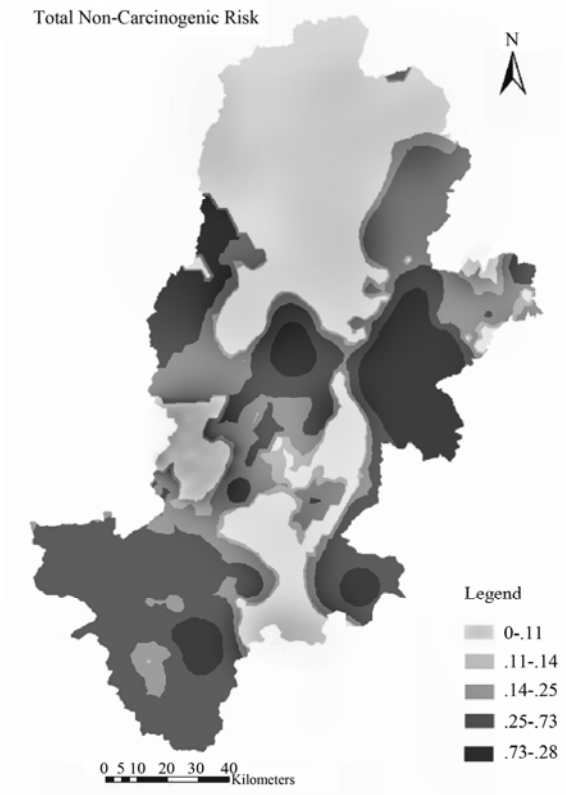

Figure 9. Total non-carcinogenic risk.

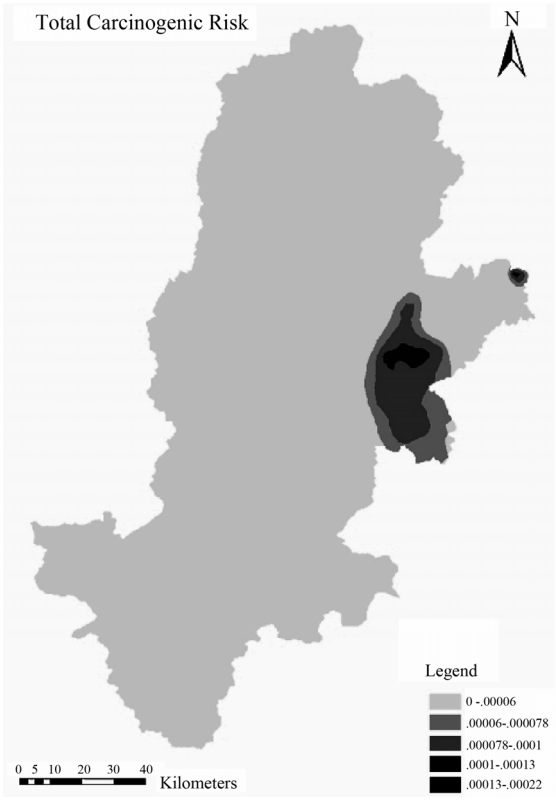

Figure 10. Total carcinogenic risk.

ceeded the drinking water management standard value of EPA. Among 12 water sources in Yucheng District, there was 7 that Cr^{6+} exceeded up to 1.6-5.2 times, 1 that As exceeded up to 107 times, 11 that As exceeded up to 86 times, 12 that Pb exceeded up to 7.9 times. Among 41 water sources in Mingshan County, there was 1 that As exceeded up to 214 times.

4.2. Single Factor Assessment of the Non-Carcinogenic Risk

From Figure 5, 6, 7 and 8, most of the non-cancerous hazard indexes of the vast majority of water sources (about 98%) were also less than the limit value 1 and will not harm the local people. The health risk of non-carcinogen comes mainly from fluoride and As, their concentrations were in the ranges of 0.1-4.2 and 0.004-0.01mg/l respectively. According to Guidelines for Drinking Water Quality of World Health Organization (Third Edition, 2008), the limit values of As and fluoride are 0.01 and 1.5mg/l respectively, the measured values of As of 1 water source in Mingshan county exceeded the limit, the measured values of fluoride of 1 water source in Shimian County, 1 water source in Hanyuan County and 2 water source in Tianquan County exceeded the limit. About 17460 residents were exposed to concentration of As and fluoride exceeding 0.01 and 1.5mg/l.

The non-cancerous hazard indexes of fluoride and As were in the range of 0.053-2.3 and 0.23-1.1 respectively

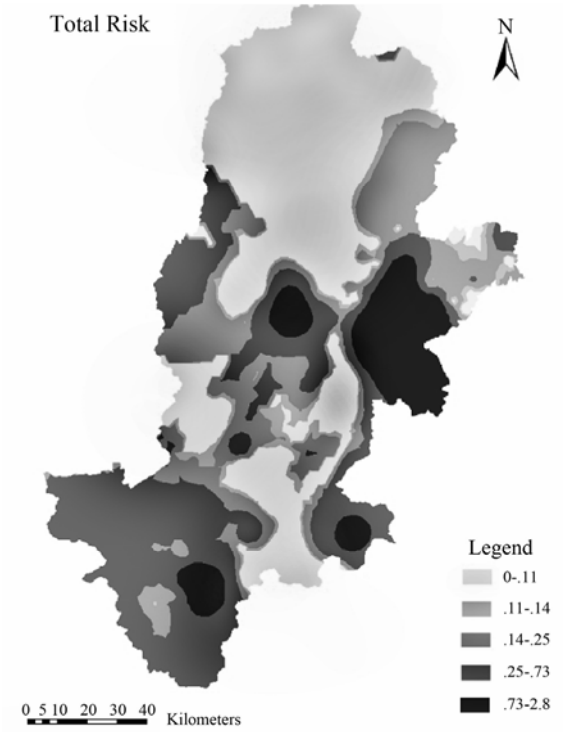

Figure 11. Total risk.

exceeded the drinking water management standard value of EPA. There was 1 water source in Mingshan County that As exceeded up to 1.11 times; There was 2,1 and 2 water sources in Shimian County, Hanyuan County and Tianquan County that fluoride exceeded up to 1.69-2.33, 1.17 and 1.22-1.33 times respectively.

4.3. Total Risk Assessment of Water Quality of the Integrate Factors

According to Figure 9, the total risk of non-carcinogenic are mainly distributed in several water sources in Yucheng District, Tianquan County, Hanyuan County and Shimian County, so we could basically confirm that drinking water supply of most water sources in Ya'an City didn't have non-carcinogenic, chronic and poisoning effects on drinking crowd. According to Figure 10, the total risk of carcinogenic mainly distributed in several water sources in Yucheng District and Mingshan County. Total risk was shown in Figure 11.

From the above Figures, the analysis results in Figure 9 and Figure 11 were comparatively similar to each other, this indicated that the total risk come mainly from the non-carcinogenic hazard, and the risk distribution areas mainly included Yucheng District, Lushan County, Shimian County, Yingjing County, etc.

The results of the integrate factors health risk assessment showed that the total cancerous risk indexes were still at the level of 10^{-6}, only 12 drinking water source investigation sites (5%) exceeded the drinking water management standard value of EPA (the limit value is 10^{-6}); the total non-cancerous risk indexes are still in the range of 10^{-2}-10^{-1}, and will not harm the local residents either, only 18 drinking water source investigation sites (8%) exceeded the drinking water management standard value of EPA (the limit value is 1).

Thus, chemical carcinogens and non-carcinogens were primary and should be removed accordingly. The effective way of decreasing the health risk and hazard was to control and dispose the rural drinking water containing As, Cr (VI), Pb and fluoride (F). The results provided important information of water quality control and the early warning for rural drinking water.

5. Conclusions

Results of this study provided more deeply and broadly scientific information to the management and protection of rural water source in Ya'an City. This study expounded the water environmental risk level of rural drinking water in the research area, and the primary and secondary of pollutants and the priority of treatment of the pollutants. By doing these may provide the scientific basis for the risk management of drinking water quality in research area, and also provided the new mode and technical platform for water quality protection in rural water sources.

Based on ESRI's ArcGIS, we did the store, the calculation, the analysis, the simulation and the display with the data of water quality of water sources. Then, thematic maps of spatial distribution of water quality risk had been drawn duly, and meanwhile the real-time monitoring, assessment and dynamic management of healthy risk of water quality of water sources were implemented. The using of ArcGIS in health risk evaluation on water quality of rural water sources has the following outstanding features such as rapidity, high accuracy, ability of dynamic monitoring, visualization and so on. A series of works done through the ArcGIS platform, such as the information input, the management, the inquiry, the analysis and the output, had provided important ways for dynamic assessment of regional water quality risk. ArcGIS integrated data from different sources, and demonstrated and made full use of the spatial information, so as to make the interpretation to the result more reasonable.

In the study, the data accuracy wasn't well satisfied the demand of water quality assessment of regional micro-scale, far more samplings of the areas with poor water quality was still needed. In the subsequent researches, detecting instruments with higher accuracy needed to detect the quality of water sources, in order to obtain more meticulous analysis and assessment. Further analysis and assessment were recommended for the next step of research work.

In this study, the exposure way just took average drinking intake into consideration which excluded other toxic substances and their routes, for instance, inhaling by dermal touch and the form of steam and dieting. Actually, the exposure risk of pollutants was underestimated. The exposure risk by drinking was also closely bound up with residence time of water in domestic pipe network, consumer's life style, consuming habit and career. So more complicated exposure assessment method was needed to get the average exposure dose by consumer touch, the daily distribution of pollutants exposure dose and the main exposure chance that individual was affected by pollutants [38].

6. Acknowledgement

This study was financed jointly by Sichuan Agricultural University youth science and technology innovation fund (00530300) and Sichuan Agricultural University introduced the talented person fund (00530301).

7. References

[1] F. M. Geng, *et al*., "Risk degree assessment on water quality health hazard of drinking water sources," Journal of Hydraulic Engineering, Vol. 37, No. 10, pp. 1242−1245, October 2006.

[2] E. X. Li and B. Ling, "Effect of water pollution on human health," Sanitary Engineering of China, Vol. 5, No. 1, pp. 3−5, May 2006.

[3] Y. R. Yin and Z. L. Deng, "Analysis on relationship between drinking water and health," Scientific and Technological Information of China, pp .219−221, December 2006.

[4] J. Z. Qian, R. Z. Li, *et al*., "Health risk assessment on source water quality of urban water supply," Journal of Hydraulic Engineering, pp. 1−5, August 2004.

[5] Y. H. QIN, "Processing technic and sanitation of drinking water," Chemical Industry Press, Beijing, pp. 5−54, 2002.

[6] OAK RIDGE National Laboratory, "Risk assessment information system [EB/OL]," http://rais.ornl.gov/tox /tox_values, shtml, July 2006.

[7] U. S. Environmental Protection Agency,"Integrated risk information system [EB/OL]," http://www.epa.gov/iris /index, html, March 2006.

[8] International Agency for Research on Cancer, "Cancer database [EB/OL],"http://monographs.iarc.fr /ENG/ Classification/index.php.

[9] F. Q. Ni, *et al*., "Health risk evaluation on water quality of rural water sources of western margin of Sichuan Basin," Progress in Natural Science (manuscript reviewing, awaiting publishing).

[10] X. L. Mao and Y. S. Liu, "Research progress on environmental risk assessment home and abroad," Scientific Journal of Application Foundation and Engineering, Vol. 11, No. 3, pp. 266−273, November 2003.

[11] E. B. Hu, "Practical techniques and methods of environmental risk assessment," State Environmental Science Press, Beijing, 2000.

[12] H. Hong, H. W. Chen, J. T. He, *et al*., "Theories and methods of health risk evaluation on contaminated sites," Earth Science Frontiers, Vol. 13, No. 1, pp. 216−223, 2006.

[13] Mark and D. Sobsey, "Drinking water and health research：A look to the future in the united states and globally," Journal of Water and Health, No. 4, pp. 17−22, 2006.

[14] R. Kumar, R. D. Singh, and K. D. Sharma, "Water resources of India, special section: Water," Vol. 89, No. 5, pp. 793−811, September 2005.

[15] L. J. H. Lee, C. C. Chan, and C. W. Chung, "Health risk assessment on residents exposed to chlorinated hydrocarbons contaminated in groundwater of a hazardous waste site," Journal of Toxicology and Environmental Health, Part A, No. 65, pp. 219−235, 2002.

[16] C. Carlsson and R. Fuller, "Fuzzy multiple criteria decision making: Recent developments," Fuzzy Sets and Systems, pp. 139−153, Vol. 78, 1996.

[17] R. L. Sanson, "The development of a decision support system for an animal disease emergency," Department of Veterinary clinical sciences Massey university, March 1993.

[18] Z. Y. Zang, Y. Zhao, L. Wei, *et al*., "Health risk assessment of an abandoned chemical plant in Beijing," Journal of Ecotoxicology, Vol. 3, No. 1, pp. 48−55, February 2008.

[19] L. Huang, P. C. Li, and B. W. Liu, "Health risk assessment of groundwater pollution of Yangtze river delta," Safety and Environmental Engineering, Vol. 15, No. 2, pp. 26−30, June 2008.

[20] Y. F. Liao, W. Y. Wang and L. Zhang, "Application study of GIS on urban NOx induced health risk assessment," Progress in Geography, Vol. 26, No. 4, pp. 44−53, July 2007.

[21] T. J. Wang, X. F. Zha, and W. N. Xiong, "Preliminary evaluation of health risk assessment on heavy metal contamination of Karstic groundwater in Gaoping area, Zunyi city, Guizhou province," Research of Environmental Sciences, Vol. 21, No. 1, pp. 46−51, January 2008.

[22] Z. Q. Wang, W. G. Sun, D. K. Wang, *et al*., "Appraisal report on present drinking water safety in rural areas of Ya'an city," Unpublished data sources, Ya'an Water Conservancy and Hydropower Survey and Design Research Institute, April 2005.

[23] D. K. Wang, *et al*., "Application of healthy hazard assessment in environmental quality evaluation," Environmental Pollution and Prevention, Vol. 7, No. 5, pp. 91−92, 1995.

[24] EPA, "Superfund public health evaluation manual," EPA/540/186060.

[25] U. S. EPA, "Available information on assessment exposure from pesticides in food," U. S. Environmental Protection Agency Office of Pesticides Programs, June 2000.

[26] EPA, "Supplement risk assessment," Part 1, USA: EPA, pp. 26−35, 1989.

[27] J. J. Gao, L. P. Zhang, and S. B. Huang, "Preliminary evaluation on health risk of heavy metal pollutants in drinking water sources in Beijing," Vol. 25, No. 2, pp. 47−50, 2004.

[28] G. M. Zeng, L. Zhuo, Z. L. Zhong, *et al*., "Water environmental health risk evaluation model," Advances in Hydroscience , Vol. 9, No. 3, pp. 212−217, 1998.

[29] L. G. Chen, M. J. Chen, and L. H. Feng, "Safety evaluation of water source quality based on health risk assessment," Journal of Hydraulic Engineering, Vol. 39, No. 2, pp. 235−244, February 2008.

[30] H. B. Luo, R. XU, X. L. Liu, *et al*., "The system design of water environmental health risk assessment in river," Proceedings of the 5th International Conference on Urban Watershed Management & Mountain River Protection and Development, Chengdu, China, April 3−5, 2007.

[31] L. LI, W. Z. Zhang and W. Y. Chen, "GIS Technology and Application in Environmental Protection," http:// www. tzwhx.com/ newOperate/html/5/51/511 /941.html.

[32] L. Zhang and T. J. Yan, "Application of GIS in resource and environment filed," http: // qkzz.net/ magazine/ 1672−3198/ 2007/09/2110036.html.

[33] "Dynamic monitoring system of river water quality based

on GIS," http://www.ck365.cn/anli/1674.html.

[34] "Application of GIS in provincial water environment function regionalization," Information Center of Environmental Protection in GanSu Province, Environmental Monitoring Center of Gansu Province, 2006.

[35] X. H. Zhou, X. J. Li, and C. R. Gao, "Application of geo-statistical analysis in water quality assessment based on GIS-A case study of Linhe city in Inner Mongolia," Journal of Capital Normal University (Natural Science Edition), Vol. 29, No. 4, pp. 52−58, 2008.

[36] Y. S. Yang and J. L. Wang, "GIS-based dynamic risk assessment for groundwater nitrate pollution from agricultural diffuse sources," Journal of Jilin University (Earth Science Edition), Vol. 37, No. 2, pp. 311−318, March 2007.

[37] Y. F. Hu, L. J. Deng, S. R. Zhang, F. Q. Ni and J. Zhang, "Spatial variability characteristics of iron and manganese contents in shallow groundwater of western margin of Sichuan Basin," Journal of Ecology, Vol. 29, No. 2, pp. 797−803, February 2009.

[38] F. Q. Ni, *et al*., "Health risk assessment on rural drinking water safety: A case study in rain city district of Ya'an city of Sichuan province," Journal of Water Resource and Protection, No. 2, pp. 128−135, 2009, doi:10.4236/ jwarp. 2009.12017 Published Online August 2009 (SciRP.org/ journal/ jwarp/).

J. Water Resource and Protection, **2009, 1, 362-367**
doi:10.4236/jwarp.2009.15043 Published Online November 2009 (http://www.sciRP.org/journal/jwarp).

Two Modified QUICK Schemes for Advection-Diffusion Equation of Pollutants on Unstructured Grids

Linghang XING
Hydraulic Research Laboratory, Changjiang River Scientific Research Institute, Wuhan,China
E-mail: *xinglinghang@yahoo.com.cn*
Received June 28, 2009; *revised August* 17, 2009; *accepted August* 26, 2009

Abstract

In this paper, two modified QUICK schemes, namely Q-QUICK and UQ-QUICK, for improving the precision of convective flux approximation are verified in advection-diffusion equation of pollutants on unstructured grids. The constructed auxiliary nodes for Q-QUICK/UQ-QUICK are composed of two neighboring nodes plus the next upwind node, the later node is generated from intersection of the line of current neighboring nodes and their corresponding interfaces. 2D unsteady advection-diffusion equation of pollutants is conducted for their verifications on unstructured grids. The numerical results show that Q-QUICK and UQ-QUICK have similar computational accuracy to the central difference scheme and similar numerical stability to upwind difference scheme after applying the deferred correction method. In addition, their corresponding CPU times are approximately equivalent to those of traditional difference schemes and their abilities for adapting high grid deformation are robust.

Keywords: Unstructured Grids, Q-QUICK/UQ-QUICK, Numerical Computation, Advection-Diffusion Equation of Pollutants

1. Introduction

The physical processes of pollutant transportation in flowing water are mainly consisting of advection and diffusion, which are usually governed by advection-diffusion equation of pollutants. Generally, the action of advection process would dominate the transportation of pollutants. Thereby, it is so important to improve the precision of convective flux approximation. Till to now, many works have been done for numerical simulation of advection-diffusion equation of pollutants on structured grids [1−8]. The natural computational boundaries are irregular. If structured grids applied, the workload of CFD pretreatment would be increased and the numerical precision in the boundaries would be decreased. Unstructured grid can produce arbitrary geometry and can well fit to complex physical boundary. Presently, the computation based on unstructured grid becomes more and more popular. However, many high-precision schemes on uniform grid can not be applied to unstructured grids directly. It is significative to extend them to unstructured grid computation. In the past decade, a number of difference schemes to calculate convective flux were developed for incompressible flow simulation. They include upwind difference scheme (UDS), central differencing scheme (CDS), hybrid differencing scheme (HDS), the quadratic upstream, quadratic upstream extended and quadratic upstream extended revised difference schemes (QUICK, QUDSE, QUDSER as modified by Pollard and Siu [9]), the locally exact scheme (LEDS) (1972), and the power difference schemes (PDS) of Pantankar [10]. The unconditionally convergent schemes UDS/HDS/LEDS/PDS can be significantly inaccurate under coarse grids, thus they require considerable grid refinement to produce acceptable results. This makes them expensive. Moreover, they implicitly introduce the numerical diffusion term and distort the solution. In terms of accuracy and computational efficiency, it appears that the QUICK/QUDSE/QUDSER may offer the best compromise [11]. In uniform grids, they can have over second-order precision for convective flux approximation. However, QUICK/ QUDSE/ QUDSER need two nodes upstream. It is not so easy to apply these high-order schemes to unstructured grid directly, especially in three dimensional problems. Moreover, to find the exact locations of the next upwind node would require a very complex pointer system and consume more memory and CPU time. Davidson L. 1996 [12] introduced one method where the next upwind node is constructed by intersection from the line of two adjacent central nodes and its corresponding interface. Presently,

it is named Q-QUICK. According to the method, another similar scheme named UQ-QUICK is also introduced for comparative investigation. As for time discretization, the first-order and second-order schemes are taken into account. To this end, many compound schemes are formed and their corresponding numerical performances including numerical precision, stability and CPU time are fully demonstrated in 2D unsteady advection-diffusion equation of pollutants. In order to accelerate convergence speed for linear equations, generalized Minimum Residual (GMRES) [13] method with the Incomplete LU (ILUT) precondition is used.

2. Q-Quick and UQ-Quick

QUICK [14] is the third order approximation of the convection term. However, this high-order scheme is not easy to apply to unstructured grid directly. To find the exact location of the next upwind node would increase the geometrical complexity and consume relative more memory and CPU time. For a compromise, DAVIDSON L. introduced a modified QUCIK scheme in the end of his paper [12]. However, little work has been done later for this recommended scheme. Thus, it is necessary for fully studying its numerical characteristics including numerical precision, convergent stability and CPU time. As for comparison, another modified QUICK scheme is also introduced, namely UQ-QUICK.

2.1. QUICK

In a uniform grid (Figure 1 for definitions of points WW, W, P, E, EE etc.), the quadratic upstream difference scheme of Leonard [14] at the east cell-face can be written as

$$\begin{aligned}\phi_e &= \frac{1}{2}(\phi_P+\phi_E)-\frac{1}{8}(\phi_W-2\phi_P+\phi_E) \quad (u\ge 0)\\ \phi_e &= \frac{1}{2}(\phi_P+\phi_E)-\frac{1}{8}(\phi_{EE}-2\phi_E+\phi_P) \quad (u<0)\end{aligned} \tag{1}$$

It is a third order approximation of the convection term.

2.2. Q-QUICK

Considering Figure 2(a), the next upwind node *U* is constructed by intersection of line $\overline{PA}$ and its corresponding interface. A better way is probably to use reconstruction schemes, namely to compute the gradient in node *P* and use Taylor expansion to obtain the value at point *U*.

$$\begin{aligned}\phi_U &= \phi_P+\vec{r}_{PU}\cdot(\nabla\phi)_P+\frac{1}{2}(\vec{r}_{PU})^2:(\nabla\nabla\phi)_P\\ &+\cdots+\frac{1}{n!}(\vec{r}_{PU})^n\vdots\underbrace{(\nabla\nabla\cdot\cdot\nabla}_{n}\phi)_P+\cdots\end{aligned} \tag{2}$$

For present study, the second order approximation is considered. Thus the first two terms from the right of the equation are kept. And then, it is imperative to estimate

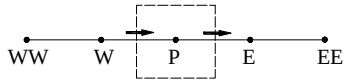

Figure 1. QUICK scheme in uniform grid.

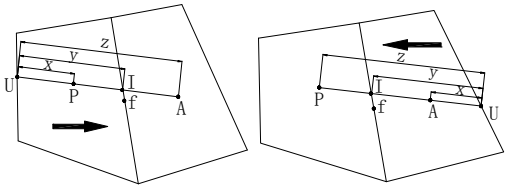

(a) $\vec{u}\cdot\vec{n}>0$ **(b)** $\vec{u}\cdot\vec{n}<0$

Figure 2. The next upwind node reconstruction for Q-QUICK.

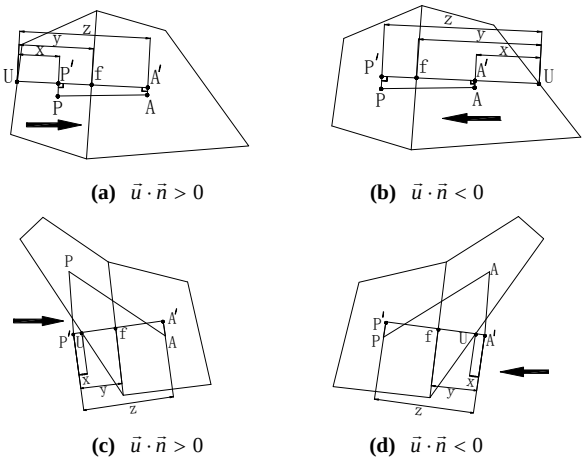

(a) $\vec{u}\cdot\vec{n}>0$ **(b)** $\vec{u}\cdot\vec{n}<0$

(c) $\vec{u}\cdot\vec{n}>0$ **(d)** $\vec{u}\cdot\vec{n}<0$

Figure 3. The next upwind node reconstruction for UQ-QUICK.

the face value at interface f .In doing this, it is assumed that the flow direction is from right to left. To this end,the face value can be interpolated by QUICK method as the same way acted on the structured grid. So the normal face value ϕ_f is derived according as

$$\phi_f=\phi_P+f_1\nabla\phi_P\cdot\vec{r}_{PU}+f_2(\phi_A-\phi_P)+\nabla\phi_I\cdot\vec{r}_{If} \tag{3}$$

where, $f_1=-(z-y)(y-x)/x/z$； $0\le y\le 2$

If the flow direction is inverse (see Figure 2(b)), the same Formula (3) can be derived.

2.3. UQ-QUICK

The reconstruction method of NQ-QUICK has no intrinsic difference to that of Q-QUICK except that the three auxiliary nodes U , P' and A' (see Figure 3) in a line are perpendicular to interface f . In addition, the node values of P' and A' should be obtained first before interpolation by QUICK method. However, a tough problem here is that the relative positions of nodes U , P' and A' are not as simple as those of Q-QUICK. In present study, two cases are summarized as follows.

- Case 1

If $\vec{u}\cdot\vec{n}>0$ (see Figure 3(a))

$$\phi_f=\phi_{P'}-f_1(\phi_{P'}-\phi_U)+f_2(\phi_{A'}-\phi_{P'}) \tag{4}$$

where, $f_1=-(z-y)(y-x)/x/z$; $f_2=y(y-x)/z/(z-x)$

If $\vec{u}\cdot\vec{n}<0$ (see Figure 3(b)), similar to that of case 1 ($\vec{u}\cdot\vec{n}>0$).

- Case 2

If $\vec{u}\cdot\vec{n}>0$ (see Figure 3(c))

$$\phi_f=\phi_{P'}-f_1'(\phi_{P'}-\phi_U)+f_2'(\phi_{A'}-\phi_{P'}) \tag{5}$$

where, $f_1'=1-f_1-f_2$; $f_2'=f_2$, f_1 and f_2 have the same formulas as written in (4).

On high twisted grid, the coefficients of f_1 and f_2 in (5) may be much larger, which can cause the face value abnormal and result in the whole computation failure. So some flexible method should be implemented for the whole computational continuity. A better way for mending the defect may use the linear interpolation method for assuring a second-order precision at least. Then, the interface value can be written as

$$\phi_f=\omega\phi_{P'}+(1-\omega)\phi_{A'} \tag{6}$$

where, ω is the linear interpolation factor.

To this end, the coefficients of f_1' and f_2' are as follows

$$f_1'=0;\ f_2'=1-\omega \tag{7}$$

If $\vec{u}\cdot\vec{n}<0$ (see Figure 3(d)), similar to that of case 2($\vec{u}\cdot\vec{n}>0$).

3. Numerical Verification

In present study, a two-dimensional advection-diffusion equation of pollutants is discretized by compounds of different time schemes and different convective flux schemes. The former includes UDS and Crank-Nicolson and the later consists of UDS, CDS, HDS, PDS, Q-QUICK and UQ-QUICK. To this end, comprehensive comparisons for their numerical performances are investigated, including relative errors, CPU time and numerical stability.

3.1. Governing Equation and Initial Condition

In general, a two-dimensional advection-diffusion equation of pollutants can be written as

$$\frac{\partial C}{\partial t}+u\frac{\partial C}{\partial x}+v\frac{\partial C}{\partial y}=\frac{\partial}{\partial x}\left(D_x\frac{\partial C}{\partial x}\right)+\frac{\partial}{\partial y}\left(D_y\frac{\partial C}{\partial y}\right)+S_\phi \tag{8}$$

where, C is concentration of pollutants, u and v are velocities along x and y directions; D_x and D_y are diffusive coefficients;S_ϕ is the source item.

The initial computational condition is governed by a unit Gauss impulse within a rectangular plane. It is depicted as follow:

Table 1. Definition of F_f^H.

Schemes	F_f^H
UDS/CDS/ HDS/PDS	$-F_f\nabla\phi_f\cdot\vec{r}_{lf}$
Q-QUICK	$-\max(F_f,0)\left[f_1\nabla\phi_P\cdot r_{PU}+f_2(\phi_A-\phi_P)\right]$ $-\min(F_f,0)\left[f_3\nabla\phi_A\cdot r_{AU}+f_4(\phi_P-\phi_A)\right]$ $-F_f\nabla\phi_f\cdot\vec{r}_{lf}$
NQ-QUICK	$-\max(F_f,0)\left\{f_2(\phi_A-\phi_P)+f_2\nabla\phi_A\cdot\vec{r}_{AA'}\right.$ $\left.+\nabla\phi_P\cdot\left[(1-f_2)\vec{r}_{PP'}+f_1\vec{r}_{PU}\right]\right\}+$ $\min(F_f,0)\left\{f_4(\phi_P-\phi_A)+f_4\nabla\phi_P\cdot\vec{r}_{PP'}+\right.$ $\left.\nabla\phi_A\cdot\left[(1-f_4)\vec{r}_{AA'}+f_3\vec{r}_{AU}\right]\right\}$

$$C(x,y,0)=\exp(-(x-0.5)^2/D_x-(y-0.5)^2/D_y) \tag{9}$$

Its corresponding resolution is [15]

$$C(x,y,t)=\frac{1}{4t+1}\exp\left(-\frac{(x-0.5-ut)^2}{D_x(4t+1)}-\frac{(y-0.5-vt)^2}{D_y(4t+1)}\right) \tag{10}$$

where, $D_x = D_y= 0.01\text{m}^2/\text{s}$; u=v=0.8m/s; x and y are defined as $0\le x\le 2$ m, $0\le y\le 2$ m (see Figure 4(a)); the time step is set as $\Delta t=0.00625$ s.

3.2. Numerical Discretization

Generally, the advection-diffusion equation of pollutants can be first integrated over a control volume and then using the Gauss's divergence theorem, finally the common form over a CV is

$$\sum_f F_f^t+\sum_f F_f^c=\sum_f F_f^d+\int_V S_\phi dV \tag{11}$$

where, F_f^t is listed for time discretization; $F_f^c=(A\vec{u}\cdot\vec{n})_f C_f$, $F_f^d=(A\Gamma_C\nabla C\cdot\vec{n})_f$ standing for the convection and diffusion fluxes through one interface f respectively, and $\vec{n}$ is the surface outwardly normal vector.

In the following section, the first-order and second-order schemes for time discretization are both considered and the corresponding common equations for convenience of program compiling are also illuminated. In addition, over-relaxed approach [16−18] is adopted for cross derivative term approximation in the numerical computation.

First-order time discretization (UDS)

A common form for first-order time discretization along with different schemes for convective flux discretization can be derived as follow:

$$\begin{aligned}&\left[\frac{\Delta V_P}{\Delta t}+\sum_f D_f A(|P_f|)+2(1-\omega_f)\max(-F_f,0)+\max(F_f,0)\right]C_P\\&-\sum_f\left[D_f A(|P_f|)+2(1-\omega_f)\max(-F_f,0)\right]C_A=\left\{\frac{\Delta V_P}{\Delta t}C_P^0-\right.\\&\left.\sum_f\min(F_f,0)C_P+\sum_f A_f(\Gamma_C)_f(\nabla C)_f\cdot\vec{k}+\int_V b dV\right\}+\sum_f F_f^H\end{aligned} \tag{12}$$

where, $F_f=\vec{u}_f\cdot\vec{n}_f A_f$; $D_f=\left|\vec{\Delta}\right|_f(\Gamma_C)_f A_f/d_{AP}$, $\vec{\Delta}$ and $\vec{k}$ are the splitting vectors; $P_f=F_f/D_f$; F_f^H has different form for

each scheme and its definition is tabulated in Table 1.

Second-order time discretization (Crank-Nicolson)

A common form for Crank-Nicolson can be written as

$$a_P C_P = \sum_{nb} a_{nb} C_{nb} + b_P \tag{13}$$

where, different coefficients are as a follow

$$a_P = \sum_{nb} a_{nb} + \sum_f \max(F_f, 0) + S_P V_P + \frac{2V_P}{\Delta t}$$

$$a_{nb} = D_f A(|P_f|) + 2(1-\omega_f)\max(-F_f, 0)$$

$$b_P = -\sum_f \min(F_f, 0) C_P + \frac{2V_P}{\Delta t} C_P + S_C V_P + \sum_f A_f (\Gamma_\phi)_f (\nabla C)_f \cdot \vec{k}$$
$$+ \sum_f F_f^H + F_P^0; F_P^0 = \left(\sum_{nb} a_{nb} C_{nb} + b_P - a_P \phi_P \right)^0$$

The definition of F_f^H is the same as above, superscript '0' denotes the last time step.

3.3. Numerical Results

The verification of Q-QUICK/UQ-QUICK has been investigated on three values of unstructured mesh numbers: 454, 1770 and 3955 with quadrilateral grids only. As it can be seen from Figure 4, the computational Grid 1 and Grid 2 are intentionally twisted along the pollutant downstream. Generalized Minimum Residual (GMRES (30)) method with the Incomplete LU (ILUT) precondition is used to accelerate the convergence of the linear equation. The numerical precision is indicated by relative errors defined as follow:

$$\varepsilon = \sum_i |C_i - C_{i0}| \Big/ \sum_i C_{i0} \tag{14}$$

If t=1.25s, the relative errors and CPU time of different schemes are listed in Table 2, concentrations of each scheme along line $y=x$ are also illuminated in Figure 5.

- Numerical precision: At the same scheme of time discretization, the numerical precision of Q-QUICK/ UQ-QUICK/ CDS are much better than UDS/HDS/PDS, as for Q-QUICK/ UQ-QUICK/ CDS themselves, Q-QUICK/ UQ-QUICK exhibit a little lower relative errors that those of CDS especially on sparse grids. In addition, Q-QUICK and UQ-QUICK show a similar numerical precision. Furthermore, with the increasing mesh numbers, Q- QUICK/ UQ-QUICK/CDS can fit well to the benchmarks quickly and on Grid 3 they can perform a perfectly match.
- CPU time: Q-QUICK and UQ-QUICK consume a slight longer CPU times than those of other schemes. As for comparison by them, Q-QUICK seems a little economical. This is reasonable for its little auxiliary nodes in scheme reconstruction.
- Numerical stability: After applying the deferred correction method for Q-QUICK/UQ-QUICK and over-relaxed approach for cross derivative term approximation, most of the schemes can keep a good numerical stability except that CDS has a little vibration on relative sparse grids. In addition, these schemes are in sensitive to high grid deformation.

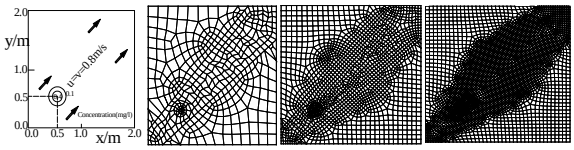

(a) Domain and initialization (b) Grid1 (c) Grid2 (d) Grid3

Figure 4. Computational domain and grids.

Table 2. Relative errors and CPU time.

Time Discretization	Convective Flux Discretization	Grid1		Grid2		Grid3	
		Errors	*CPU Time (s)*	*Errors*	*CPU Time (s)*	*Errors*	*CPU Time (s)*
UDS	UDS	0.6758	0.36	0.5042	1.85	0.4087	5.30
	CDS	0.3794	0.34	0.1726	1.69	0.1463	4.50
	HDS	0.6001	0.28	0.3700	1.36	0.2371	3.81
	PDS	0.6037	0.37	0.3835	1.78	0.2780	4.86
	Q-QUICK	0.2395	0.41	0.1597	1.93	0.1450	5.47
	UQ-QUICK	0.2483	0.41	0.1585	1.97	0.1454	5.55
Crank-Nicolson	UDS	0.6562	0.32	0.4625	1.50	0.3494	4.10
	CDS	0.3720	0.31	0.1011	1.39	0.0410	3.66
	HDS	0.5737	0.28	0.3039	1.22	0.1330	3.17
	PDS	0.5764	0.34	0.3201	1.52	0.1858	4.03
	Q-QUICK	0.1570	0.35	0.0507	1.58	0.0298	4.26
	UQ-QUICK	0.1600	0.36	0.0508	1.64	0.0309	4.38

For further clearly representing the numerical precision by each scheme, the distributions of concentration at 1.25s within the whole computational domain are also illustrated in Figure 6 (Grid 1, Crank-Nicolson). As referenced to analytic solution, the suggested scheme Q-QUICK or UQ-QUICK can keep pollutant cloud shape well more similar to that of benchmark, UDS and HDS numerically dissipate a lot and the corresponding shape almost distort, UDS exhibits better than the former two schemes, however, its shape shows not so matching especially in the left part.

4. Conclusions

In present study, two modified QUICK namely Q-QUICK and UQ-QUICK are introduced and their verifications were conducted on 2D unsteady advection-diffusion equation of pollutants. The main conclusions are as follow:

1) For comparisons in relative error and computational time amongst various schemes on unstructured grids, it can be seen that Q-QUICK and UQ-QUICK have similar computational accuracy to the central difference scheme and similar numerical stability to upwind difference scheme after applying the deferred correction method.

2) Q-QUICK and UQ-QUICK's corresponding CPU times are approximately equivalent to those of traditional difference schemes and their abilities for adapting high grid deformation are robust.

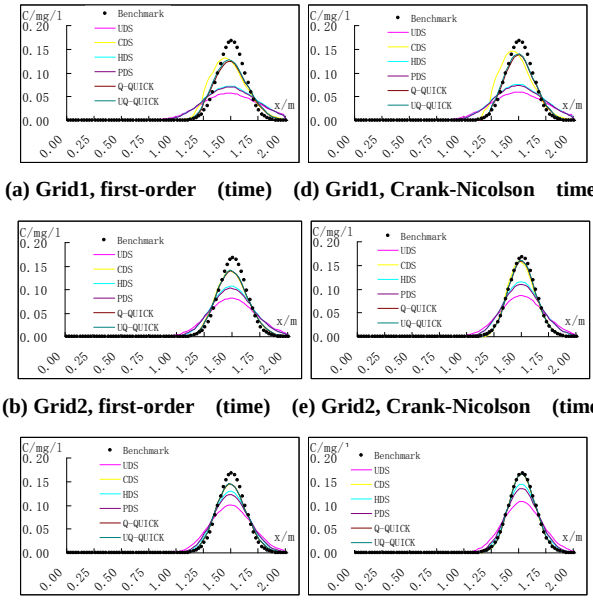

(a) Grid1, first-order (time) (d) Grid1, Crank-Nicolson time)

(b) Grid2, first-order (time) (e) Grid2, Crank-Nicolson (time)

(c) Grid3, first-order (time) (f) Grid3, Crank-Nicolson (time)

Figure 5. Illustration of comparisons of concentration along line *y*=*x* at *t*=1.25s.

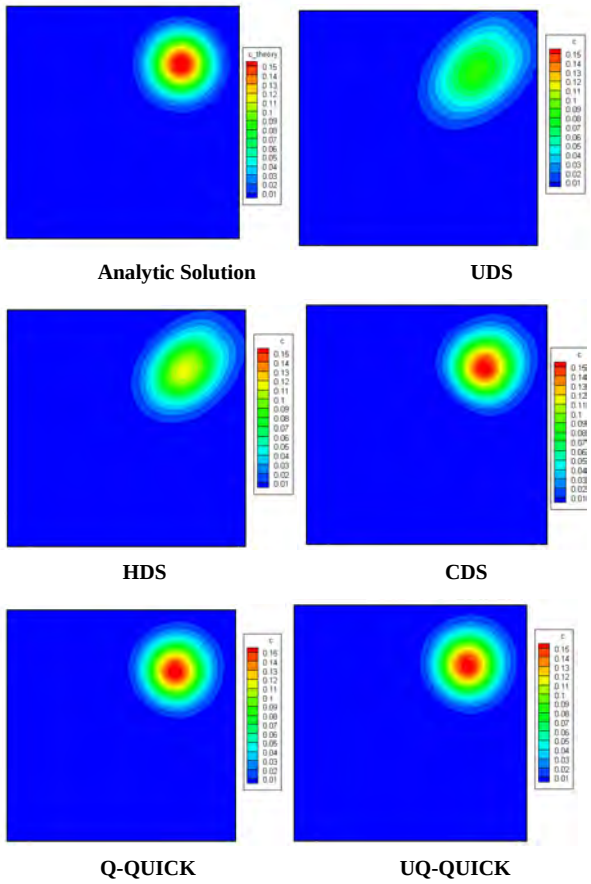

Figure 6. Illustration of comparisons of concentration in the plane at *t*=1.25s. (Grid1, Crank-Nicolson).

3) It is so promising to apply the suggested schemes to simulate pollutant transportation in shallow water with the merit of higher numerical precision.

5. Acknowledgments

This research was sponsored by Research Initiation Funds for Doctor (No.YJJ0906/SL01) of Changjiang River Scientific Research Institute ; 2009 National Public Research Institutes for Basic R & D Operating Expenses Special Project (No.YWF0901 and No.YWF0905); National Basic Research Program of China (No.2007CB714100, No. 2007CB714106).

6. References

[1] R. S~mkiewiez, “Oscillation-free solution of shallow water equations for nonstaggered grid,” Journal of Hydraulic Engineering, ASCE, Vol. 119, No. 10, pp. 1118−1137, 1993.

[2] J. Fletcher, “Computational techniques for fluid dyrtaralcs,” 8pfinger-Vedag, Berlin, No. 1, 1991.

[3] J. Shi and E. F. Toro, “Fully discrete high-order shock-eaptunng numerical schemes,” Internationa1 Journal for Numerical Methods in Fluids, Vol. 23, pp. 241−269, 1996.

[4] S. Sankaranarayanan, N. J. Shankar, and H. F. Cheoag, “Three-dimensional finite difference model for transport conservative pollutants,” Ocean Engneering, Vol. 25, No. 6, pp. 425−442, 1998.

[5] R. J. Sobey, “Fraetional step algorithm for estruaine mass transport,” International Journal for Numerical Methods in Fluids, Vol. 3, pp. 567−581, 1983.

[6] B. P. Leonard, “Simple high accuracy resolution program for convective modelling of discontinuities” International Journal for Numerical Methods in Fluids, Vol. 8, pp. 1291−1318, 1988.

[7] B. J. Noye and H. H. Tan, “A third-order semi-implicit finite difference method for solving one-dimensional eonvectlon-dlffusion equation,” International Journal for Numerical Method in Engineering, Vol. 26, pp. 1615−1629, 1988.

[8] B. J. Noye and H. H. Tan, “Finite difference method for the two-dimensional advetion difusion equation” International Journal for Numerical Methods in Fluids, Vol. 9, pp. 75−98, 1989.

[9] A. Pollard, A. L. Siu, and L. W. Siu, “The calculation of some laminar flows using various discretization schemes,” Comp. Meth. Appl. Mech. Eng., Vol. 35, pp. 293−313, 1982.

[10] S. V. Pantankar, Numerical Heat Transfer, McGraw−Hill, New York, 1980.

[11] M. K. Patel and N. C. Markatos, “An evaluation of eight discretization schemes for two-dimensional convection-diffusion equations,” International Journal for Numerical Methods in Fluids, Vol. 6, pp. 129−154, 1986.

[12] L. Davidson, "A pressure correction method for unstructured meshes with arbitrary control volumes," International Journal for Numerical Methods in Fluids, Vol. 22, pp. 265−281, 1996.

[13] Y. Saad and M. H. Schultz, "Gmres: A generalized minimal residual algorithm for solving nonsymmetric linear systems," SIAM. J. Sci. Stat. Comput., Vol. 7, 1986.

[14] B. P. Leonard, "Third-order finite-difference method for steady two-dimensional convection," Numerical Methods in Laminar and Turbulent Flow, pp. 807−819, 1978.

[15] S. I. Karaa and J. Zhan, "High order ADI method for solving unsteady convection diffusion problems," Journal of Computational Physics, Vol. 198, No. 1, pp. 1−9, 2004.

[16] H. Jasak, "Error analysis and estimation for the finite volume method with applications to fluid flows," Ph.D. thesis, Imperial College, University of London, London, 1996.

[17] B. Basara, "Employment of the second-moment turbulence closure on arbitrary unstructured grids," International Journal of Numerical Methods in Fluids, Vol. 44, pp. 377−407, 2001.

[18] Y. Y. Tsui and Y. F. Pan, "A pressure-correction method for incompressible flows using unstructured methes," Numerical Heat Transfer, Part B, Vol. 49, pp. 43−65, 2006.

J. Water Resource and Protection, **2009, 1, 368-375**
doi:10.4236/jwarp.2009.15044 Published Online November 2009 (http://www.sciRP.org/journal/jwarp).

Forecasting of Runoff and Sediment Yield Using Artificial Neural Networks

Avinash AGARWAL[1], R. K. RAI[2], Alka UPADHYAY[2]
[1]*National Institute of Hydrology, Roorkee, Uttarakhand, India*
[2]*DHI (India) Water & Environment Pvt. Ltd., New Delhi, India*
E-mail: *rai.raveendra@gmail.com*
Received June 16, 2009; *revised July* 16, 2009; *accepted July* 27, 2009

Abstract

Runoff and sediment yield from an Indian watershed during the monsoon period were forecasted for different time periods (daily and weekly) using the back propagation artificial neural network (BPANN) modeling technique. The results were compared with those of single- and multi-input linear transfer function models. In BPANN, the maximum value of variable was considered for normalization of input, and a pattern learning algorithm was developed. Input variables in the model were obtained by comparing the response with their respective standard error. The network parsimony was achieved by pruning the network using error sensitivity - weight criterion, and model generalization by cross validation. The performance was evaluated using correlation coefficient (CC), coefficient of efficiency (CE), and root mean square error (RMSE). The single input linear transfer function (SI-LTF) runoff and sediment yield forecasting models were more efficacious than the multi input linear transfer function (MI-LTF) and ANN models.

Keywords: Artificial Neural Network, Forecasting, Runoff, Sediment Yield

1. Introduction

Rainfall-runoff-sediment yield is the most complex hydrological phenomenon to comprehend due to tremendous spatial variability of watershed characteristics and precipitation patterns, making the physical modeling quite complex and involved. The quantity of runoff and sediment yield resulting from a given rainfall depends mainly on rainfall intensity, duration, and distribution besides others, such as initial soil moisture, land use, slope, etc. The runoff is critical to many water resources activities, for example, design of flood protection works, protection of agricultural lands, planning of water storage and release, etc. The erosion in the watershed may be occurred due to rainfall and runoff, and degrades its land. The sediment transport caused the reduction of storage capacity of rivers and reservoirs. Also, sediments can carry pollutants such as radioactive materials, pesticides and nutrients, and their transportation is generally avoided.

A number of linear and non-linear hydrological models have been developed since 1930's for describing the processes of rainfall-runoff, runoff-sediment yield, and rainfall-runoff-sediment yield in a watershed fluvial system, and these are also useful in forecasting. These models can be broadly classified as lumped, conceptual, hydrological, and hydraulic models. The physically based classical models requires wide range of parameters related to land uses, soil characteristics, soil horizon, watershed treatment, man made activities, conservation practices, soil moisture variation, topographic data, surface roughness, etc. These parameters vary significantly over a space and time, and very difficult to monitor. Under these circumstances, classical models require assumption of the parameters. Most common assumption to be made for describing the rainfall-runoff-sediment yield process is: sediment produced in the catchments is uniformly distributed over the catchments, uniform soil group, approximation of slopes, etc. These assumptions create lumped-ness in the physically based distributed classical model. On the other hand, ANN based approach yields satisfactory results without going into the details of catchments characteristics. The artificial neural network (ANN) approach comprises both linear and non-linear concepts in model building, and can be operated with the dynamic or memory less input-output system. It has the following major advantages [1]. 1) An ANN model does not require a prior knowledge of the system and, therefore, can be applied to solve the problems not clearly defined, 2) The model has more tolerance to noise and incomplete data, and thus, requires less data

for model development, and 3) The results are the outcome of the collective behavior of data, and thereby, the effect of outlier is minimized. In ANN, the gradient descent search optimization embedded with back propagation algorithm [2] is quite popular in ANN for exploring diverse areas such as bio-medical, engineering, image processing, water resources, and others [3,4].

The hydrologic applications of ANN include modeling of daily rainfall-runoff-sediment yield process, snow-rainfall process; assessment of stream ecological and hydrological responses to climate change; rainfall-runoff forecasting, sediment transport and groundwater quality forecasting, and groundwater remediation. A good overview of ANN application to rainfall-runoff simulation and forecasting is available elsewhere [5−16]. Imrie improved the generalization by adding a guidance system to the cascade correlation learning architecture and extrapolation properties using an activation function. Wilby interpreted the internal behavior of an ANN-based rainfall-runoff model by deleting all the nodes other than the hidden nodes and comparing the state variables and internal fluxes. Danh and Elshorbagy proposed back propagation artificial neural network (BPANN) models for runoff forecasting using fixed stopping criterion and independent variables, respectively, and compared them for performance with the available conceptual models.

It is apparent from above that the generalization of ANN models for varying data sets and their application to sediment modeling do not appear to have been studied extensively or even attempted. Thus, the objective of the study is to develop memory-based linear transfer function, ANN-based runoff and sediment yield forecasting models for daily and weekly time periods; and to evaluate the model performance for their forecasting abilities using the data of the Vamsadhara River watershed of India.

2. Model Development

The linear transfer function (LTF) models require minimum input and computation, and yield the results of desired accuracy [17]. In an LTF, two or more time-dependent observations are linked as:

$$S_t = \sum_{j=1}^{p} a_j S_{t-j} + \sum_{j=1}^{q} b_j R_{t-j+1} + \sum_{j=1}^{r} c_j Q_{t-j+1} \quad \cdots\cdots(1)$$

where, S_t is the dependent observation; R_t and Q_t are independent observations; p, q, r are the response or time memory; and a_j, b_j, c_j are the parameters associated with the j^{th} variable. Least square method can be used to solve the set of t linear equations for parameters. Representing $[a_1, a_2,\ldots, a_p, b_1, b_2,\ldots,b_q, c_1, c_2,\ldots,c_r]^T$ as $\hat{H}$, the variance of the response {var ($\hat{H}$)} is given as [17]: Var ($\hat{H}$) = $[A^T A]^{-1} \sigma^2$, where A is the input matrix and σ^2 is the variance of error term (e_t) expressed as:

$$\sigma^2 = (t-p-q-r)^{-1} \sum_{j=1}^{t} e_j^{\,2} \qquad (2)$$

The Var ($\hat{H}$) helps in parsimonious selection of response or time memory by comparing the respective standard error (SE) associated with each response ($\hat{H} \geq \sqrt{\mathrm{Var}(\hat{H})}$) as follows. The initially selected response value is increased one by one and if the resulting $\hat{H}$ is less than the respective standard error {$\sqrt{\mathrm{Var}(\hat{H})}$}, otherwise the response value is decreased one by one. The obtained response value represents the number of successive past events of the variable affecting output [17].

In a feed forward BPANN scheme, nodes of the input layer receive the normalized data set (input). The weighted sum corresponding to each node of next layer is calculated and passed to next layer usually through a sigmoid activation function. For updating the weights of interconnection, the error (E) is calculated at the output as;

$$E = \frac{1}{2} \sum_{1}^{k} [d_{(k)} - O_{(k)}]^2 \qquad (3)$$

This error is propagated back to hidden layer and finally to input layer. Here, $d_{(k)}$ is the observed output at the k^{th} node of the output layer and $O_{(k)}$ is the estimated output at the k^{th} node of the output layer. In all iterations, weights are updated using $W_{(ij)\,n+1} = W_{(ij)\,n} + \Delta W_{(ij)\,n}$.

The speed of convergence in gradient descent is normally increased by introducing a momentum term β ($0 < \beta < 1$) considering the effect of previous weight change as:

$$W_{(ij)\,n+1} = W_{(ij)n} + \Delta W_{(ij)n} + \beta[W_{(ij)n} - W_{(ij)n-1}] \qquad (4)$$

The change in weights (ΔW) in the direction of negative gradient is given by $\Delta W_{(ij)} = -\alpha\ \partial E/\partial W_{(ij)}$, where α is learning rate such that $0 < \alpha < 1$. The learning rate governs the rate of change of weights.

The network parsimony (minimum network structure) can be achieved through A information criterion (AIC) [18], B information criterion (BIC) [19], or by pruning of network [20]. AIC and BIC utilize SE statistic for deciding the number of free parameters [21]. In pruning, [20] suggested the use of error sensitivity $Se_{(ij)}$ with respect to weight $W_{(ij)}$ for elimination of the respective weight without involvement of excessive calculations. $Se_{(ij)}$ is defined as:

$$Se_{(ij)} = -\frac{\partial E}{\partial W_{(ij)}} \int_{W^f_{(ij)}}^{W^i_{(ij)}=0} W^f_{(ij)} \qquad (5)$$

Finally, $Se_{(ij)}$ with respect to $W_{(ij)}$ reduces to:

$$Se_{(ij)} = \sum_{1}^{it} \frac{\Delta W_{(ij)}^{\,2}}{\alpha} \cdot \frac{W^f{}_{(ij)}}{W^f{}_{(ij)} - W^i{}_{(ij)}} \quad \cdots\cdots\cdots(6)$$

Table 1. Summary of annual hydrological data of Vamsadhara River basin.

Year	Weighted Average Rainfall (mm)	Runoff (m^3/s)	Runoff (mm)	Sediment yield (kg/s)	Runoff-Rainfall Ratio	Sediment Yield-runoff ratio/ Sediment Concentration ($kg/m^{3)}$
1984	965.2	13245.2	146.3	28917.2	0.15	2.18
1985	1079.6	17195.9	190	29802.3	0.18	1.73
1986	971.7	20519.6	226.7	36233	0.23	1.77
1987	715.8	6506.6	71.9	12230.4	0.1	1.88
1988	1053.7	25454.9	281.2	42742.8	0.27	1.68
1989	1074.2	19789.9	218.7	30699.6	0.2	1.55
1992	1028.7	40017.2	442.1	62668.2	0.43	1.57
1993	773.3	15005.5	165.8	20177.2	0.21	1.34
1994	1142.3	31896.4	352.4	33675.8	0.31	1.06
1995	1010.6	34237.4	378.3	30291.5	0.37	0.88

where, i and f indicate the initial and final values of weights. Since the weight update is available during learning, only summation of squares of change in weight, i.e. $\Sigma \Delta W_{(ij)}{}^2$, is determined for estimation of the sensitivity of error. A comparatively low sensitivity suggests the pruning of the corresponding node.

The model can be generalized by cross-validation, but without ascribing a level of accuracy in the beginning of model formulation. The performance of the developed model is checked in all iterations. In this method, the network is trained on training data set and its statistical performance is evaluated on training and cross-validation data sets. The method monitors the generalized performance, and the process of learning is stopped when there is no more improvement in training along with the performance in cross validation period. For performance, the following statistical and hydrological criteria were used in the present analysis.

2.1. Correlation Coefficient (CC)

The correlation between the observed and estimated values is accounted by the correlation coefficient expressed as follows.

$$CC = \frac{\sum_{j=1}^{n}\{(Y_j - \bar{Y})(\hat{Y}_j - \bar{\hat{Y}})\}}{\{\sum_{j=1}^{n}(Y_j - \bar{Y})^2 \sum_{j=1}^{n}(\hat{Y}_j - \bar{\hat{Y}})^2\}^{1/2}} \times 100 \qquad (7)$$

where, $\bar{Y}$ and $\bar{\hat{Y}}$ are mean of observed and estimated values, Y and $\hat{Y}$ are the observed and estimated values respectively and n is the number of observation.

2.2. Coefficient of Efficiency (CE)

Nash and Sutcliffe proposed this non-dimensional criterion on the basis of standardization of the residual variance with initial variance. It is estimated as follows:

$$CE = \left\{1 - \frac{\text{Residual Variance}}{\text{Initial Variance}}\right\} x100 = \left\{1 - \frac{\sum_{j=1}^{n}(Y_j - \hat{Y}_j)^2}{\sum_{j=1}^{n}(Y_j - \bar{Y})^2}\right\} x100 \quad \cdots\cdots(8)$$

A perfect agreement between the observed and estimated values yields the coefficient of efficiency as 100 percent. For zero agreement, all the estimated values must be equal to the observed mean. A negative efficiency shows that the estimated values are less than the observed mean. It can be used to compare the model's relative performance on different watersheds.

2.3. Root Mean Square Error (RMSE)

An alternate criterion of residual error is the root mean square error [22] which is expressed as the measure of mean of the residual variance summed over the period, that is:

$$RMSE = \sqrt{\frac{\text{residual variance}}{n}} = \left(\frac{\sum_{j=1}^{n}(Y_j - \hat{Y}_j)^2}{n}\right)^{1/2} \qquad (9)$$

3. Study Area

The Vamsadhara river basin is located between $18^0$15' to $19^0$55' north latitudes and $83^0$20' to $84^0$20' east longitudes (Figure 1) situated between Mahanadi and Godavari river basins in South India. The river originates from Kalahandi and travels through a distance of about 254 km before it joins the Bay of Bengal. Its principal tributaries are Chauldua, Phaphalia, Ganguda, Sanna Nadi, and Mahendrathanaya. The watershed (7820 km^2) has six raingauge stations: Kutraguda, Mohana, Gudari, Mohandragarh, Gunur, and Kashinagar. Weighted rainfall for study was estimated by considering the Thiessen po-

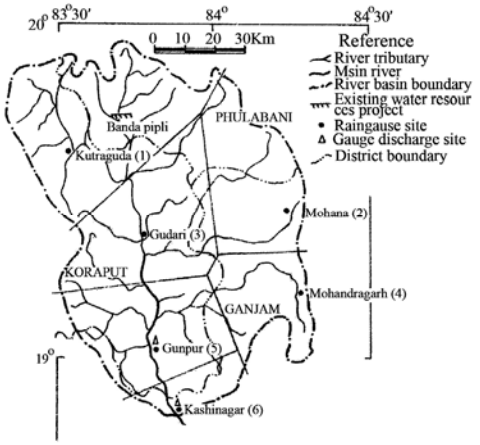

Figure 1. Index map of Vamsadhara River basin showing catchment details.

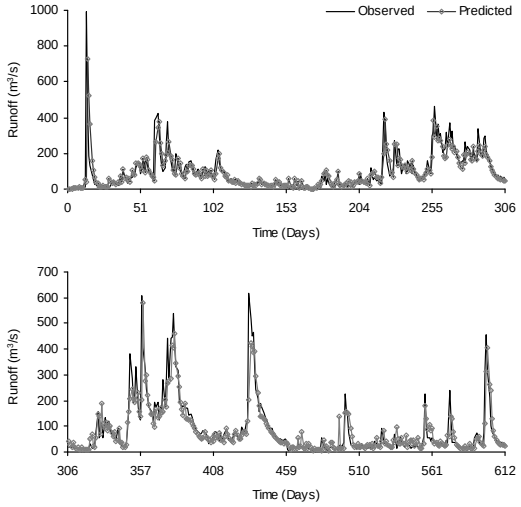

Figure 2. Daily observed and predicted runoff from SI-LTF model during calibration period (1984-87).

lygons as shown in Figure 1. The calculated weights for each rainguage, starting from rainfall stations one to six were 0.2640, 0.1835, 0.2696, 0.1096 and 0.0224 respectively. The yearly weighted rainfall, runoff and sediment yield are shown in Table 1. The mean annual rainfall and temperature varies from 170 to 1280 mm, and 10 to 43 °C, respectively and humidity is above 95% during the monsoon. The soils of area can be classified into mixed red, black soils, red sandy soils, yellow soils, coastal sands, and forest soils, and its surface is mostly covered with *Kankar* and *Murum*. The hydro-meteorological data are being collected by India Meterological Department (IMD) and Central Water Commission (CWC), Godavari Mahanadi Circle Division, South Eastern Region, Bhubaneswar, Orissa. The measurements include rainfall, stage and sediment concentration in a one litre of sample. Rainfall is measured by India Meteorological Department (IMD) in the units of mm/day using a self recording raingauge. The runoff is recorded by CWC by area velocity method and observed once in a day starting at 8.00 h. The velocities are measured by current metre and using sounding rod. The runoff recorded by CWC is reported in the units of m^3/s. The sediment yield, that is the suspended is measured by taking 1*l* water sample and is reported in the units of kg/m^3.

In this study, the daily rainfall, runoff, and sediment yield data of monsoon period (June 1–October 31) for 1984-1987 were used for model calibration, and the data of 1988-89 and 1992-95 for cross validation and verification.

4. Analysis of the Results

In the present study, the acceptable significance limits only for CC and CE for the model were considered as > 75% and > 60% respectively. The criterion RMSE is basically used to compare the models and therefore no limits for these criteria have been fixed for evaluating the performance of a particular model. The descriptive statistic of data used in model development, cross-validation, and verification is shown in Table 1. It is seen that runoff-rainfall ratios for 1992, 1994, and 1995 are higher than those in other years, implying that the verification with former years data may underestimate the runoff. However, sediment concentration values in 1993, 1994, and 1995 are lower than those in the other years, and therefore, the developed models may overestimate the sediment yield in those verification years.

4.1. Runoff Forecasting

4.1.1. Model development

1) SI-LTF model:

Following the above-described procedure, the single-input linear transfer function (SI-LTF) rainfall (R)-runoff (Q) models were developed for daily and weekly time steps, and the results are shown in Table 2. In this table, the value of time memory for input rainfall is a maximum, and for runoff, it is a maximum of three. The time memories of runoff are 3 and 2 respectively for daily and weekly models, indicating that the lumping of time periods from daily to weekly reduced the time memory of the runoff. It can be inferred from the values of CC and CE that the daily runoff forecasting model performed better than the weekly model (Table 2). Daily observed and predicted runoff by SI-LTF model during calibration period is shown in Figure 2.

2) MI-LTF model:

The multi-input linear transfer function (MI-LTF) models account for the spatial variation of rainfall over the watershed. Therefore, rainfall values of all raingauge stations, viz., R1 to R6 along with runoff (Q) were utilized in models of the considered time steps, and the results are shown in Table 2. It is observed that the rainfall

Table 2. Model order and corresponding parameters for different time periods of runoff forecasting in SI-LTF and MI-LTF models for Vamsadhara River basin.

Model and variable		Model Parameter Associated with Input time Memory			Performance of Developed Model		
		t-1	t-2	t-3	CC (%)	CE (%)	RMSE
SI-LTF (Daily)	**R**	3.390	--	--	--	--	--
	Q	0.524	0.127	0.181	80.0	64.0	65.0
SI-LTF (Weekly)	**R**	6.192	--	--	--	--	--
	Q	0.332	0.202	--	62.7	37.9	490.0
MI-LTF (Daily)	**R1**	0.728	0.479	--	--	--	--
	R5	0.296	--	--	--	--	--
	R6	2.166	--	--	--	--	--
	Q	0.448	0.249	--	80.0	63.3	66.0
MI-LTF (Weekly)	**R4**	0.894	--	--	--	--	--
	R6	5.173	--	--	--	--	--
	Q	0.333	0.203	--	62.9	38.1	490.0

at Mohana (R2) and Gudari (R3) does not influence the output of any time scale model though these areas are located near the centroid of the watershed. It may be attributed to the presence of a dense forested area in the middle of the watershed acting as a sink. The time memory of the runoff in multi-input daily and weekly is 2. Again the results infer that the daily runoff forecasting model performed better than weekly model.

3) ANN model:

Artificial neural network (ANN) models developed for daily and weekly bases with sigmoid as activation function by pattern learning were subjected to maximum 5000 iterations. The highest value of respective variable in series was considered for normalization of input and output variables. The learning rate (α) and momentum term (β) were assumed constant (0.5) for error convergence. All interconnecting weights were updated using the error of input-output pairs. The pattern learning is governed by the error of each data set, and the interconnecting weights simultaneously adjusted. The processing is however slow as it continuously improved the weights for each data set.

The three-layer network structure was selected so that the number of nodes in the input layer equaled the number of input variables. Due to non-availability of guidelines [1], the number of hidden nodes in the hidden layer(s) was initially taken twice the input nodes [23] and it was increased by one at a time considering the improved generalization and the above pruning criterion. Corresponding to one output, only one node was taken in the output layer. Thus, a three-layer network structure with varying numbers of hidden nodes in the hidden layer was tried, and the performance, in both cross-validation and validation, of the finally selected ANN models for all above mentioned time steps for pattern learning is shown in Table 3. In this table, the generalized case exhibits least errors in both calibration and cross-validation. Here, the data of 1984 to 1987 were used in calibration, and the data of 1988 to 1989 and 1992 to 1995 in cross-validation, referred as the first and second verification periods in the text, respectively. Performance of daily models both in calibration and cross-validation is better than the weekly model suggesting that the daily model is better than weekly model.

4.2. Sediment Yield Forecasting

4.2.1. Model Development

1) SI-LTF model:

These models consisted of rainfall (R), runoff (Q), and sediment yield (Sy), and the results are given in Table 5. Apparently, the results of daily model show the effect of one day preceding sediment yield on today's computed sediment yield. Daily observed and predicted sediment yield by SI-LTF model during calibration period is shown in Figure 5. On the other hand, the weekly model has no preceding sediment yield term(s) in the model, implying that the preceding weekly or higher time step sediment yield have no effect on the current output. The model performance reduces with increased lumping of data to larger time periods. Based on the evaluation criteria, though no model passes the criteria, these could be used cautiously for the study area.

2) MI-LTF model:

Similar to the above, the rainfall values of six rainfall gauging sites were considered in the models developed for various time periods, and the results are given in

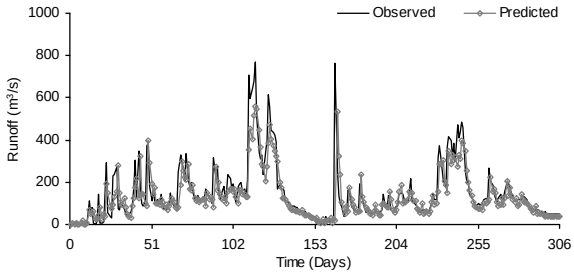

Figure 3. Daily observed and predicted runoff from SI-LTF model during verification period (1988-89).

Table 3. Pattern learned artificial neural network runoff forecasting models for different time periods for Vamsadhara River basin.

Model	Structure	Iteration	Performance in model development, %					
			Calibration (1984-1987)			Cross validation (1988-1989)		
			CC (%)	CE (%)	RMSE	CC (%)	CE (%)	RMSE
Daily	4,8,1	2490	83.8	70.1	60.0	79.5	62.5	82.0
Weekly	3,6,1	53	65.7	43.2	470.0	68.1	37.7	600.0

Table 4. Performance evaluation of SI-LTF, MI-LTF and ANN runoff forecasting models during verification stages.

Model	Performance evaluation criteria					
	Verification (1988 – 1989)			Verification (1992 - 1995)		
	CC, %	CE, %	RMSE	CC, %	CE, %	RMSE
SI-LTF (Daily)	80.7	63.5	80	86.7	72.4	103
SI-LTF (Weekly)	68.9	37.8	590	70.7	40.4	956
MI-LTF (Daily)	80.6	62.8	82	85.6	60.7	108
MI-LTF (Weekly)	68.2	39.5	592	70.6	39.9	961
ANN (Daily)	--	--	--	84.5	63.9	--
ANN (Weekly)	--	--	--	71.4	26.3	--

Table 5. Model order and corresponding parameters for different time periods of sediment yield forecasting in SI-LTF and MI-LTF models for Vamsadhara River basin.

Model and variable		Model parameters associated with input time			Performance evaluation of developed model		
		t-1	t-2	t-3	CC, %	CE, %	RMSE
SI-LTF (Daily)	R	15.98	--	--	--	--	--
	Q	0.31	0.23	--	--	--	--
	Sy	0.15	--	--	64.4	41.4	284.0
SI-LTF (Weekly)	R	17.60	3.21	--	--	--	--
	Q	0.25	--	--	--	--	--
	Sy	--	--	--	35.0	8.7	1551.0
MI-LTF (Daily)	R5	3.54	--	--	--	--	--
	R6	13.56	0.58	--	--	--	--
	Q	0.61	--	--	--	--	--
	Sy	0.07	--	--	65.0	42.2	282.0
MI-LTF (Weekly)	R4	10.73	4.79	--	--	--	--
	R6	4.95	--	--	--	--	--
	Q	0.17	--	--	--	--	--
	Sy	--	--	--	40.7	13.8	1507.0

Table 6. Pattern learned artificial neural network sediment yield forecasting models for different time periods for Vamsadhara River basin.

Model	Structure	Iteration	Performance in model development					
			Calibration (1984-1987)			Cross validation (1988-1989)		
			CC	CE	RMSE	CC	CE (%)	RMSE
Daily	4,8,1	65	63.4	40.0	290	57.3	31.0	280.0
Weekly	3,6,1	793	46.8	21.7	1400	44.0	15.7	1300.0

Table 7. Performance evaluation of SI-LTF, MI-LTF and ANN sediment yield forecasting models during verification stages.

Model	Performance evaluation criteria					
	Verification period (1988 – 1989)			Verification period (1992 - 1995)		
	CC	CE	RMSE	CC	CE	RMSE
SI-LTF (Daily)	60.3	35.3	268	67.9	45.0	347
SI-LTF (Weekly)	39.1	1.4	1367	45.5	18.6	2143
MI-LTF (Daily)	60.4	33.4	276	67.6	45.5	349
MI-LTF (Weekly)	40.4	3.1	1355	48.1	17.4	2158
ANN (Daily)	--	--	--	67.2	44.8	351
ANN (Weekly)	--	--	--	25.7	5.1	2300

Table 5. Similar to the single-input model, the daily multi-input model indicated the effect of successive past sediment yield on the output whereas weekly did not. In addition, the rainfall of Kutraguda (R1), Mohan (R2) and Gudari (R3) did not influence the output of any of the models despite their being in the center and upper part of the watershed, perhaps due to the presence of forest and better soil conservation practices in the Koraput district, which covers the polygon area of Kutraguda, Mohan and Gudari rain gauge sites (Figure 1). As seen and inferred from Table 5, the lumping of time periods improved the model performance in calibration.

3) ANN model:

Similar to above, the ANN models for various time steps were developed for sediment yield. The models were calibrated on 1984 to 1987 data set, cross-validated for maximum generalization with the data of first verification period (1988-1989). The ANN structure was selected as explained earlier, and the number of hidden nodes were selected on the bases of improved generalization and pruning criteria. The values of CC and CE indicated no model to perform well.

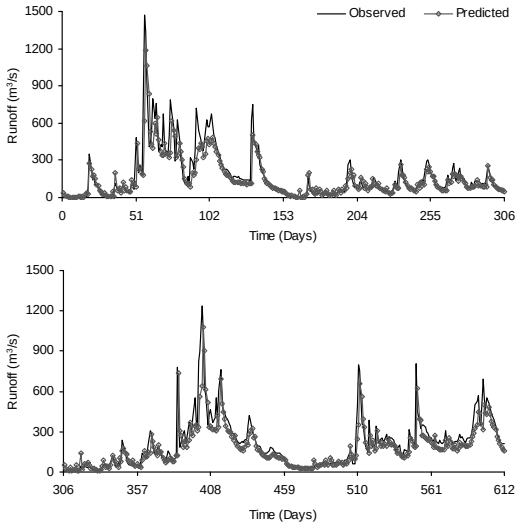

Figure 4. Daily observed and predicted runoff from SI-LTF model during verification period (1992-95).

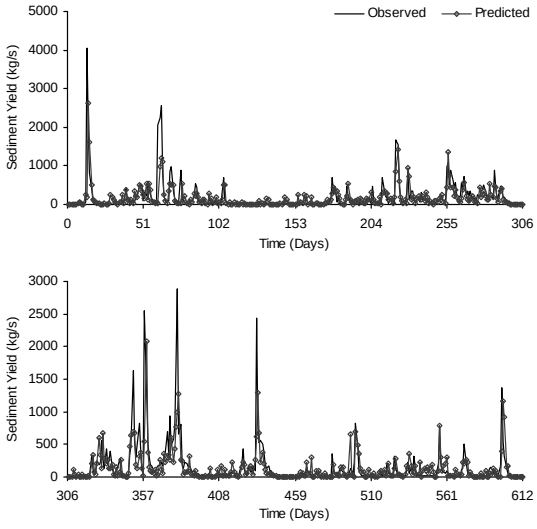

Figure 5. Daily observed and predicted sediment yield from SI-LTF model during calibration period (1984-87).

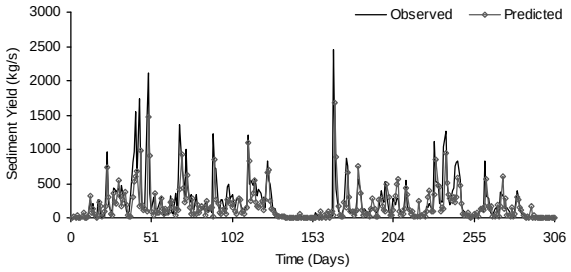

Figure 6. Daily observed and predicted sediment yield from SI-LTF model during verification period (1988-89).

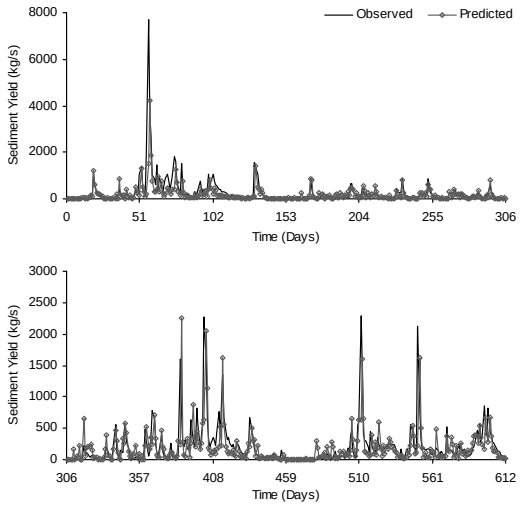

Figure 7. Daily observed and predicted sediment yield from SI-LTF model during verification period (1992-95).

4.2.2. Model Verification

Similar to the models performance in calibration, Table 7 shows non-workability of all the models in verification probably due to high variation of sediment concentration (Table 1) and nonhomogeneous data. However, the daily model worked better than the weekly model. Daily observed and predicted sediment yield by SI-LTF model during both the verification periods is shown in Figure 6 and 7.

5. Conclusions

The following conclusions can be drawn from the study:

1) A three-layered ANN structure with the number of

nodes in hidden layer as twice of the input nodes was the best generalized model obtained in less than 5000 iterations.

2) The daily SI-LTF, MI-LTF, ANN models worked well in runoff forecasting, whereas others failed in calibration as well as in both the verification periods. The daily SI-LTF model was superior to daily MI-LTF model in calibration as well as in both the verification periods. However, the daily ANN model showed an improvement over the former in calibration, but was slightly poor in cross-validation as well as in verification.

3) Any of the proposed SI-LTF, MI-LTF, ANN models can be useful for sediment yield forecasting with little variation in accuracy.

5. References

[1] A. S. Tokar and M. Markus, "Precipitation-runoff modelling using artificial neural networks and conceptual models," Journal of Hydrologic Engineering, Vol. 5, No. 2, pp. 156−161, 2000.

[2] D. E. Rumelhart, G. E. Hinton, and R. J. Williams, "Learning internal representations by error propagation," Parallel Distributed Processing, MIT Press, Cambridge, Vol. I, pp. 318−362, 1986.

[3] D. E. Rumelhart, B. Widrow, and M. A. Letr, "The basic ideas in neural networks" Communications of the ACM, Vol. 37, No. 3, pp. 87−92, 1994.

[4] A. Y. Shamseldin, K. M. O'Connor, and G. C. Liang, "Methods for combining the outputs of different rainfall-runoff models," Journal of Hydrology, Vol. 197, pp. 203−229, 1997.

[5] "ASCE (2000a) Task Committee on application of artificial neural networks in hydrology," Artificial Neural Networks in Hydrology, I: Preliminary Concepts, Journal of Hydrologic Engineering, ASCE, Vol. 5, No. 2, pp. 124−137.

[6] "ASCE (2000b) Task Committee on application of artificial neural networks in hydrology" Artificial Neural Networks in Hydrology, II: Hydrologic Application, Journal of Hydrologic Engineering, ASCE, Vol. 5, No. 2, pp. 115−123.

[7] A. Jagadeesh, B. Zhang, and R. S. Govindaraju, "Comparison of ANNs and empirical approaches for predicting watershed runoff," Journal of Water Resources Planning and Management, Vol. 126, No. 3, pp. 156−166, 2000.

[8] A. S. Tokar and M. Markus, "Precipitation-runoff modelling using artificial neural networks and conceptual models," Journal of Hydrologic Engineering, Vol. 5, No. 2, pp. 156−161, 2000.

[9] H. M. Nagy, K. Watanabe, and M. Hirano, "Prediction of sediment load concentration in rivers using artificial neural network model," J. Hydraulic Engrg., Vol. 128, No. 6, pp. 588−595, 2002.

[10] M. P. Rajurkar, U. C. Kothyari, and U. C. Chaube, "Modeling of the daily rainfall-runoff relationship with artificial neural networks," Journal of Hydrology, Vol. 285, pp. 96−113, 2004.

[11] K. P. Sudheer and S. K. Jain, "Radial basis function neural network for modeling rating curves." J. Hydrologic Engrg., Vol. 8, No. 3, pp. 161−164, 2003.

[12] T. W. Kim and J. B. Valdes, "Nonlinear model for drought forecasting based on a conjunction of wavelet transforms and neural networks," J. Hydrologic Engrg., Vol. 8, No. 6, pp. 319−328, 2003.

[13] H. Moradkhani, K. L. Hsu, H. V. Gupta, and S. Sorooshian, "Improved streamflow forecasting using self-organizing radial basis function artificial neural networks," Journal of Hydrology, Vol. 295, pp. 246−262, 2004.

[14] J. Olsson, C. B. Uvo, K. Jinno, A. Kawamura, K. Nishiyama, N. Koreeda, T. Nakashima, and O. Morita, "Neural networks for rainfall forecasting by atmospheric downscaling." J. Hydrologic Engrg., Vol. 9, No. 1, pp. 1−12, 2004.

[15] Keskin, M. Erol, and T. Özlem, "Artificial neural network models of daily pan evaporation" Journal of Hydrologic Engrg., Vol. 11, No. 1, pp. 65−70. 2006

[16] N. S. Raghuwanshi, R. Singh, and L. S. Reddy, "Runoff and sediment yield modeling using artificial neural networks: Upper siwane river," J. Hydrologic Engrg., India, Vol. 11, No. 1, pp. 71−79, 2006.

[17] J. Johnston, Econometric Methods, McGraw Hill, Tokyo, 1972.

[18] H. Akaike, "A new look at the statistical model identification," IEEE Transactions on Automatic Control, Vol. AC-19, pp. 716−723, 1974.

[19] Rissanenj, "Modeling by short data description," Automation, Vol. 14, pp. 465−471, 1978.

[20] E. D. Karnin, "A simple procedure for pruning back propagation trained neural networks," Institute of Electrical and Electronics Engineers Transactions on Neural Networks, Vol. 1, No. 20, pp. 239−242, 1990.

[21] Z. X. Xu and J. Y. Lijy, "Short term inflow forecasting using an artificial neural network model," Hydrological Process, Vol. 16, pp. 2423−2439, 2002.

[22] P. S. Yu, C. L. Liu, and T. Y. Lee, "Application of a transfer function model to a storage runoff process," Stochastic and Statistical Methods in Hydrology and Environmental Engineering, Vol. 3, pp. 87−97, 1994.

[23] K. W. Hipel, A. Ian, U. S. Panum, and V. P. Singh, "Stochastic and statistical methods in hydrology and environmental engineering," The series analysis in hydrology and environmental engineering, Kluwer Academic Publishers, The Netherlands, Vol. 3, 1994.

J. Water Resource and Protection, **2009, 1, 376-380**
doi:10.4236/jwarp.2009.15045 Published Online November 2009 (http://www.scirp.org/journal/jwarp)

Biological Nitrogen and COD Removal of Nutrient-Rich Wastewater Using Aerobic and Anaerobic Reactors

Florante A. MAGNAYE[1,2], Pag-asa D. GASPILLO[1], Joseph L. AURESENIA[1]
[1]*Chemical Engineering Department, De La Salle University-Manila, Manila, Philippines*
[2]*Chemical Engineering Department, Technological Institute of the Philippines-Manila, Manila, Philippines*
E-mail: *magnayef@yahoo.com*
Received September 2, 2009; *revised September* 30, 2009; *accepted October* 16, 2009

Abstract

A preliminary study on nitrogen and organic removal efficiency of a lab-scale system using aerobic and anaerobic reactors was performed. A simulated wastewater containing elevated levels of nitrogen was used. This paper aims to compare the efficiency of aerobic and anaerobic reactors in achieving nitrogen and chemical oxygen demand (COD) removal of nutrient-rich wastewater. It also presents the start-up experimentation conducted on simulated wastewater using two different reactors configured as aerobic and anaerobic. Start-up experiments were carried out using a 5-liter acrylic aerobic reactor and a 4-liter flask anaerobic reactor containing activated sludge taken from De La Salle University (DLSU) wastewater treatment plant as a source of inoculum. Simulated wastewater was continuously fed to the two reactors and the time course of biomass growth was monitored by measuring the biomass concentration represented by mixed liquor volatile solids (MLVS). The time course of organic pollutant reduction by measuring the chemical oxygen demand (COD) was conducted until steady state condition was reached. On the other hand, COD and nitrogen tests such as Ammonia nitrogen (NH_3-N), Nitrite nitrogen (NO_2^--N), Nitrate nitrogen (NO_3^--N) were also performed using 5 batch aerobic reactors containing different concentrations of wastewater and a single batch anaerobic reactor to see the effect of different feed concentrations in the removal of nitrogen. Preliminary results showed that 98% reduction in COD was obtained in aerobic reactor, as supported by increasing concentration of MLVS, with a hydraulic retention time (HRT) of 5 hours after 11 days while 34% reduction in COD was obtained in anaerobic reactor with the same HRT after 14 days.

Keywords: COD, MLVS, HRT, Aerobic, Anaerobic Reactors

1. Introduction

Nitrogen pollution of the world's oceans is harming marine ecosystem and contributing to global warming. Researches, which involved dozens of scientists from around the world, show that human activity is dramatically altering nitrogen cycles in Earth's oceans, soils and atmosphere. Nitrogen produced by human activity is responsible for nitrous oxide and carbon dioxide input to the world's ocean each year. The accumulation of reactive nitrogen in the environment at alarming rates may be as serious as putting carbon dioxide in the atmosphere [1]. The excess nitrogen can deplete essential oxygen levels in the water and has significant effects on climate, food production, and ecosystems all over the world [2], promote eutrophication and toxicity to aquatic organisms [3] and can cause several problems when discharged into the environment [4] as it is extremely harmful due to the high toxicity of free ammonia at a pH higher than 8 [5]. Because of this tremendous challenge of the global environment, it is, therefore, necessary to remove such substances from wastewater. Further, as environmental and legislative constraints increase, specifically the Philippine Clean Water Act, there is a considerable impetus for reducing the nitrogenous substances for wastewater before its reuse or deposit to the water body. The treatment of wastewater by biological technology has been widely adopted because of its easy operation and low pollution generation [6].

For many years, the traditional method for nitrogen removal from wastewater has been the combination of nitrification-denitrification processes [7]. With the aim to obtain better process stability, some researchers have been focusing on combinations of anaerobic and aerobic processes [8]. Different reactor configurations and sys-

tems working with one or two reactors can be used [9]. Simultaneous removal of nitrogen and COD can be achieved using the conventional nitrification and denitrification systems. However, over the past few years, new technologies for nitrogen removal have been developed mainly because of the increasing financial costs of traditional wastewater treatment technologies [7]. Some of the novel microbial nitrogen removal processes that have been developed are Single reactor system for High Ammonium Over Nitrite (SHARON) which involves part conversion of ammonium to nitrite, Anaerobic Ammonium Oxidation (ANAMMOX) process which involves anaerobic oxidation of ammonium and the Completely Autotrophic Nitrogen removal Over Nitrite (CANON) process which involves nitrogen removal within one reactor under oxygen-limited conditions [10]. There are other processes that have been developed such as Oxygen Limited Autotrophic Nitrification-Denitrification (OLAND) and a wetland based systems, all with high potential for nitrogen removal.

The development of the above novel microbial nitrogen removal processes is useful in attaining higher efficiency of nitrogen and COD removal from wastewater containing elevated level of nitrogen at a low cost. Prior to the use of these technologies, a preliminary study on the efficiency of nitrogen and organic removal of nutrient-rich simulated wastewater using two different reactors, aerobic and anaerobic, was conducted. This also aims to present the start-up experimentation from these reactors as reference for future study employing any of the above novel nitrogen removal processes.

2. Materials and Methods

Experiments were carried out using aerobic and anaerobic reactors. A continuous aerobic reactor was made up of acrylic board with a working volume of 5 liters where an air pump was used for aerobic zone. On the other hand, a continuous anaerobic reactor was made up of a 4-liter Erlenmeyer flask equipped with magnetic stirrer and stir bar to facilitate continuous stirring within the reactor. A photograph of the reactors used in this study is shown in Figure 1. Ports were provided for feeding the sample solution and withdrawing samples for analysis. Two 20-liter buckets were used to collect the effluent from both reactors. The seeding sludge for the laboratory reactors was taken from DLSU- Sequencing Batch Reactor (SBR) wastewater treatment plant.

A simulated wastewater containing glucose as carbon source and ammonium chloride as nitrogen source was prepared as feed to the reactors. It has an approximate COD concentration of 300 ppm and NH_3-N of 250 ppm. This simulated wastewater was continuously fed to aerobic and anaerobic reactors separately. COD test, mixed liquor volatile solid (MLVS), temperature and pH were performed regularly to monitor the time course until steady state condition was reached.

Batch reactors as shown in Figure 2 were made up of 5 1-liter imhoff cones supported by iron stand and iron ring with different concentrations of wastewater. Air pumps were also used for each reactor for aeration. Wastewater with different concentrations of NH_3-N and COD were

Figure 1. Aerobic and anaerobic reactors.

Figure 2. Batch reactors.

Table 1. Initial and final nitrogen concentrations in aerobic batch reactors.

COD (ppm)	Ammonia Nitrogen		Nitrite Nitrogen		Nitrate Nitrogen	
	Initial (ppm)	Final (ppm)	Initial (ppm)	Final (ppm)	Initial (ppm)	Final (ppm)
500 ppm Aerobic	18.89	0	0	9.60	0.2707	8.7934
1000 ppm Aerobic	30.91	0	0	19.20	0.1374	8.7542
1500 ppm Aerobic	103.13	0	0	93.80	0.1726	8.7267
2000 ppm Aerobic	137.50	0	0	120.40	0.2863	8.6954
2500 ppm Aerobic	171.86	0	0	160.00	0.2354	8.6679

fed to these reactors to see the effect of various feed concentrations in the removal of nitrogen as shown in Table 1. Furthermore, the same anaerobic reactor was used for batch mode operation. Unless otherwise specified, all parameters in this study were analyzed in accordance with the procedures stipulated in APHA Standard Methods [11].

3. Results and Discussions

The COD concentration profile in continuous aerobic reactor was shown in Figure 3 while that of continuous anaerobic reactor was shown in Figure 4. An initial COD of 300 ppm was fed to both reactors until steady state condition was reached. A COD value of 5.47 ppm as shown in Figure 3 was obtained and it became constant after 276 hours or approximately 11 days. Preliminary results showed that 98% reduction in COD was obtained in aerobic reactor as supported by increasing concentration of MLVS. On the other hand, the COD concentration profile of anaerobic reactor is shown in Figure 4. The same concentration of feed was introduced in the reactor and the COD value of 194.54 ppm was obtained and it became constant after 330 hours, that is approximately at steady state condition after 14 days. Only 34 % reduction of COD was obtained. The above data showed that aerobic bacteria have a higher capability to degrade faster the organic pollutant in wastewater as compared to anaerobic bacteria with the same hydraulic retention time (HRT) of 5 hours in the two reactors.

Figure 5 showed the COD concentration profile of 5 aerobic batch reactors with initial concentrations of 500, 1000, 1500, 2000 and 2500 ppm. It was found out that 71 to 97 percent reduction in COD was achieved under aerobic conditions within an average time of 4 to 5 days. The figure also revealed that the higher the COD concentrations, the faster its degradation in its early stage as shown by 2500, 2000 and 1500 ppm of COD. On the other hand, 1000 and 500 ppm of COD revealed that it takes a longer time to degrade. High COD loading resulted in a low COD removal of 71%. The absence of trend in these results maybe attributed to the various MLVS concentrations in the reactors since the carbon to nitrogen (C/N) ratio in all reactors were almost the same.

Initially, ammonia concentrations of the aerobic batch reactors were 18.89, 30.91, 103.13, 137.50 and 171.86 ppm. Wastewater sample had no nitrite-nitrogen but nitrate was present in a small amount as shown in Table 1. It was very evident that ammonia has been totally degraded at the end of 5 days to nitrite and nitrate with the help of ammonium oxidizing bacteria (AOB) that live in an aerobic environment. However, it was also observed that the higher the concentration, the longer it takes to degrade ammonia.

Figures 6 and 7 showed the nitrogen concentration

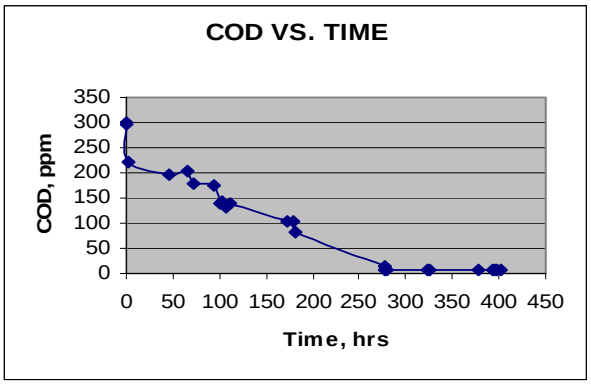

Figure 3. COD *vs.* Time.
(Continuous aerobic)

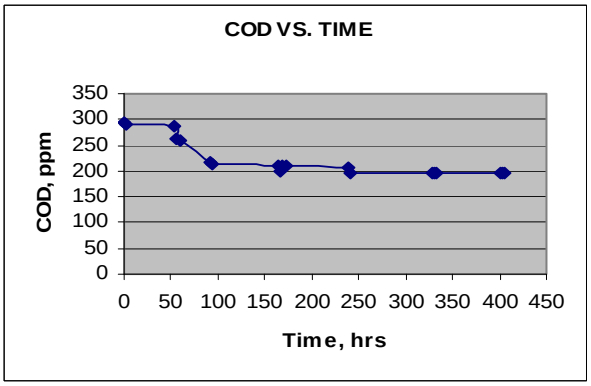

Figure 4. COD vs. Time.
(Continuous anaerobic)

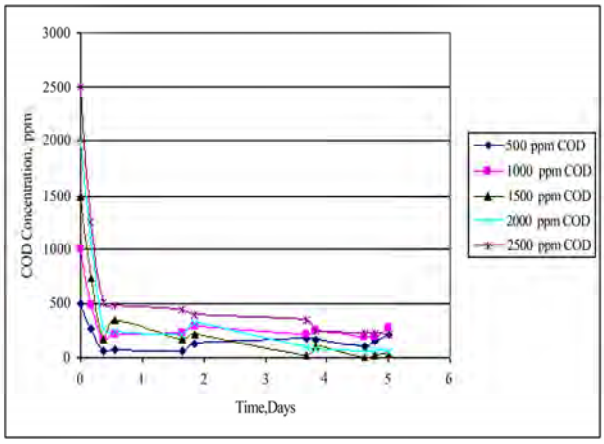

Figure 5. COD concentration profile in aerobic batch reactors.

profile in aerobic batch reactors. The lowest concentration used for NH_3-N was 18.89 ppm as shown in Figure 6 and the highest concentration used for NH_3-N was 171.86 ppm as shown in Figure 7. It was very evident from Figure 6 that the 18.89 ppm NH_3-N be-

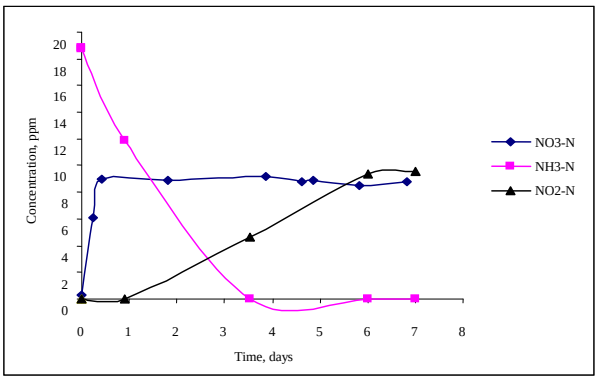

Figure 6. Nitrogen concentration profile in aerobic batch reactor (500 ppm of COD).

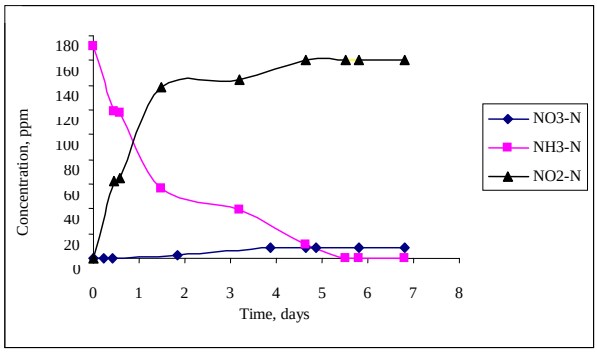

Figure 7. Nitrogen concentration profile in aerobic batch reactor (2500 ppm of COD).

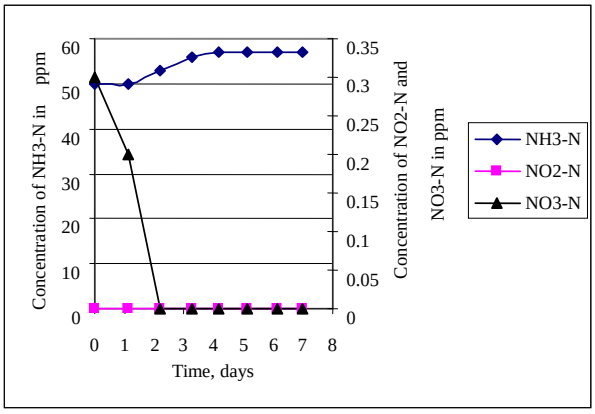

Figure 8. Nitrogen concentration profile in anaerobic batch reactor.

came totally degraded after 3.5 days while 171.86 ppm NH_3-N was totally degraded after 5.5 days. This revealed that the time to degrade NH_3-N also depends on the concentration of the feed, that is, the higher the concentration of NH_3-N, the longer the time required for its degradation assuming the same condition and biomass concentration in the reactor. It was also found out that the concentrations of NO_2-N and NO_3-N increased in both reactors. These results could be attributed to the activity of ammonium oxidizing bacteria (AOB) converting NH_3-N to NO_2-N and NO_3-N in aerobic environment. On the other hand, NO_2-N also increased in both reactors while there was a slight increase in NO_3-N concentration. It was suspected that the concentration of dissolved oxygen in the reactor was limited for further oxidation of nitrite to nitrate due to the higher affinity to oxygen of the ammonia than the nitrite oxidizing bacteria (NOB). One possible reason is maybe due to uncontrolled pH in the reactor resulting in partial nitrification. Presence of inhibitors for nitrite oxidizing bacteria may also be possible for low conversion of nitrite to nitrate though the microorganisms can adapt to the inhibitor after a long period of application and decrease its inhibiting efficiency [12].

Figure 8 showed the nitrogen concentration profiles of 50 ppm NH_3-N and 1000 ppm of COD in an anaerobic batch reactor. Theoretically, no ammonia conversion was expected in an anaerobic environment, only nitrate or nitrite conversions. Autotrophic nitrifiers need oxygen to be able to convert ammonia to nitrite and then to nitrate. However, from the result of the experiments, ammonia concentration was observed to have increased slightly. This may be attributed to the formation of ammonia from the protein content of wastewater dissociated in water. Based on the previous study, the effluent ammonia concentration sometimes exceeded the corresponding influent ammonia concentration due to ammonification of organic nitrogenous compounds under anaerobic conditions [13]. This may also be due to some organic compounds that have been found to be degraded to simple organic acids, alcohol, etc., rather than CO_2 and H_2O under anaerobic conditions which also limited COD reduction in the same condition [14]. Initially, there was no nitrite in the reactor and remained constant throughout. On the other hand, 0.3 ppm nitrate nitrogen was totally degraded under anaerobic condition due to denitrification process where nitrate was reduced to nitrogen gas. COD reduction in anaerobic environment maybe attributed to synthesis of biomass and methane gas [15,16].

The time course of biomass growth was monitored by measuring the biomass concentration represented by mixed liquor volatile solids (MLVS). The increasing concentration of MLVS suggested that the removal of nitrogen and COD in the two reactors is possible.

4. Conclusions

From the experimental results obtained, the following conclusions can be drawn:

1) At the same HRT, 98% reduction in COD was obtained in aerobic reactor against 34 % reduction in anaerobic reactor, therefore, anaerobic bacteria have a slower capability to degrade organics.

2) Nitrite accumulation and low nitrate build up in aerobic reactor was observed because of the low activity

of NOB maybe due to the presence of inhibitors or uncontrolled pH in the reactor during nitrification.

3) Aerobic process requires longer aeration time and produces large amount of sludge but they can remove ammonium nitrogen.

4) Anaerobic treatment methods usually offer advantages such as higher organic loading rates and production of usable biogas, however a relatively higher effluent concentration and incapability to remove ammonium nitrogen are some of its disadvantages.

5) Therefore, based on the above findings, it is more attractive to use combined anaerobic and aerobic systems for simultaneous removal of nitrogen and COD.

5. Acknowledgments

The authors wish to thank the Department of Science and Technology- Philippine Council for Industry and Energy Research and Development (DOST-PCIERD) and CH-ED Center for Excellence in Chemical Engineering for the financial support for this research project, De La Salle University-Manila and Technological Institute of the Philippines-Manila. Special thanks to Mr.Lucky Uy, Mr. Jorich Gaw and Ms. Diane Dy.

6. References

[1] J. N. Galloway, "Transformation of the nitrogen cycle: Recent trends, questions and potential solutions," Science Journal, May 2008.

[2] R. A. Duce, "Impacts of atmospheric anthropogenic nitrogen on the open ocean," Science Journal, May 2008.

[3] F. Moharram and R. Bhargava, "The Optimum stage for nitrification efficiency in the biofilm-ASP reactor," ICWNR'04, pp 24−31, 2003.

[4] M. Kermani, B. J. Bina, H. Movahedian, M. M. Amin, and M. Nikaeen, "Biological phosphorous and nitrogen removal from wastewater using moving bed biofilm process," Iranian Journal of Biotechnology, Vol. 7, No. 1, 2009.

[5] V. Reginatto, R. M. Teixeira, F. Pereira, W. Schmidell, J. A. Furigo, R. Menes, C. Etchebehere, and H. M. Soares, "Anaerobic ammonium oxidation in a bioreactor treating slaughterhouse wastewater," Brazilian Journal of Chemical Engineering, Vol. 22, No. 4, 2005.

[6] X. Zheng, J. Tong, H. J. Li, and Y. G. Chen, "The investigation of effect of organic carbon sources addition in anaerobic-aerobic (low dissolved oxygen) sequencing batch reactor for nutrients removal from wastewaters," Bioresource Technology, Vol. 100, pp. 2515−2520, 2009.

[7] D. Paredes, P. Kuschk, T. S. A. Mbwette, F. Stange, R. A. Muller, and H. Koser, "New aspects of microbial nitrogen transformations in the context of wastewater treatment: A review," Engineering Life Science, Vol. 7, No. 1, pp. 13−25, 2007.

[8] S. W. Hu, F. L. Yang, S. T Liu, and L. G. Yu, "The development of a novel hybrid aerating membrane-anaerobic baffled reactor for the simultaneous nitrogen and organic carbon removal from wastewater," Water Research, Vol. 43, pp. 381−388, 2009.

[9] C. P. L Grady, G. Daigger, and H. Lim, "Biological wastewater treatment," 2nd Edition, Revised and Expanded, Marcel Dekker Inc., N.Y., 1999.

[10] T. Khin and A. P. Annachhatre, "Novel microbial nitrogen processes," Biotechnology Advances, Vol. 22, No. 7, pp. 519−532, 2004.

[11] APHA/AWWA/WEF, "Standard methods for the examination of water and wastewater," 18th Ed., Washinton DC, USA., 1992.

[12] A. M. Corral, F. Gonzalez, J. L. Campos, and R. Mendez, "Partial nitrification in sharon reactor in the presence of salts and organic carbon compounds," Process Biochemistry, Vol. 40, pp. 3109−3118, 2005.

[13] R. He, X. W. Liu, Z. J. Zhang, and D. S. Shen, "Characteristics of the bioreactor landfill system using an anaerobic-aerobic process for nitrogen removal," Bioresource Technology, Vol. 98, pp. 2526−2532, 2007.

[14] W. Li and S. K. Zheng, "A combination of anaerobic and aerobic treatment for ammonia-laden coke plant effluent: The pilot study," International Society for Environmental Information Sciences, Vol. 2, pp. 602−610, 2004.

[15] S. Chen, D. Z. Sun, and J. S. Chung, "Simultanoeous removal of COD and ammonium from landfill leachate using an anaerobic-aerobic moving bed biofilm reactor system," Waste Management, Vol. 28, pp. 339−346, 2008.

[16] J. H. Im, H. J. Woo, M. W. Choi, K. B. Han, and C. W. Kim, "Simultaneous organic and nitrogen removal from municipal landfill leachate using an anaerobic-aerobic system," Water Research, Vol. 35, pp. 2403−2410, 2001.

Call For Papers

IEEE EMB iCBBE

Environmental Pollution and Public Health (EPPH2010)

Special Track within iCBBE

环境污染与人类健康国际学术会议征文

June 21-23, 2010 Chengdu, China

http://www.icbbe.org/epph2010/

The International conference on Environmental Pollution and Public Health (EPPH2010), a special track within iCBBE 2010, will be held from June 21st to 23rd, 2010 in Chengdu, China. You are invited to submit papers in all areas of environmental pollution and related health problems. As we did in EPPH 2009 and 2008, all papers accepted will be included in IEEE Xplore and cited by Ei Compendex and ISTP.

Topics

Water Quality and Public Health

- Purification of drinking-water supplies
- Treatment, disposal and discharge of wastewater
- New wastewater treatment technologies
- Methods of monitoring water quality
- Modeling and measuring of water pollution
- New water purification technologies
- Ground water pollution control
- Water resources and quality assessment
- Water resource protection and sustainable use
- Hydrobiology and water pollution
- Other topics related to water pollution

Air Pollution and Public Health

- Effects of air pollution on public health
- Sources of air pollution
- Air pollution monitoring and modeling
- Air pollution prevention and control
- Urban/indoor air pollution and control
- Air quality measurement and management
- Global climate change and air pollution

Other Related Issues

- Chemical pollutants and its effects on health
- Land pollution and its effects on health
- Radiation safety in atomic industry
- Food and drug safety control
- Hazardous materials management
- Solid waste management
- Environmental toxicology
- Risk assessment of contaminated environments
- Ecosystem restoration
- Global climate changes and human health

Important Dates

- Paper Submission Due: Oct. 30, 2009
- Acceptance Notification: Dec. 31, 2009
- Conference: Jun. 21-23, 2010

Contact Information

Website:http://www.icbbe.org/epph2010/

E-mail: epph@icbbe.org

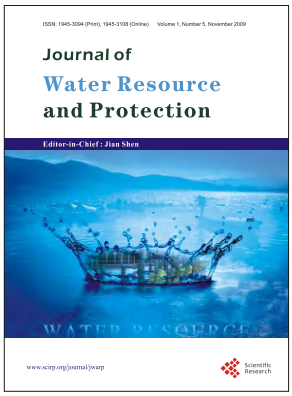

Call For Papers

Journal of Water Resource and Protection (JWARP)

http://www.scirp.org/journal/jwarp
ISSN:1945-3094 (Print), 1945-3108 (Online)

JWARP is an international refereed journal dedicated to the latest advancement of water resource and protection. The goal of this journal is to keep a record of the state-of-the-art research and promote the research work in these fast moving areas.

Editor-in-Chief

Editorial Board

Subject Coverage

This journal invites original research and review papers that address the following issues in water resource and protection. Topics of interest include, but are not limited to:

- Water resources and quality assessment
- Rivers, lakes and estuary systems
- Wastewater treatment and sludge biotreatment
- Water purification and water supply
- Water source protection and sustainable use
- Modeling, measuring and prediction of water pollution
- Ground water pollution control
- Reactions and degradation of wastewater contaminants
- Other topics about water pollution

We are also interested in short papers (letters) that clearly address a specific problem, and short survey or position papers that sketch the results or problems on a specific topic. Authors of selected short papers would be invited to write a regular paper on the same topic for future issues of the *JWARP.*

Notes for Intending Authors

Submitted papers should not have been previously published nor be currently under consideration for publication elsewhere. Paper submission will be handled electronically through the website. All papers are refereed through a peer review process. For more details about the submissions, please access the website.

Website and E-Mail

http://www.scirp.org/journal/jwarp Email: jwarp@scirp.org

J. Water Resource and Protection, 2009, 1, 299-380.
Published Online November 2009 in SciRes (http://www.SciRP.org/journal/jwarp).

TABLE OF CONTENTS

Volume 1 Number 5 **November 2009**

9771945309004 05